Slow and fast light effects in semiconductor optical amplifiers for applications in microwave photonics

Xue, Weiqi; Mørk, Jesper; Sales, Salvador; Öhman, Filip

Publication date:
2010

Document Version
Publisher's PDF, also known as Version of record

TECHNICAL UNIVERSITY OF DENMARK

Slow and Fast Light Effects in Semiconductor Optical Amplifiers for Applications in Microwave Photonics

by

Weiqi Xue

at

DTU Fotonik

Department of Photonics Engineering

Danmarks Tekniske Universitet

JUNE 2010

TECHNICAL UNIVERSITY OF DENMARK

Abstract

Slow and fast light effects have generated great interest in optical signal processing for applications in optical communications and microwave photonics. This thesis experimentally and theoretically analyzes semiconductor optical amplifiers (SOAs) based slow and fast light effects. The proposed devices are promising candidates for implementing optical signal processing especially in microwave photonic fields such as microwave phase shifters or delay lines. This thesis describes the achievement of 360^o microwave phase shifts by slow and fast light effects in SOAs, which also satisfies some basic requirements of microwave photonic systems.

In this work, we initially explore the physical limitations of the coherent population oscillations based slow and fast light in SOAs and present a theoretical model, in the context of four wave mixing, to simulate the microwave phase changes induced by controlling the group velocity of light. Based on these understandings, we propose a new configuration by optical filtering to enhance slow light effects. This method has been demonstrated to produce up to $\sim 150^o$ microwave phase shifts at such high microwave frequency as 40 GHz. Then we characterize this new configuration in detail by investigating the microwave operation bandwidth and initial chirp dependence. The most promising result of this thesis is the achievement of 360^o microwave phase shifters through a cascaded slow light structure. The multi-current control of the cascaded

structure has been experimentally assessed and has allowed simultaneous manipulation of both microwave phase and power. In addition, fully tunable microwave notch filters have been experimentally realized with free spectral ranges of 9.4 MHz and 300 MHz, respectively, where slow light based phase shifters provide 100 percent fractional tuning over the whole free spectral range. This thesis then deals with the noise characterization by mainly focusing on intensity noise and single sideband phase noise. The relation between these two noise is analyzed theoretically and the analytical model is also verified experimentally. Finally, we propose a cross gain modulation (XGM) based slow light scheme. By operating XGM in a counter-propagation configuration, a 10.5 ps continuously tunable true time delay over a microwave bandwidth of several tens of GHz is achieved.

TECHNICAL UNIVERSITY OF DENMARK

Resumé

Egenskaberne ved langsomt og hurtigt lys har skabt stor interesse inden for optisk signalbehandling til anvendelse inden for optisk kommunikation og mikrobølgefotonik. Denne afhandling analyserer, teoretisk såvel som eksperimentelt, optiske halvlederforstærkere (Semiconductor Optical Amplifier -SOA'ere) baseret på langsomt samt hurtigt lys. De foreslåede strukturer er lovende kandidater til gennemførelse af optisk signalbehandling, især til brug indenfor mikrobølgefotonik med henblik på faseforskydning eller forsinkelse linjer. Denne afhandling beskriver muliggørelsen af 360^o mikrobølge faseskift benyttende langsomt og hurtigt lys i SOA'ere, som også opfylder nogle grundlæggende krav i fotoniske mikrobølgesystemer.

I dette arbejde udforsker vi først de fysiske begrænsninger af kohærente optiske oscillationer (Coherent Population Oscillations -CPO) med fokus på langsomt samt hurtigt lys i SOA'ere. Der præsenteres en teoretisk model, baseret på firebølgeblanding, til at simulere mikrobølge faseforandringer induceret af den kontrollable gruppehastighed af lyset. Ud fra på de fundne resultater, fremsættes en ny konfiguration med optisk filtrering for således at optimere effekterne af langsomt lys. Med denne metode demonstreres et faseskift på op til 150^o ved frekvenser på 40 GHz. Herefter karakteriseres denne nye konfiguration i detaljer ved at undersøge mikrobølgebåndbredden samt chirp-afhængigheden. Det mest

lovende resultat af denne afhandling, er opnåelsen af 360^o faseforskydning gennem en kaskadebaseret struktur. Den multistrøms-baserede kontrol med kaskadestrukturerne er blevet eksperimentelt undersøgt og har muliggjort kontrol af både mikrobølge-fase samt amplitude. Desuden er fuldt tunebare mikrobølge-notchfiltre blevet eksperimentelt realiseret med en fri spektral afstande på 9,4 MHz hhv. 300 MHz, hvor langsomt lysbaseret faseforskydning giver 100 procent tuning over hele den fri spektrale afstand.

Afhandlingen omhandler dernæst karakteristik af støj med primær fokus på intensitetsstøj samt enkeltsidebånds-fasestøj. Forholdet mellem disse to typer støj analyseres teoretisk, og en analytisk model verificeres eksperimentelt. Endelig foreslår vi en krydsforstærkningsmodulation (cross gain modulation -XGM) baseret langsomt lys. Ved at operere XGM i en kontra-propagerende konfiguration, kan der opnås en kontinuerlig tunebar signal forsinkelse på op til 10,5 ps over en båndbredde på tocifrede GHz.

Acknowledgements

During the three years of this Ph.D. project, between July 2007 and June 2010, many people have contributed to the work presented in this thesis in many different ways. First and foremost, I would like to show my sincere gratitude to my supervisor Prof. Jesper Mørk. His professional knowledge and skills have been an invaluable assistance on all the work discussed here. Working with him has been a great learning experience for me both professionally and personally. My warmest gratitude also goes to Prof. Salvador Sales and Prof. José Capmany in Universidad Politécnica de Valencia for their endless inspirations in microwave photonics and great support during my professional career. I would especially like to thank Salvador for all fun discussions related to research and life. Without his guidance and help I would never survive, particularly when I was in Valencia.

I have been extremely fortunate to work with many of former and current colleagues at Fotonik. Firstly I would like to thank Filip Öhman and Søren Blaaberg, who were my first mentors and guided me into the project swiftly. I am also very grateful to Kresten Yvind and David Larsson for their active help on device fabrications and tricky noise measurements in the lab. In addition, I am very grateful to all of my group members, especially my partner Yaohui Chen, with whom I have worked for last three years and struggled through many nerve-wracking problems.

A great number of people from the High-Speed Optical Communications group, Leif Oxenløwe, Christophe Peucheret, Michael Galili, Hans Christian Hansen Mulvad and Hao Hu are thanked for letting me "steal"

devices from their magic blue cabinets, especially Christophe for constantly knocking his door with problems. Moreover, my sincere appreciation goes to Xianbin Yu, Lei Wei, Minhao Pu and Jing Xu for inspired cooperations on other interesting areas, and Kamau Prince for being the first reader and proofreading the thesis.

I owe my deepest gratitude to the guys in Optical and Quantum Communications group of Universidad Politécnica de Valencia, Gustavo Puerto, Raimundo Garcia, Juan Sancho and Juan Lloret, for the good collaboration and supplying state-of-the-art devices for the experiments.

Last but not least, endless love to my fantastic wife Hua Ji for inspiring me and taking care of me.

Contents

Acronyms

ADCs	**A**nalog to **D**igital **C**onversions
ASE	**A**mplified **S**pontaneous **E**mission
CPO	**C**oherent **P**opulation **O**scillations
CW	**C**ontinuous **W**ave
DA-MZM	**D**ual **A**rm **M**ach **Z**ehner **M**odulator
EA	**E**lectro **A**bsorber
EDFA	**E**rbium **D**oped **F**iber **A**mplifier
EIT	**E**lectromagnetically **I**nduced **T**ransparency
EOM	**E**lectrical **O**ptical **M**odulator
FBG	**F**iber **B**ragg **G**rating
FSR	**F**ree **S**pectral **R**ange
FWM	**F**our **W**ave **M**ixings
MEMS	**M**icro **E**lectro **M**echanical **S**ystems
MZ-modulator	**M**ach **Z**ehnder **M**odulator
PC	**P**olarization **C**ontroller
PD	**P**hoto **D**etector
RF	**R**adio **F**requency

RIN	**R**elative **I**ntensity **N**oise
SOA	**S**emiconductor **O**ptical **A**mplifier
SMF	**S**ingle **M**ode **F**iber
SNR	**S**ignal to **N**oise **R**atio
SSB	**S**ingle **S**ide**B**and
VOA	**V**ariable **O**ptical **A**ttenuator
XGM	**C**ross **G**ain **M**odulation

Chapter 1

Introduction

The speed of light has been a hot issue and extensively researched for over one hundred years in the optics community. Especially during recent several decades, the swift and enormous progress of optical communications and all-optical signal processing has stimulated the motivation of controlling the speed of light, which is named as "slow and fast light". Normally, two kinds of velocities, phase and group velocities, are employed to describe the light propagation in a dispersive media [1, 2]. To physically understand slow and fast light effects, it is extremely crucial to distinguish between these two velocities. The phase velocity is the propagation speed of the phase front of the electric or magnetic fields used to describe the propagating light wave. The group velocity refers to the propagation speed of the envelope of light waves. In an optical signal processing or communication system, information is normally carried by the envelope of light waves, and hence propagates at the group velocity. Therefore, controlling the group velocity using slow and fast light

effects shows great potentials for myriad applications. In this thesis, I will mainly focus on the possible applications in microwave fields.

1.1 Motivations: microwave photonics - phase shift and true time delay

Due to the explosive increase of the throughput of the current generation wireless telecommunication networks, the microwave[1] carrier frequency is spreading into the millimeter-wave regime. 38.6∼40 GHz is already used for licensed high-speed microwave data links. In the nearby future, available wireless spectra in 71∼76, 81∼86 and 92∼95 GHz bands will be exploited for point-to-point high-bandwidth communication links [3]. Furthermore, the capacity of multi-band operation, light weight, small size, and low power consumption are highly desired in many current communication radars and future reconfigurable radio frequency (RF) front-ends, such as those required for mobile communication systems. Nowadays, all kinds of microwave or millimeter-wave signal processing functionalities in such wireless communication systems are widely implemented using digital electronics. However, the speed and bandwidth of such methods are significantly limited by the electronic sampling rate, especially at millimeter-wave frequencies [4]. To satisfy the requirements for higher carrier frequencies and larger bandwidth, photonic technologies are being exploited to realize various functions in microwave fields, some of which are very complex, or even impossible to do directly in the microwave domain. This interdisciplinary field is well known as "microwave photonics" [5, 6] and has been growing dramatically over the last several decades.

[1] In following chapters of this thesis, "microwave" also includes "millimeter-wave".

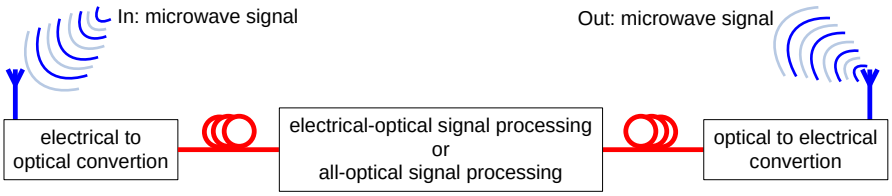

FIGURE 1.1: Schematic of a microwave photonic system. The red curves are optical fibers, which can enable ultra-long distance transmission with very low loss, typically 0.2 dB/km.

The reason is that photonic technology can provide many unique advantages, such as huge bandwidth, low loss, light weight, and immunity to electromagnetic interference. Figure 1.1 shows a typical schematic of a microwave photonic system. The microwave signal is commonly transported via the intensity modulated envelope of a propagating laser beam. The modulation is typically implemented using an electrical-optical convertor. This conversion enables the microwave signal propagation and processing to be directly implemented in the optical domain. After the desired signal processing, the optical signal is converted back into the microwave domain and broadcasted to users.

In the block of electrical-optical or all-optical signal processing, a tunable and wideband microwave delay line or phase shifter is highly essential in order to achieve more flexible and adaptable configurations [4, 7]. Here we mainly discuss two widely developed applications, tunable photonic microwave filters and optically steered phased array antennas.

1.1.1 Tunable photonic microwave filters

Microwave filters are widely used, in all kinds of wireless communication systems, to combine or separate multi-frequency bands and to suppress

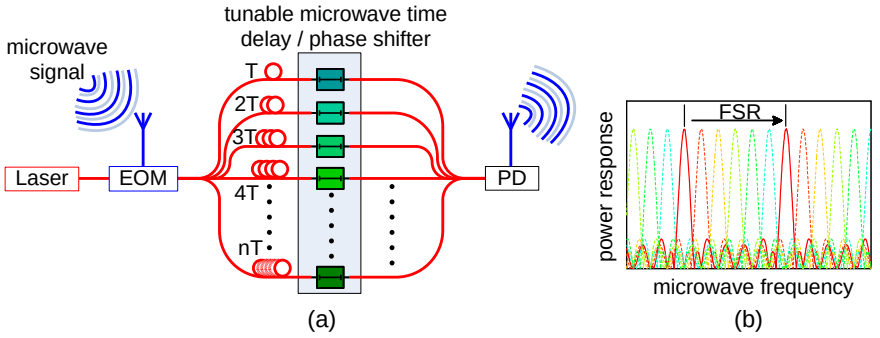

FIGURE 1.2: (a) Basic configuration of photonic microwave filters. (b) A typical microwave power response. The black arrow shows that the filter response is continuously tuned by properly adjusting microwave phase shifter within each branch. EOM: electrical-optical modulator. FSR: free spectral range. PD: photo detector.

noise or unwanted signals [8, 9]. Figure 1.2 shows a photonic implementation of microwave filters. The microwave signal is modulated onto a laser beam by means of an electrical-optical modulator. The optical signal is then split into n branches. There is a fixed time delay T between pairs of adjacent arms, as shown in Fig. 1.2(a), which could be easily realized by an optical fiber with a certain length. After the combination, due to the interference between signals propagating along different branches, the microwave power response versus the microwave frequency can be imagined and plotted in Fig. 1.2(b), as the red solid line shows. The free spectral range (FSR) of the filter response is decided by T. By employing a tunable photonic microwave delay line or phase shifter at each branch, the resonance peak can be easily tuned, which enables a tunable filter. In a real system, in order to avoid alterations of the FSR and the shape of the filter response when the resonance band is tuned, a constant microwave phase shifter is preferable rather than a time delay [10]. It can be clearly seen, as shown by the colored dashed lines in Fig. 1.2(b), that by introducing suitable microwave phase shifts for each

branch, the filter can be tuned over the whole FSR range, meantime, both the FSR and the shape of the filter keep undisturbed.

1.1.2 Optically steered phased array antennas

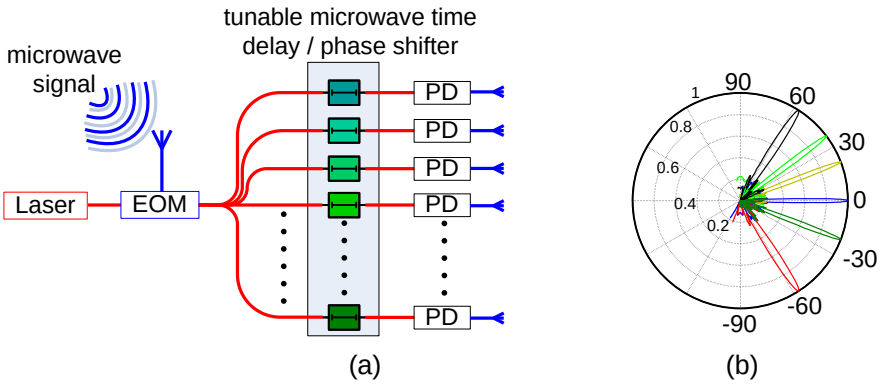

FIGURE 1.3: (a) Basic configuration of optically steered phased array antennas. (b) A typical far-field power distribution. The colored curves represent the radiation patterns with different beam directions, which is achieved by properly introducing time delay or phase shift in each branch.

Another interesting application is optically steered phased array antenna. Compared to Fig. 1.2(a), the main difference here is that the signal propagating along each branch is independently converted back to the microwave domain and broadcasted through a photo detector (PD) and radiation element, as shown in Fig. 1.3(a). Based on the electromagnetic field theory [11], the far-field distribution can be depicted in Fig. 1.3(b), as one of curves shows. By changing the tunable delay line or phase shifter in each arm, the radiation direction of the antenna can be continually steered, as shown by the different colored lines. However, microwave phase shifters inevitably induce beam squinting effects,

where the main lobe of the radiation pattern drifts away from the desired angle with changes in operating frequency. This beam squinting limits the antenna's instantaneous bandwidth and hence precludes the use of phased arrays in broadband applications, such as target-ID radar and spread-spectrum communication systems. An optically generated true-time delay can not only compensate for this squinting, but can also provide many inherent benefits [12, 13].

1.1.3 Slow and fast light enabled microwave photonic delay

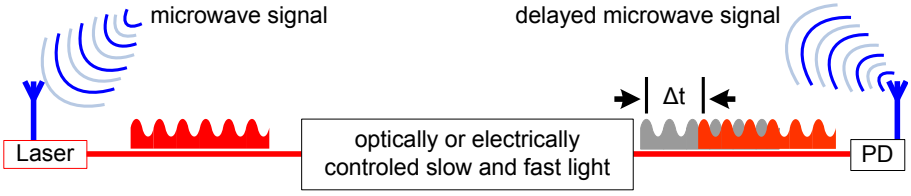

FIGURE 1.4: Basic configuration of a microwave tunable delay line based on slow and fast light effects.

As previously mentioned, a tunable microwave delay line is a key component in microwave photonic systems in which a flexible tunability is desired. For a laser beam, whose intensity is modulated by a microwave signal, changing the group velocity of light can be naturally converted into a time delay or phase shift experienced by the microwave signal carried by the laser. Figure 1.4 depicts a basic accomplishment of slow and fast light based microwave photonic tunable delay lines. By optically or electrically controlling the group velocity of optical signal in a slow or fast light medium, the arriving time, at the PD, of the output optical signal can be continually tuned. Therefore, after the conversion back into the microwave domain, a tunable time delay Δt is achieved.

For a given microwave modulation frequency f_{RF}, this Δt can also be expressed as a phase shift $2\pi f_{RF}\Delta t$. Thus, slow and fast light enabled microwave photonic time delay or phase shifter is extremely attractive for microwave photonic systems [6]. Although several of experimental observations of slow and fast light have been reported before 1990s [14–17], the most significant attention and progress have started from 1999 since a landmark achievement of slowing the group velocity of light down to 17 meters per second was reported within an ultra cold atomic gas [18].

1.2 Basic analysis of slow and fast light

When a light propagates through a dispersive medium, the group velocity can be mathematically described as [19]

$$v_g = \frac{c}{n + \omega dn/d\omega} \equiv \frac{c}{n_g} \tag{1.1}$$

$$n_g = n + \omega dn/d\omega \tag{1.2}$$

where c is the speed of light in vacuum, ω is the angular frequency of light, n is the refractive index, and n_g is defined as the group velocity index. For a given medium, the refractive index is not easily tunable. Therefore, control of the group velocity invariably relies on the second term of Eq. (1.2), the frequency dependence of the refractive index, also called dispersion. Any resonance, such as gain or loss resonance, will induce a rapid variation of the refractive index in the vicinity of the resonance. Normally, the refractive index is complex and can be rewritten as

$$\tilde{n} = n + in' \tag{1.3}$$

Here the real part n and imaginary part n' stand for the refractive index used in Eq. (1.2) and the absorbtion (loss) or gain, respectively.

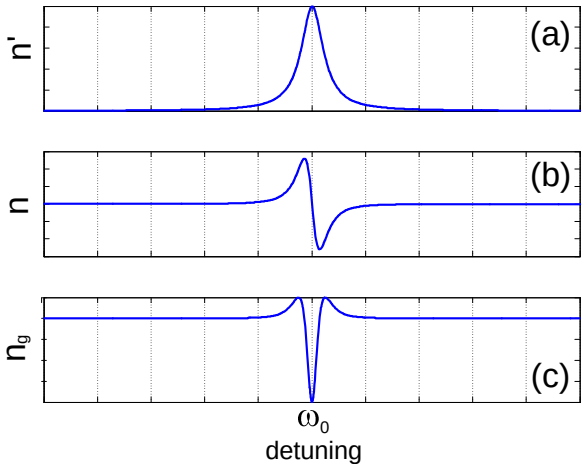

FIGURE 1.5: The origin of slow and fast light in a resonance. (a) the imaginary part, (b) the real part and (c) the group refractive index as a function of the detuning from the resonance frequency.

To physically understand how a resonance induces slow and fast light effects, let's consider an example with a material resonance peak at a optical frequency ω_0, as Fig. 1.5(a) shows. Based on the famous Kramers-Krönig relations [20], the resonance in the imaginary part of the refractive index leads to a rapid change or large dispersion of the real part, $dn/d\omega$, as shown in Fig. 1.5(b). Thus, from Eq. (1.2), the group refractive index n_g in the vicinity of the resonance will experience a significant increase (slow light) or decrease (fast light), as shown in Fig. 1.5(c). The narrower the resonance is, the larger the group velocity can be changed. If the width of the resonance is somehow tunable, the group velocity of light will also become tunable. The tunability can be achieved both optically, by injecting a strong control light, and electrically, by changing the electrical injection into the material.

1.3 Overview of various schemes to control the group velocity of light

During the last decade, several schemes were proposed to achieve slow and fast light by introducing a resonance. Several initial works employed the effects of Electromagnetically Induced Transparency (EIT) in atomic gases [18, 21, 22]. The speed of light was incredibly slowed down to the human scale. However, because EIT requires quantum mechanical interference between the electronic states of the energy levels, it is not easily performed at room temperature. Furthermore, the bandwidth of EIT-based slow and fast light is relatively small ($\sim MHz$). From an application point of view, it is highly desirable for slow and fast light effects to be operable at room temperature and over a large bandwidth ($\sim GHz$). Recently, using Coherent Population Oscillations (CPO) [23–25], stimulated scattering effects [26–30], and dispersion engineering structures [31–34], room-temperature slow and fast light effects were intensively demonstrated. Among these, slow and fast light in active semiconductor waveguides, such as semiconductor optical amplifiers (SOAs) and electro-absorbers (EAs), appear more promising because they can provide both very fast (on the order of several hundreds of picoseconds) electrically and optically controlled tunability over a microwave bandwidth of several tens of GHz in a compact device with a control voltage of a few volts [35–37]. This $\sim GHz$ operation bandwidth is absolutely necessary to satisfy the bandwidth requirements for practical applications in microwave systems.

1.4 Structure of the thesis

This thesis reports on demonstrations of slow and fast light effects within the aforementioned microwave photonic applications. To satisfy some basic requirements of applications such as 360^o phase shifts, large microwave operation bandwidth (up to 100 GHz) and possible control on microwave power, Chapter 2 analyzes the basic principles of CPO based slow and fast light effects in SOAs. A theoretical model is presented to directly describe microwave phase shifts caused by slow light effects. Furthermore, the effects of the conjugate sideband due to four wave mixing are theoretically examined. The limitations of conventional slow light configuration are analyzed physically. In Chapter 3, an optical filtering enhanced slow light configuration is proposed and experimentally verified to conquer the limitations of the conventional case. The underlying physics is elucidated through a perturbation method. The proposed new structure is then characterized in term of the initial modulation chirp and the microwave operation frequency. By taking advantage of the initial chirp dependence, both microwave phase advance and delay are realized. As a preliminary application demonstration, a fully tunable microwave photonic notch filter with a 9.4 MHz FSR is reported. Chapter 4 reports on the use of a red-shifted sideband regenerator to enable the cascadability of the slow light stages that were proposed in Chapter 3. It ultimately leads to the achievement of 360^o microwave phase shifts. The possibility of flexible controls on both microwave phase and power is also discussed. Finally, a upgraded microwave photonic filter with a 300 MHz FSR is presented. Chapter 5 is devoted to the noise properties of slow light based microwave phase shifts. Firstly, a detailed theoretical model is developed to characterize the input optical signal with focusing on the intensity noise of the optical signal and the Single Sideband (SSB)

phase noise of the electrical microwave source. After including the slow light devices, the SSB noise spectrum is investigated experimentally, and a possibility to improve signal to noise ratio is finally suggested. Chapter 6 presents a microwave photonic true time delay, which is more desired than a microwave phase shifter for applications in phased array antennas. The physical principle is cross gain modulation enabled control of the group velocity. Two configurations, co-propagation and counter-propagation, are experimentally investigated. A 10.5 ps true time delay over a microwave bandwidth of $\sim$40 GHz is obtained. The conclusions and outlooks are presented in Chapter 7.

Chapter 2

Slow and fast light effects in semiconductor optical amplifiers

2.1 Background

During past several decades, due to their various nonlinear properties, for instance, self phase modulation, cross gain modulation, cross phase modulation and four wave mixing (FWM) effects, SOAs have been well researched and developed to accomplish all kinds of optical signal processing in optical communication systems. Key applications have included wavelength conversion [38], optical gates [39], and optical regeneration [40]. Some integrated devices are already commercially available [41]. These progressions in the development of optical signal processing,

as well as its distinct advantages, have indicated that SOAs are promising devices for current and future optical systems. The first demonstration of slow light in SOAs [25, 42] has recently excited significant interests because these devices can operate at room temperature and be easily integrated with other optical systems. More importantly, for an optical signal carrying a microwave signal, slow light in SOAs can provide $\sim GHz$ bandwidth [43–46]. On the other hand, for a ultrashort pulse signal, $\sim THz$ bandwidth can also be achieved [47–49]. Because microwave intensity modulated optical signal is more interesting for microwave photonic systems, the first case will be investigated in this chapter.

Coherent population oscillations (CPO) effects [23] have been used to realize slow and fast light in SOAs. Basically, CPO effects are due to the interaction between light and the propagation medium. When two laser beams with slightly different optical frequencies, which we will denote as the strong "pump" and weaker "probe", propagate through a SOA, the carrier population in the active region will oscillate at the frequency difference between the pump and the probe. This oscillation in carrier population leads to both refractive index and gain grating. In turn, the grating scatters the energy of the pump onto the weak probe and consequently changes the refractive index and gain experienced by the probe. Due to the limitation imposed by the carrier lifetime, the efficiency of optically induced population oscillation strongly changes as a function of the detuning frequency between the pump and the probe. Therefore, according to Eq. (1.2), this dispersion property will allow the possibility of changing the group velocity of the probe. The group velocity can be tuned optically by varying the pump power or electrically by changing the injection current. Many previous and promising results have

already been reported, significant highlights include the record achievements of $\sim 200^o$ phase shifts at a microwave frequency of $\sim$1 GHz [46] and $\sim$ 120^o phase shifts at $\sim$3 GHz while at the same time allowing some power control [45, 50]. These two achievements were realized, respectively, by using a 2.5 mm long quantum-well SOA and switching between operations in gain (SOA) and absorption (EA) regimes or by concatenating SOA-EA pairs.

2.2 Wave mixing enabled coherent population oscillations

In SOAs, CPO based slow and fast light effects require two laser beams operating at different optical frequencies. Although two individual lasers can be used as sources, it is difficult to accurately control the frequency difference between independent optical sources, in order to operate in the frequency region required for microwave applications.

2.2.1 Experimental technique to perform slow and fast light

In most cases, the required strong pump and weak probe signals can be easily realized by electro-optical intensity modulation technique [23, 24]. This technique is also well used in microwave photonic systems for the photonic generation of microwave signals [51, 52], which makes the experimental realization more compatible with real-world applications. Figure 2.1 shows the experimental realization of the pump and probe. A continuous wave (CW) laser is injected into an electro-optical intensity modulator, which is modulated by a microwave signal having an angular

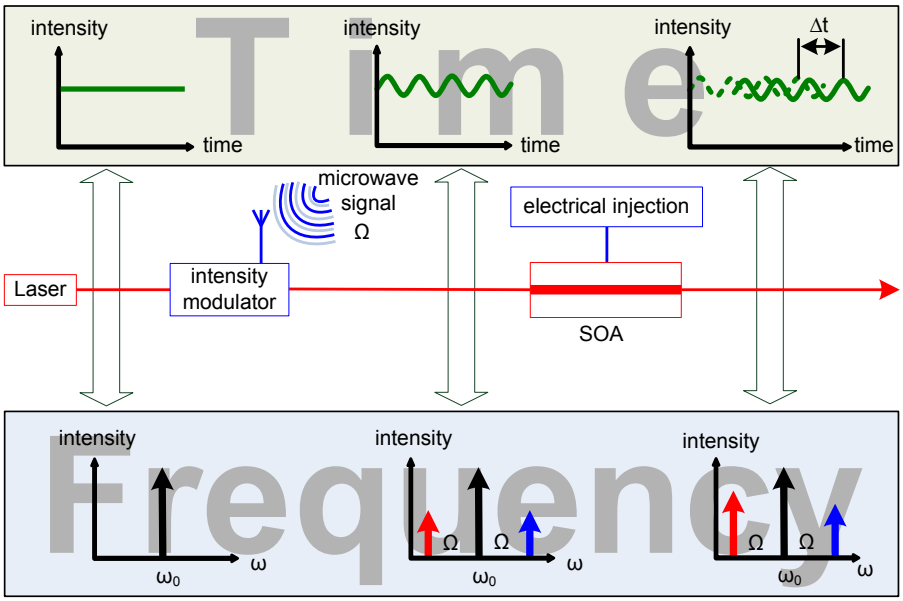

FIGURE 2.1: Basic realization of slow and fast light effects in semiconductor optical amplifiers

frequency Ω. A chirp-free Mach-Zehnder modulator (MZ-modulator) can be used to achieve pure intensity modulation. It is straightforward that in the time domain, the output optical signal from the modulator will be a sinusoidal waveform, as shown in the top row of Fig. 2.1. However, in the frequency domain, the input electrical field of the laser beam and microwave signal can be expressed as:

$$E_{in}(t) = A_0 \cdot exp(i\omega_0 t) \tag{2.1}$$

$$V_{RF_{in}}(t) = V_0 \cdot exp(i\Omega t) \tag{2.2}$$

where A_0 denotes the electrical field amplitude of the CW laser, ω is its angular frequency, and V_0 is the voltage amplitude of the microwave signal. Here, we neglect the initial phase and any noise for both the laser and microwave signal. These effects will be taken into account in

Chapter 5. Due to the intensity modulation, the electrical field of the output optical signal from the modulator can be expressed as:

$$\begin{aligned} E_{out}(t) &= A_0 \cdot cos\{\gamma \cdot cos(\Omega t) + \phi_{DC}\} \cdot e^{i\omega_o t} \\ &\approx \frac{\sqrt{2}}{2} A_0 \cdot J_0(\gamma) \cdot e^{i\omega_0 t} \\ &\quad -\frac{\sqrt{2}}{2} A_0 \cdot J_1(\gamma) \cdot e^{i(\omega_0+\Omega)t} - \frac{\sqrt{2}}{2} A_0 \cdot J_1(\gamma) \cdot e^{i(\omega_0-\Omega)t} \end{aligned} \tag{2.3}$$

Here $\gamma = \pi/2 \cdot (V_0/V_\pi)$ is the modulation index, ϕ_{DC} $(=\frac{\pi}{2})$ is the phase shift determined by the DC bias of the MZ-modulator, V_π is the half-wave voltage of the modulator, and J_0 and J_1 are the first kind Bessel functions. Compared with the first order optical sidebands, all higher order ones are omitted for a small signal modulation. From Eq. (2.3), there are two extra sidebands, E_{+1} and E_{-1}, are introduced by the intensity modulation and can be described by Eq. (2.4).

$$\begin{cases} E_0(t) = \dfrac{\sqrt{2}}{2} A_0 \cdot J_0(\gamma) \cdot e^{i\omega_0 t} \\ E_{+1}(t) = -\dfrac{\sqrt{2}}{2} A_0 \cdot J_1(\gamma) \cdot e^{i(\omega_0+\Omega)t} \\ E_{-1}(t) = -\dfrac{\sqrt{2}}{2} A_0 \cdot J_1(\gamma) \cdot e^{i(\omega_0-\Omega)t} \end{cases} \tag{2.4}$$

The frequency difference between the carrier and sidebands is decided by the microwave frequency Ω. Energy distribution cross three output optical frequencies can be controlled by varying the modulation index γ. When the optical signal propagates through the SOA, the strong carrier will act as the pump, while two weak sidebands as the probe. Due to CPO effects in term of four wave mixing (FWM), in the frequency domain, the gain and refractive index experienced by one sideband can be modified by the carrier and the other sideband through adjusting either the optical power level or electrical injection. Therefore, after the

SOA and optical-to-electrical conversion, a time delay or advance of Δt appears in the time domain, as shown in Fig. 2.1. In principle, the received microwave signal can be written as:

$$V_{RF_{out}}(t) = 2\Re {A_0}^2 J_0(\gamma) J_1(\gamma) \cdot e^{i\Omega t + i\Omega \Delta t} \tag{2.5}$$

Here $\Re$ is the responsivity of the optical-to-electrical convertor, which also takes into account the resistance of the optical-to-electrical convertor. For those applications in which a microwave phase shift is more revelent, a time delay Δt corresponds to a phase shift of $\Omega \Delta t$.

Since all time delays or phase shifts are relative, in order to measure the changing magnitude of light slow down or speed up, a reference is required. Figure 2.2 gives a typical experimental set-up to measure slow light effects by comparing the microwave phase of the modulated envelope before and after the SOA. The initial electrical microwave signal from the network analyzer is modulated onto a laser beam through a MZ-modulator. After passing through the SOA, the optical signal is converted back to the electrical domain and detected by the network analyzer, which will measure the microwave phase changes relative to the internal microwave drive signal. An EDFA and variable optical attenuator are included at the input of the SOA to tune the input optical power level. Because the MZ-modulator and SOA are sensitive to the polarization, two polarization controllers are also employed. To measure the microwave phase shift induced by slow and fast light effects in the SOA in isolation, a careful calibration measurement has to be performed to exclude any possible phase shifts caused by any other devices, especially the PD, which was demonstrated to possibly bring some phase shifts [53].

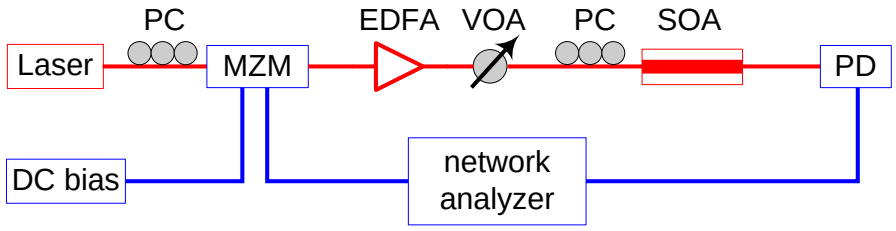

FIGURE 2.2: Basic experimental set-up to measure microwave phase shifts induced by slow and fast light effects in a SOA. PC: polarization controller. MZM: Mach-Zehnder modulator. EDFA: erbium doped fiber amplifier. PD: photo detector. DC: direct current.

2.2.2 Theoretical expressions for microwave application-oriented slow light

In order to benefit the applications of slow and fast light effects in microwave fields, in this section, we will derive a theoretical model to directly govern the microwave phase shifts achieved by the slow and fast light effects in SOAs. Since CPO effects involve interactions between several optical frequency components and SOAs, it is straightforward to describe it in the frequency domain using a wave mixing frame [54, 55]. In the case where the input optical signal is created by intensity modulation of a single-frequency CW laser, as mentioned in section 2.2.1, propagations in the SOA for pump, E_0, and two probes ,E_{+1} and E_{-1}, are governed by Eq. (2.6) [43, 44, 56].

$$\begin{cases} \dfrac{\partial E_0}{\partial z} = \gamma_0 E_0 \\ \dfrac{\partial E_{+1}}{\partial z} = \gamma_0 E_{+1} + \xi_{+1}[|E_0|^2 E_{+1} + E_0^2 E_{-1}^*] \\ \dfrac{\partial E_{-1}}{\partial z} = \gamma_0 E_{-1} + \xi_{-1}[|E_0|^2 E_{-1} + E_0^2 E_{+1}^*] \end{cases} \tag{2.6}$$

$$\gamma_0 = \frac{1}{2}[g_{sat}(1 - i\alpha) - a] \qquad S = \frac{|E_0|^2 + |E_{+1}|^2 + |E_{-1}|^2}{P_{sat}}$$

$$g_{sat} = \frac{\Gamma g_0}{1 + S} \qquad \xi_{\pm 1} = -\frac{1}{2}\frac{g_{sat}}{P_{sat}}\frac{1 + S \pm \alpha\Omega\tau_s - i\alpha(1 + S) \pm i\Omega\tau_s}{(1 + S)^2 + (\Omega\tau_s)^2}$$

where Γg_0 is the linear gain, α is the linewidth enhancement factor, a is the internal loss, P_{sat} is the saturation power, S is a normalized optical intensity by the saturation power, and τ_s is the carrier lifetime.

For the applications in microwave photonic systems, the microwave signal is carried as the beating, P_{RF}, between the pump, E_0, and the probes, E_{+1} and E_{-1}. It is recovered by the electrical-to-optical conversion after the SOA.

$$P_{RF} = E_0^* \cdot E_{+1} + E_{-1}^* \cdot E_0 \tag{2.7}$$

$$P_{DC} = |E_0|^2 + |E_{+1}|^2 + |E_{-1}|^2 \approx |E_0|^2 \tag{2.8}$$

By substituting Eq. (2.7) and (2.8) into Eq. (2.6), the propagation equations of the microwave signal P_{RF} and DC part P_{DC} can be derived:

$$\begin{cases} \dfrac{\partial P_{DC}}{\partial z} = (\gamma_0 + \gamma_0^*) \cdot P_{DC} \\ \dfrac{\partial P_{RF}}{\partial z} = (\gamma_0 + \gamma_0^*) \cdot P_{RF} + (\xi_{+1} + \xi_{-1}^*) \cdot P_{DC} P_{RF} \end{cases} \tag{2.9}$$

From an application point of view, Eq. (2.9) gives a direct prediction of how the microwave signal is delayed or advanced by slow and fast light effects in SOAs.

2.2.3 Simulation results of slow and fast light effects in SOAs

In general, slow-down or speed-up of a signal centered at the probe frequency corresponds to a positive or negative dispersion of the refractive index seen by the probe, with respect to the detuning frequency between the pump and probe. However, because here the microwave photonic signal is generated by the technique of modulation, it is composed of three discrete optical frequency components. Hence, one of the sidebands will be affected not only by the strong carrier but also by the other sideband. It makes the situation more complicated compared with the basic CPO case, where the signal is only affected by the strong pump. To simplify the situation, we can initially neglect one of the sidebands when the signal propagates in the SOA, which provides us a basic insight. The Eq. (2.6) then can be simplified to,

$$\begin{cases} \dfrac{\partial E_0}{\partial z} = \gamma_0 E_0 \\ \dfrac{\partial E_{+1}}{\partial z} = \gamma_0 E_{+1} + \xi_{+1}|E_0|^2 E_{+1} \quad or \quad \dfrac{\partial E_{-1}}{\partial z} = \gamma_0 E_{-1} + \xi_{-1}|E_0|^2 E_{-1} \end{cases} \tag{2.10}$$

From Eq. (2.10), the susceptibility of the remained sideband can be fully understood theoretically. The main parameters used in the calculations are: $|E_0|^2 = 10mW$, $P_{sat} = 2.5mW$, $\tau_s = 100ps$, $\Gamma g_0 = 1.2 \times 10^4 m^{-1}$, and the length of the SOA is $500\mu m$.

Figure 2.3 shows both the real and imaginary parts of the susceptibility of the sideband and the resulted group refractive index as a function of the microwave frequency Ω for several different linewidth enhancement factors α. The positive/negative Ω represents that the blue-shifted/red-shifted sideband is considered. For $\alpha = 0$, Fig. 2.3(a) gives a standard

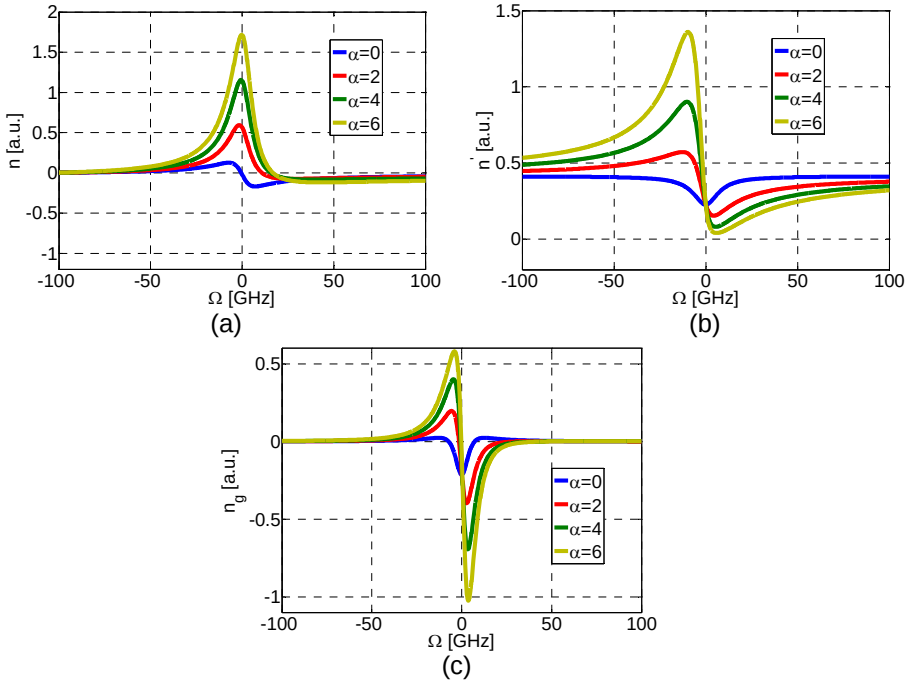

FIGURE 2.3: Simulations of slow and fast light in a SOA with one sideband included. (a) the real part, (b) the imaginary part, and (c) the group refractive index as a function of the microwave modulation frequency Ω for different linewidth enhancement factor α.

dispersion dependence, which is related to the gain change of the sideband shown in Fig. 2.3(b) and, therefore, induces a small fast light at the resonance. But when $\alpha \neq 0$, the carrier density modulation will induce not only a gain grating but also a refractive index grating. The dependence of the refractive index on the carrier density introduces asymmetric spectra for the gain and refractive index, as shown in Fig. 2.3(a) and (b) [55, 57]. Compared with the case $\alpha = 0$, this asymmetric dispersion thus leads to a larger slow light for the red-shifted sideband or fast light for the blue-shifted sideband. The peak positions of the group refractive index, shown in Fig. 2.3(c), are determined by the inverse of

the carrier lifetime τ_s.

From Eq. (2.9), it is easy to obtain the final microwave time delays caused by the group refractive index changes of the sideband. The results are shown in Fig. 2.4(a). It can be concluded that the refractive index dynamics related to a non-zero α contributes much larger time delays than the gain dynamics. The corresponding microwave phase shifts are also depicted in Fig. 2.4(b) and show that the microwave operation bandwidth is limited by the carrier lifetime.

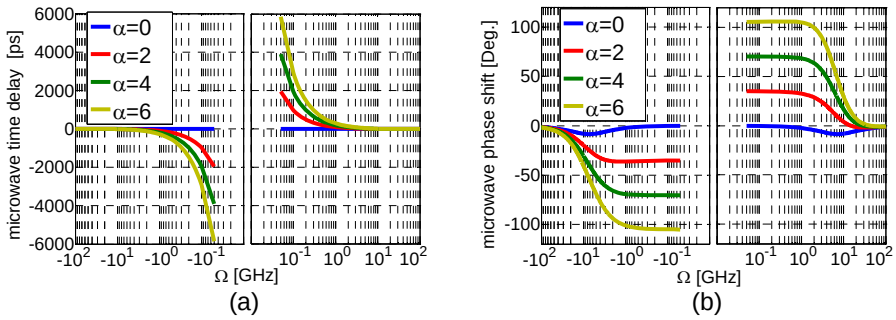

FIGURE 2.4: Calculated (a) microwave time delays and (b) microwave phase shifts by slow and fast light in a SOA with one sideband included.

However, due to two sidebands at input and strong wave mixing effects in the SOA, the interaction between two sidebands can not be ignored. By including both sidebands, Figure 2.5 presents the calculated susceptibility and group refractive index experienced by the sidebands. Compared with the results in Fig. 2.3, the most distinct difference is that the refractive dispersion shows a blue shift as α increases. Consequently, the group refractive index at the blue-shifted sideband can be modified at even higher microwave frequencies, as shown in Fig. 2.5(c)

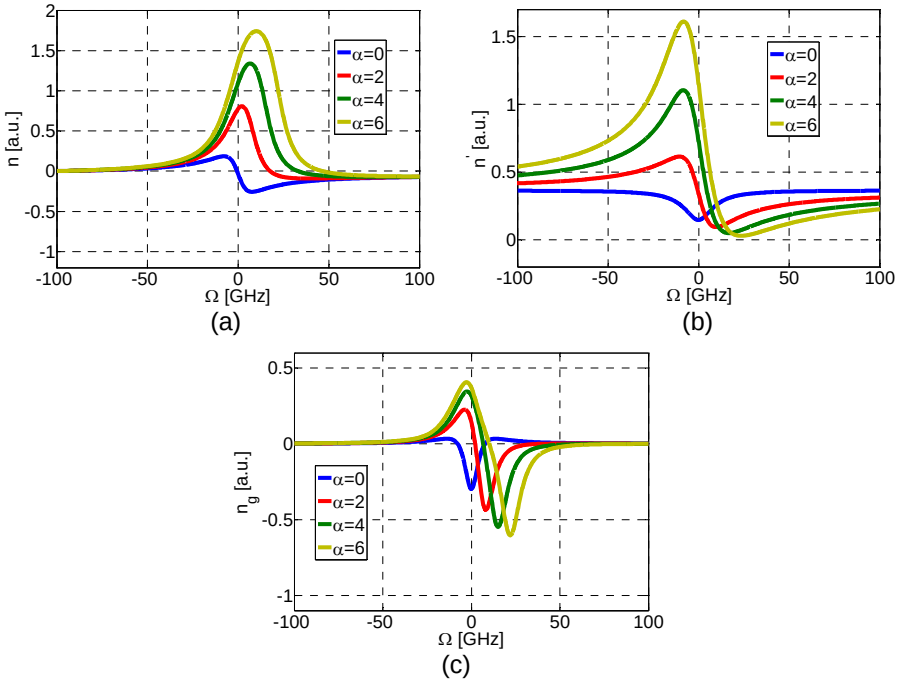

FIGURE 2.5: Simulations of slow and fast light in a SOA including the conjugate sideband effects. (a) the real part, (b) the imaginary part, and (c) the group refractive index as a function of the microwave modulation frequency Ω for different linewidth enhancement factor α.

After propagating through the SOA, the optical signal, which is composed of the strong carrier and two weak sidebands, is detected and converted to electrical signal by a high speed PD. The induced microwave time delays and phase shifts are calculated and shown in Fig. 2.6. Since the group velocity related to the non-zero α factors changes in the opposite directions for two sidebands, the slow and fast light effects generated by the refractive index dynamics will significantly cancel each other due to the double sideband detection. Therefore, the detected microwave time delay or phase shift is mainly determined by the gain dynamics. Consequently, Fig. 2.6 indicates similar values for both $\alpha = 0$ and $\alpha \neq 0$.

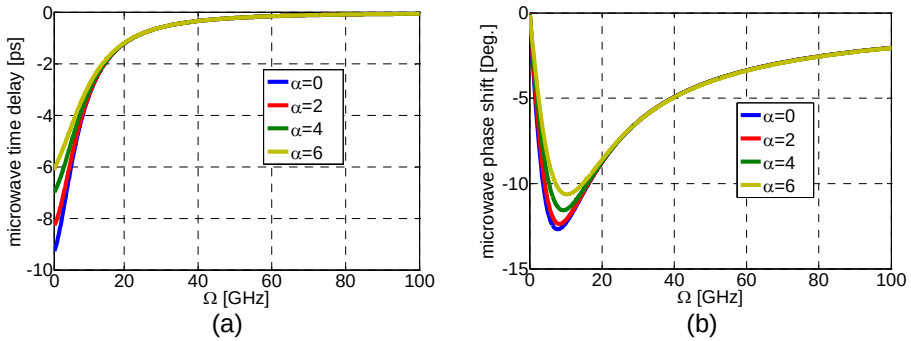

FIGURE 2.6: Calculated (a) microwave time delays and (b) microwave phase shifts by slow and fast light in a SOA with both sidebands included.

2.3 General discussions

To facilitate the applications of slow and fast light in microwave photonic systems, especially those operating at the X or K band, the achievement of a 360^o microwave phase shift is important in order to realize full functionality. Since a single element, like an SOA, only realizes a microwave phase shift of a few tens of degrees, there have been a number of proposals and investigations to increase the phase shift. One idea, resulting in a phase shift of more than 180^o [46], is to switch between the regimes of gain and absorption. However, this implies a very large change in the net transmission of the microwave signal through the device when changing the light speed. Furthermore, the operating frequency is limited by the longest carrier lifetime achieved, i.e., under operation as an SOA. In [46] the large phase shift was thus obtained at an operating frequency of 1 GHz. On the other hand, although a EA is a promising candidate due to its much shorter carrier lifetime, its loss is a main limitation for practical applications. In order to solve this problem, a solution is to combine an EA with an SOA to compensate for the

loss, and even concatenate several EA-SOA pairs in order to increase the absolute value of the microwave phase shift [50]. However, we have already discussed that an SOA introduces an advancement of the microwave phase, corresponding to the fast light effect, which thus might counteract the slow light effect of an EA. Therefore, the achievement of a sizable net, microwave phase shift relies on a complicated choice of the operation conditions of all involved SOAs and EAs. Moreover, its operating frequency is still limited to a few GHz.

In previously reported cases, the input optical signal is composed of a strong carrier, the pump, and two weak sidebands, the probes in the optical frequency domain. The physical effects inducing light slow-down or speed-up in semiconductor waveguides are CPO effects. For an SOA, the gain and refractive index are modulated in time, and the corresponding temporal gratings subsequently scatter the pump fields and alter their amplitude and phase. The resulting detuning dependence of the probe phase, described in terms of an effective index, leads to a change in the group velocity experienced by the probe signals. Based on the theoretical investigations in this chapter, it has already been shown that the contribution of the temporal index grating leads to an antisymmetric detuning dependence of the probe phase. Upon detection of both sidebands, this effect cancels out and hence the phase change is governed solely by the gain dynamics. In this regime, the slow/fast light effects can be described as the effect of absorption/gain saturation and is limited in frequency and magnitude by the carrier recovery time of EAs/SOAs [43, 58]. Therefore, the removal of the cancelation between the two sidebands is a suggestion for moving beyond these limitations.

Chapter 3

Enhanced light slow-down by optical filtering

3.1 Basic idea by optical filtering

As we discussed in Chapter 2, the refractive index dynamics associated with a non-zero linewidth enhancement factor α could induce much larger slow or fast light effects at even higher microwave frequencies. However, due to the cancelation of the group velocity changes between two sidebands, the refractive index dynamics do not contribute to the final microwave phase shift. Hence, it is worth to figure out how to avoid the cancelation of the refractive index dynamics by removing one of the sidebands in order to achieve greater microwave phase shifts.

3.1.1 Optical filtering at input

In [57, 59], it was suggested that utilizing a single sideband signal at the input can enhance the group velocity change that can be achieved in SOAs. We have experimentally investigated this possibility by blocking one of the sidebands before the SOA. Figure 3.1 shows the experimental set-up along with the transmission spectrum of the employed a fiber Bragg grating (FBG) notch filter. The 3 dB and 20 dB bandwidths of the FBG filter are 0.1 nm and 0.06 nm, respectively. The notch suppression is larger than 30 dB. Additionally, the FBG notch filter can be slightly tuned by mechanically pulling. All these properties make it possible that one of the sidebands can easily be removed without influencing the other sideband or the carrier when the microwave frequency is larger than 5 GHz.

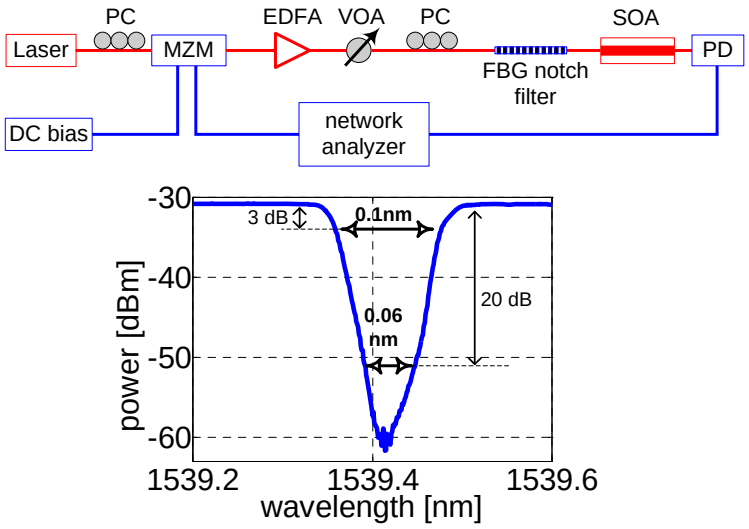

FIGURE 3.1: Experimental set-up for single sideband at input and the transmission spectrum of the FBG notch filter. FBG: fiber Bragg grating.

However, as demonstrated in Fig. 3.2(a), hardly any difference of the induced phase shift is observed between the three cases with one of the sidebands or both at input. The optical spectra both before and after the SOA are also shown in Fig. 3.2(b). The top, middle and bottom rows show results obtained with the cases of double-sideband at input, only red-shifted sideband at input or only blue-shifted sideband at input, respectively. Due to the fast build-up of a conjugate sideband during propagation in the SOA, the output signal possesses a similar spectrum for all three cases. Therefore, the phase change of that mirror sideband tends to reduce the effect of the single sideband input and make the refractive index dynamics cancel out again.

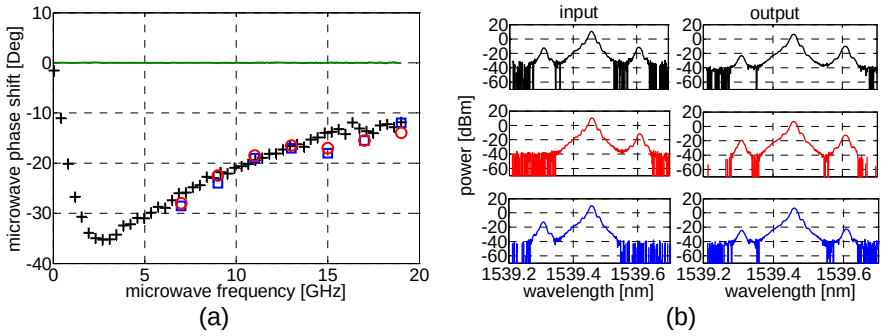

FIGURE 3.2: (a) Measured microwave phase shift vs. microwave frequency for the input signal with double sidebands (black "+"), only red-shifted sideband (red "o") or only blue-shifted sideband (blue "□"). The SOA is biased at 160 mA and the microwave phase shift is obtained when the input optical power changes from -10.3 dBm to 13.6 dBm. The green solid line is the reference when the input power level at the minimum value of -10.3 dBm. (b) Measured input spectra before the SOA (left column) and output spectra after the SOA (right column) for the three different input signals.

3.1.2 Optical filtering at output

Instead, we proposed another method for exploiting the refractive index dynamics to enhance the microwave phase shift [60]. In this case, a double sideband signal is launched at the input, and after propagation through the SOA, one of the sidebands is blocked by an optical notch filter. Figure 3.3 shows the basic scheme of optical filtering at output. By tuning the notch filter, either of the sidebands can be completely removed before the detection.

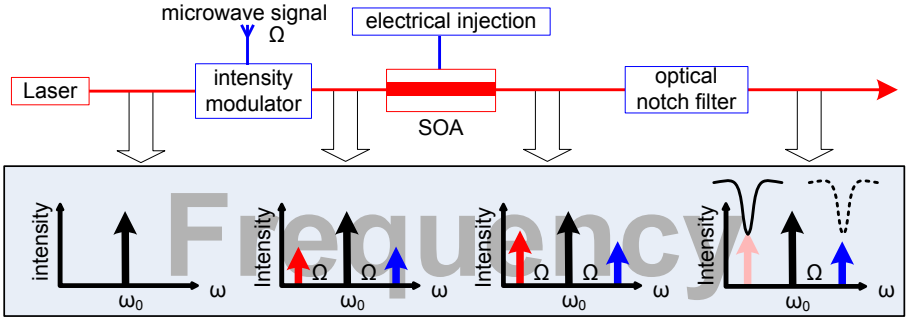

FIGURE 3.3: Basic scheme to exploit the refractive index dynamics by employing optical filtering after the SOA.

The physics involved in the optical filtering after the SOA can be qualitatively understood from a perturbation treatment of the model presented in Chapter 2 in the limit of relatively small propagation length δL. From Eq. (2.7), the final detected microwave signal can be rewritten:

$$P_{RF} \quad = \quad E_0^* \cdot E_{+1} + E_{-1}^* \cdot E_0 \equiv P_{+1} + P_{-1} \tag{3.1}$$

where P_{+1}, P_{-1} and P_{RF}, respectively, correspond to the modulated part

of the detected signal when blocking the red-shifted sideband E_{-1}, blocking the blue-shifted sideband E_{+1}, or without optical filtering. Therefore, Eq. (2.9) can be extended as:

$$\begin{cases} \dfrac{\partial P_{DC}}{\partial z} = (\gamma_0 + \gamma_0^*) \cdot P_{DC} \\ \dfrac{\partial P_{RF}}{\partial z} = (\gamma_0 + \gamma_0^*) \cdot P_{RF} + (\xi_{+1} + \xi_{-1}^*) \cdot P_{DC} P_{RF} \\ \dfrac{\partial P_{+1}}{\partial z} = (\gamma_0 + \gamma_0^*) \cdot P_{+1} + \xi_{+1} \cdot P_{DC} P_{RF} \\ \dfrac{\partial P_{-1}}{\partial z} = (\gamma_0 + \gamma_0^*) \cdot P_{-1} + \xi_{-1}^* \cdot P_{DC} P_{RF} \end{cases} \tag{3.2}$$

For a small propagation distance in the SOA, the spatial variation of the saturation induced by the DC field can be neglected. Then, the output values of P_{RF}, P_{+1} and P_{-1} can be approximately derived as:

$$\begin{cases} P_{RF}(\delta L) = P_{RF}(0) + \Delta P_{RF} \\ \qquad\qquad = 2|E_0 E_{+1}|[1 + (g_{sat} - a + \gamma_1)\delta L + i\beta_1 \delta L] \\ P_{+1}(\delta L) = P_{+1}(0) + \Delta P_{+1} \\ \qquad\qquad = |E_0 E_{+1}|[1 + (g_{sat} - a + \gamma_1 + \alpha\beta_1)\delta L + i(\beta_1 - \alpha\gamma_1)\delta L] \\ P_{-1}(\delta L) = P_{-1}(0) + \Delta P_{-1} \\ \qquad\qquad = |E_0 E_{+1}|[1 + (g_{sat} - a + \gamma_1 - \alpha\beta_1)\delta L + i(\beta_1 + \alpha\gamma_1)\delta L] \end{cases} \tag{3.3}$$

We have assumed that, at the input of the SOA, the fields corresponding to the two sidebands are equal and real with a normalized value of $|E_0 E_{+1}|$, which is also known as a chirp-free intensity modulation. The quantities γ_1 and β_1 are given by:

$$\gamma_1 = -g_{sat} \frac{(1+S)S}{(1+S)^2 + (\Omega\tau_s)^2}$$
$$\beta_1 = -g_{sat} \frac{\Omega\tau_s S}{(1+S)^2 + (\Omega\tau_s)^2}$$

Therefore, it is easy to infer that the microwave phases are determined by the arguments of Eq. (3.3) and can be expressed as,

$$\begin{cases} \delta\varphi_{RF} = arg[1 + (g_{sat} - a + \gamma_1)\delta L + i\beta_1\delta L] \\ \delta\varphi_{+1} = arg[1 + (g_{sat} - a + \gamma_1 + \alpha\beta_1)\delta L + i(\beta_1 - \alpha\gamma_1)\delta L] \\ \delta\varphi_{-1} = arg[1 + (g_{sat} - a + \gamma_1 - \alpha\beta_1)\delta L + i(\beta_1 + \alpha\gamma_1)\delta L] \end{cases} \quad (3.4)$$

For the conventional case where both sidebands are detected after the SOA, the microwave phase $\delta\varphi_{RF}$ does not depend on the linewidth enhancement factor α. This indicates that the influence from the refractive index dynamics, also quantified by α, is canceled. Hence, when the input optical power or the injection current is changed, the induced microwave phase change is solely governed by the gain dynamics [43, 44].

When employing an optical notch filter to block one of the sidebands, red-shifted or blue-shifted, before detection, the microwave phases, $\delta\varphi_{+1}$ or $\delta\varphi_{-1}$, include extra contributions $\alpha\beta_1$ and $\alpha\gamma_1$ which originate from the refractive index dynamics. Based on Eq. (3.4), it can be theoretically demonstrated that introducing optical filtering at the output can exploit the refractive index dynamics, which could enhance slow and fast light effects induced by the CPO effects in SOAs.

3.2 Experimental results of greatly enhanced microwave phase shifts

In order to experimentally investigate the role of optical filtering at the output of the SOA, the set-up shown in Fig. 3.4 is utilized. A CW laser beam with the wavelength of 1539.46 nm is modulated by a microwave synthesizer inside the network analyzer. The MZ-modulator provides

a nearly chirp-free intensity modulation. The modulated laser beam is coupled into a bulk SOA, where CPO and FWM effects will induce changes of the phase and the amplitude of the two sidebands. After the SOA, one of the sidebands can be blocked by a FBG notch filter before the detection. After the optical to electrical conversion, the detected microwave signal is compared with the initial electrical signal to assess time delays or microwave phase shifts which are caused by the SOA. The experimental controls are the input optical power to the SOA and the microwave modulation frequency. By incorporating an erbium doped optical fiber amplifier (EDFA) and a variable optical attenuator, the input optical power can be adjusted from -10.3 dBm to 13.6 dBm.

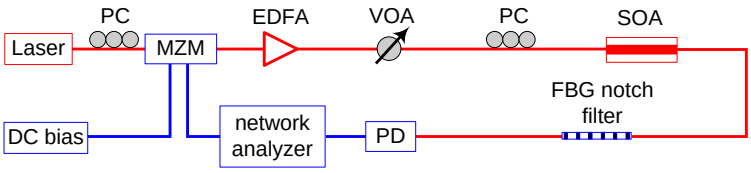

FIGURE 3.4: Experimental set-up to exploit the refractive index dynamics by employing optical filtering after the SOA.

For different optical filtering schemes, we measured the change of the phase of the intensity envelope relative to its value at the minimum input optical power of -10.3 dBm. Figure 3.5 shows the microwave phase delay (positive) or advance (negative) and microwave power changes as a function of the input optical power for a fixed injection current of 160 mA and modulation frequency of 19 GHz. The black curves in Fig. 3.5(a) show the conventional case where both sidebands are detected. A $\sim 20^o$ phase advance is obtained by increasing the input optical power from -10.3 dBm to 13 dBm and can be clearly explained by the gain saturation effects [43, 44]. However, blocking the red-shifted sideband or blue-shifted sideband results in positive and negative phase changes, corresponding, respectively, to slow light and fast light. Especially when

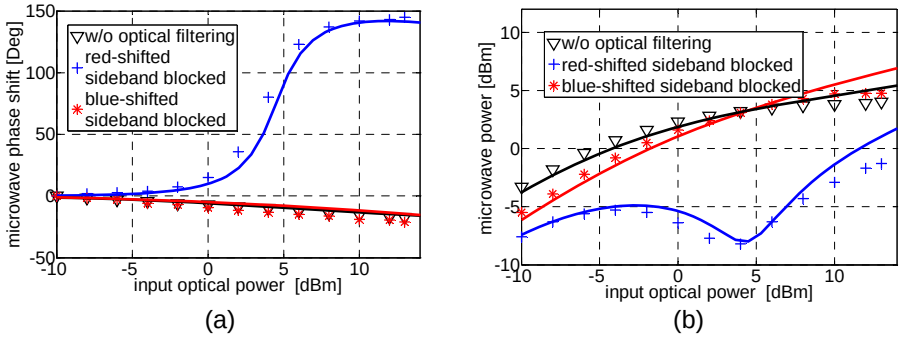

FIGURE 3.5: Experimental investigations of the role of optical filtering after the SOA. Measured (a) microwave phase shifts and (b) microwave powers as a function of the input optical power for the detection with double sidebands (black "∇"), with only blue-shifted sideband (blue "+") or with only red-shifted sideband (red "$*$"). The experimental data are taken at a microwave modulation frequency of 19 GHz and the solid curves are full simulation results based on the model presented in Chapter 2.

the red-shifted sideband is blocked, $\sim 150^o$ phase delay is achieved, which corresponds to a ten-fold increase of the maximum microwave phase shift obtained in the absence of filtering. The solid lines in Fig. 3.5 are numerical simulations based the model, presented in Chapter 2, and demonstrate a very good agreement with the experimental results. The following main parameters are used in the simulations: $P_{sat} = 10dBm$, $\tau_s = 100ps$, $g_0 = 1.15 \times 10^4 m^{-1}$, $\alpha = 6$, $\Omega = 19GHz$ and the length of the SOA $L = 500\mu m$.

However, since blocking either of the sidebands can exploit the refractive index dynamics, as demonstrated in Eq. (3.4), in order to understand why blocking red-shifted sideband induces much larger microwave phase change than blocking blue-shifted sideband, it is important to investigate the signs of terms $\alpha\beta_1$ and $\alpha\gamma_1$ which are related to α. When blocking the red-shifted sideband before detection, the microwave phase

is decided as $\delta\varphi_{+1} = arg[1+(g_{sat}-a+\gamma_1+\alpha\beta_1)\delta L+i(\beta_1-\alpha\gamma_1)\delta L]$ and demonstrates an additional large phase delay introduced by a positive (increasing) term $-\alpha\gamma_1$ in the imaginary part and a negative (decreasing) term $\alpha\beta_1$ in the real part. On the other hand, when the blue-shifted sideband is blocked, from the third equation in Eq. (3.4), we can conclude that the refractive index dynamics related to α factor still cancel out to a significant extent because the magnitudes of both real and imaginary parts are increased by two extra terms, $-\alpha\beta_1$ and $\alpha\gamma_1$. Therefore, blocking the blue-shifted sideband can not yield any distinct improvements, as the red "$*$" symbols show in Fig. 3.5(a).

When the red-shifted sideband is blocked before detection, the corresponding microwave power in Fig. 3.5(b) shows an $\sim$10 dB variation and the power drop is correlated with the sharp increase of the microwave phase and can be understood through inspecting the second equation of Eq. (3.3). For convenience, we rewrite it here.

$$\begin{aligned} P_{+1}(\delta L) &= P_{+1}(0) + \Delta P_{+1} \\ &= |E_0 E_{+1}|[1 + (g_{sat} - a + \gamma_1 + \alpha\beta_1)\delta L + i(\beta_1 - \alpha\gamma_1)\delta L] \end{aligned}$$

The microwave power is determined by $|P_{+1}(\delta L)| = \sqrt{Re^2 + Im^2}$. While the microwave phase is greatly shifted due to two terms, $\alpha\beta_1$ and $-\alpha\gamma_1$, the absolute values of the real and imaginary parts firstly decrease towards zero as $\alpha\beta_1$ and $-\alpha\gamma_1$ increase and then increase when $\alpha\beta_1$ and $\alpha\gamma_1$ totally dominate the real and imaginary parts, respectively. This is the reason why the microwave phase shift is accompanied by a power drop.

The microwave frequency dependence of the slow light based phase shifter is also investigated experimentally. For the conventional case,

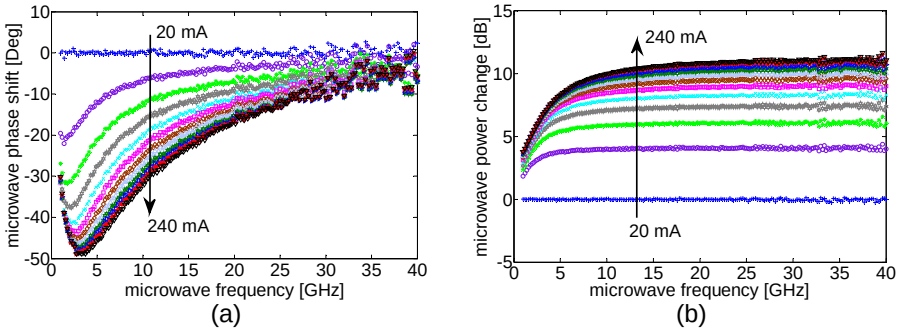

FIGURE 3.6: Microwave frequency dependence of slow and fast light effects in an SOA without optical filtering. Measured (a) microwave phase shift and (b) power change as a function of the microwave modulation frequency.

without optical filtering, Figure 3.6 presents experimental results for the microwave phase shift and power change as a function of the modulation frequency for different injection currents. The reference phase in Fig. 3.6(a) is measured at an injection current of 20 mA. During the measurements, the input optical power is fixed at 10 dBm. A tunable microwave phase shift (relative to the reference) of up to 50^o is obtained at around 3 GHz. At higher microwave frequencies, the limited response time of the SOA due to the finite carrier lifetime leads to smaller microwave phase shifts. The maximum phase shift is related to the small signal gain. The higher the injection current, the more the group velocity changes, then, the larger microwave phase shift is achieved. The measured microwave phase shifts show a good qualitative agreement with the theoretical simulation results presented in Fig. 2.6. The corresponding microwave power change, in Fig. 3.6(b), shows a low-pass filter profile which is also determined by the carrier recovery time [61, 62].

When the red-shifted sideband was blocked after the SOA, Figure 3.7(a)

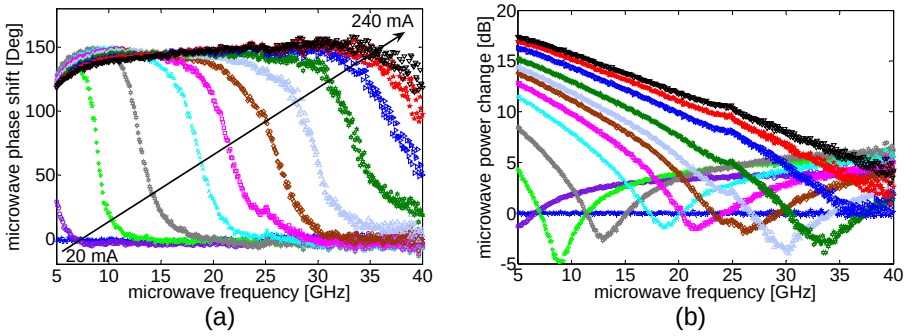

FIGURE 3.7: Microwave frequency dependence of optical filtering enhanced slow light effects in an SOA with blocking the red-shifted sideband before the detection. Measured (a) microwave phase shift and (b) power change as a function of the microwave modulation frequency.

presents the enhanced light slow-down for the microwave phase shifts and power changes as a function of the microwave frequency. It shows that $\sim 150^o$ phase delay can be obtained over the whole microwave bandwidth of 35 GHz, up to 40 GHz. The lowest microwave modulation frequency is limited by the FBG notch filter. These large improvements not only on the microwave phase shift, but also in the operating microwave bandwidth make the CPO based slow light effects in SOAs more promising in applications such as microwave photonic filters [63], waveform signal generators [64] and phased array antennas [12]. We notice that the microwave phase shift does not correspond to a true time delay, which may be a limitation for wideband phased array systems due to the beam squint effects [65]. Another possible limitation for applications is the microwave power variation which always accompanies the large microwave phase shift, as shown in Fig. 3.7(b). But in later chapters it will be demonstrated that these power variations can be greatly decreased by a new cascaded configuration.

3.3 Dependence on linewidth enhancement factor α

In previous sections, it was theoretically and experimentally shown that blocking the red-shifted sideband after the SOA can significantly enhance light slow-down by exploiting the refractive index dynamics, which are related to the gain dynamics through a non-zero linewidth enhancement factor α. Consequently, it introduces several-fold increase of the achieved microwave phase shift. Furthermore, the microwave operating frequency is greatly extended from a few GHz to several tens of GHz as well. Based on the FWM model presented in section 2.2, a numerical solution for the case of blocking the red-shifted sideband can be obtained. The full simulation results are given in Fig. 3.8(a). A similar measurement as shown in Fig. 3.7(a) can be performed as well. The measured results are presented as a contour plot in Fig. 3.8(b). Here, the injection current is fixed at 300 mA and the microwave phase is controlled by changing the input optical power instead of the injection current. This also verifies its both optical and electrical tunability. Although the FWM model gives a perfect prediction on the microwave operating frequency of the proposed microwave phase shifter, it has not been physically understood why the microwave operating bandwidth is greatly enhanced and not limited by the carrier lifetime.

Here, if we focus on the induced microwave phase, in order to get analytical solutions of Eq. (3.2), the terms only related to the amplitude in

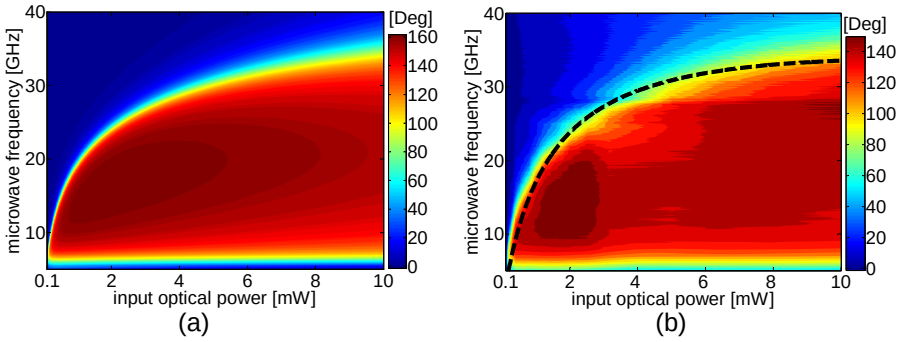

FIGURE 3.8: Contour plots of microwave frequency dependence of the proposed microwave phase shifter. (a) Numerical simulation results. (b) Experimental measurements. The black dashed curve shows the analytical result calculated from Eq. (3.9).

Eq. (3.2) can be neglected. Thus, Eq. (3.2) can be simplified as:

$$\begin{cases} \dfrac{\partial P_{RF}}{\partial z} = (\xi_{+1} + \xi_{-1}^{*}) \cdot P_{DC} P_{RF} \\ \dfrac{\partial P_{+1}}{\partial z} = \xi_{+1} \cdot P_{DC} P_{+1} + \xi_{+1} \cdot P_{DC} P_{-1} \\ \dfrac{\partial P_{-1}}{\partial z} = \xi_{-1}^{*} \cdot P_{DC} P_{+1} + \xi_{-1}^{*} \cdot P_{DC} P_{-1} \end{cases} \tag{3.5}$$

In this case, however, all information regarding the amplitude of the modulated signal is lost.

For the conventional situation without optical filtering, an analytical solution of the microwave phase shift by changing the optical power can be derived from the first equation of Eq. (3.5).

$$\delta\varphi_{RF}(z) = arg[e^{(\xi_{+1}+\xi_{-1}^{*})\cdot P_{sat} S z}] = -z\Gamma g_0 \cdot \frac{S}{1+S} \cdot \frac{\Omega\tau_s}{(1+S)^2 + (\Omega\tau_s)^2} \tag{3.6}$$

Figure 3.9 gives the results calculated from the analytical solution Eq. (3.6). A microwave phase advance is achieved by increasing the input

optical power S. Furthermore, from Eq. (3.6) it is also easy to conclude that the maximum microwave phase shift is obtained when $\Omega\tau_s = 1+S$. Thus $\Omega_{max}(\tau_s) = (1+S)/\tau_s$, which is a few GHz and only determined by the carrier lifetime τ_s.

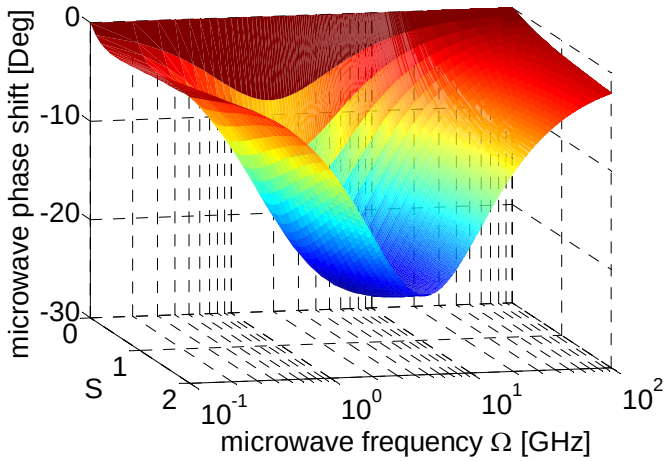

FIGURE 3.9: Analytical result of microwave frequency dependence of the slow light based microwave phase shifter without optical filtering

For the cases with optical filtering after the SOA, the analytical solutions of the second and third equations in Eq. (3.5) are:

with blocking the red-shifted sideband,

$$\delta\varphi_{+1}(z) = arg[(1-i\alpha)\cdot e^{(\xi_{+1}+\xi^*_{-1})\cdot P_{sat}Sz} + i\alpha] \tag{3.7}$$

with blocking the blue-shifted sideband,

$$\delta\varphi_{-1}(z) = arg[(1+i\alpha)\cdot e^{(\xi_{+1}+\xi^*_{-1})\cdot P_{sat}Sz} - i\alpha] \tag{3.8}$$

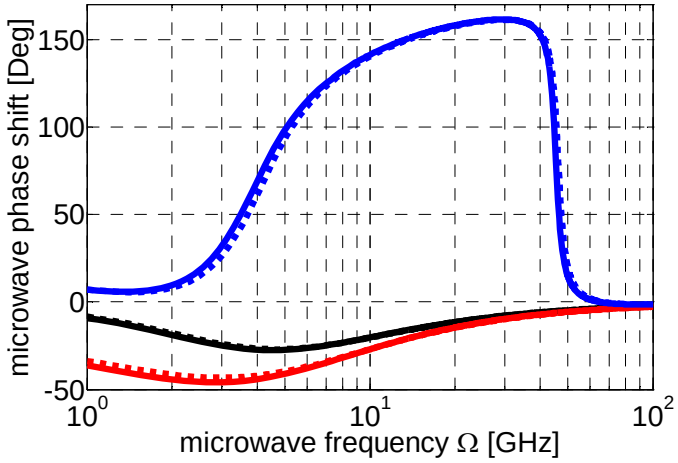

FIGURE 3.10: Compare between full numerical simulations (solid lines) and analytical solutions (dashed lines) for the microwave phase shifts. The color "black", "blue" and "red" stand for the cases without optical filtering, with blocking the red-shifted sideband and with blocking the blue-shifted sideband, respectively.

To verify the accuracy of the analytical solutions Eq. (3.6-3.8), we compare them with the full numerical simulations. The results are shown in Fig. 3.10. The microwave phase shifts for three different cases are achieved by increasing the normalized input optical power S from 0.1 to 2. The approximately analytical solutions demonstrate a very good agreement with accurate simulations.

Actually, for the more interesting case with the red-shifted sideband blocked, where a much larger phase shift can be obtained, from Eq. (3.7) we can derive the maximum microwave operation frequency.

$$\Omega_{max}(\tau_s, \alpha) = \frac{1}{\tau_s} \cdot \frac{S + \sqrt{S^2 - 4(1+S)^4 \cdot \Phi^2}}{2\Phi(1+S)} \tag{3.9}$$

where $\Phi = [\pi/2 - arctan(\alpha)]/(z\Gamma g_0)$. Hence, blocking the red-shifted

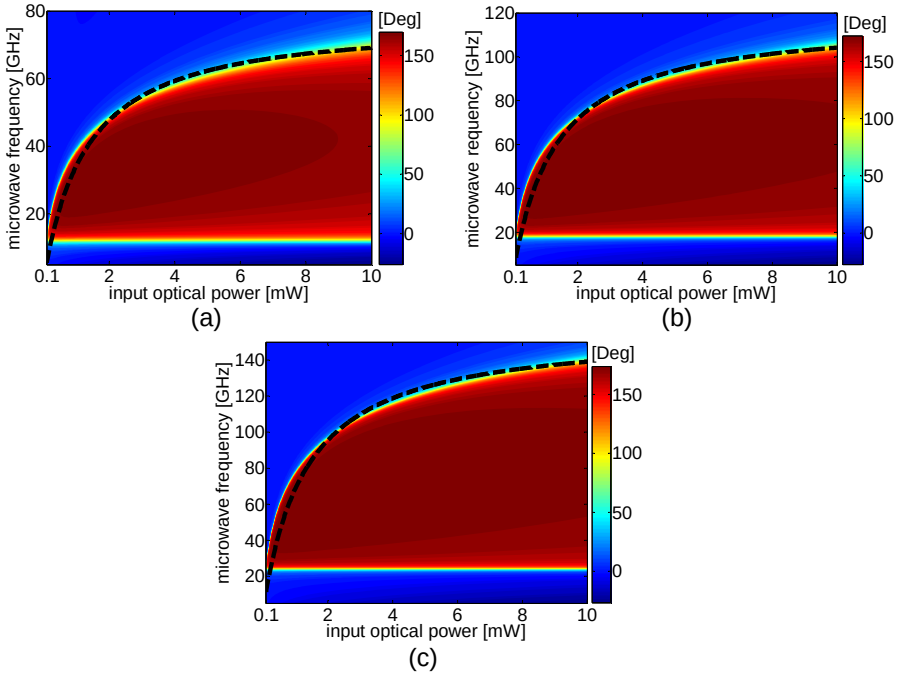

FIGURE 3.11: Numerical simulations and analytical calculations of microwave phase shifts as a function of both input optical power and microwave frequency for three different linewidth enhancement factors. (a) $\alpha = 20$. (b) $\alpha = 30$. (c) $\alpha = 40$. The black dashed lines are calculated from Eq. (3.9)

sideband by optical filtering is seen to enhance the available microwave operating frequency by a factor that depends on not only the carrier lifetime τ_s but the linewidth enhancement factor α. This can be interpreted as an equalization effect brought about by the dynamics of the refractive index, not unlike the effect used in interferometers to increase the speed of all-optical signal processing [66]. The black dashed curve in Fig. 3.8(b) is given by Eq. (3.9), and shows that the analytical result provides a good prediction of the microwave operating frequency. In

particular, by increasing α, it is possible to significantly enhance the microwave operating frequency. For a value of α of the order of 30 or more the frequency thus extends beyond 100 GHz. Figure 3.11 shows the numerical simulation results. When $\alpha = 20$, 30 or 40, the proposed microwave phase shifter can be operated at 70 GHz, 100 GHz or even 140 GHz, respectively. And the analytical results shown by the black dashed lines confirm the simulations. Such high α parameters have been realized in quantum dot active waveguides [67]. Therefore, the approximate analytical solutions Eq. (3.7-3.9) give directions for further engineering an SOA to make it operate at a specific microwave frequency band of interest.

3.4 Dependence on initial chirp

In all experiments and theoretical analysis presented previously, the optical phases of the sidebands within the input optical signal are implicitly assumed to be zero, which corresponds to a pure intensity modulated signal, also denoted as chirp-free. In this section, we will discuss that the chirp of the input signal plays an important role in the case of optical filtering assisted slow and fast light scheme. We will experimentally demonstrate that for the specific case of blocking the red-shifted sideband before detection, both $\sim 120^o$ microwave phase delay and $\sim 170^o$ phase advance can be achieved by choosing different values of the initial chirp. The experimental results are shown to agree well with numerical simulations and can be qualitatively explained using an analytical perturbation approach.

3.4.1 Theory and numerical model

The input optical signal is created by intensity modulation of a single-frequency CW laser, the sidebands, E_{+1} and E_{-1}, and carrier, E_0, of which act as probe and pump beams, respectively. For small signal modulation, in the experiments reported here, the power of the carrier is 20 dB larger than that of the sidebands, thus $|E_0|^2 >> |E_{+1}|^2, |E_{-1}|^2$. By taking into account the initial modulation chirp of the input optical signal, the three electrical fields at input can be expressed as,

$$\begin{cases} E_0(0) = |E_0(0)| \cdot e^{i\theta_0} \\ E_{+1}(0) = |E_{+1}(0)| \cdot e^{i\theta_1} \\ E_{-1}(0) = E_{+1}(0) \end{cases} \tag{3.10}$$

By inserting Eq. (3.10) into (3.1), we can obtain the initial conditions of the microwave modulated parts of the optical signal, $P_{+1}(z)$, $P_{-1}(z)$ and $P_{RF}(z)$.

$$\begin{cases} P_{RF}(0) = 2|E_0(0) \cdot E_{+1}(0)|cos(\Delta\theta) \\ P_{+1}(0) = |E_0(0) \cdot E_{+1}(0)|[cos(\Delta\theta) + i \cdot sin(\Delta\theta)] \\ P_{-1}(0) = |E_0(0) \cdot E_{+1}(0)|[cos(\Delta\theta) - i \cdot sin(\Delta\theta)] \end{cases} \tag{3.11}$$

where $\Delta\theta = \theta_1 - \theta_0$ is the initial optical phase difference between the carrier and sidebands, and reflects the degree of the initial chirp induced by the modulation [68]. Based on Eq. (3.2) and the initial conditions expressed by Eq. (3.11), the initial chirp dependence of the achieved microwave phase shift can be analyzed numerically.

Figure 3.12 depicts the calculated microwave phase shifts as a function of $\Delta\theta$. For each $\Delta\theta$, the microwave phase shift occurs upon increasing the

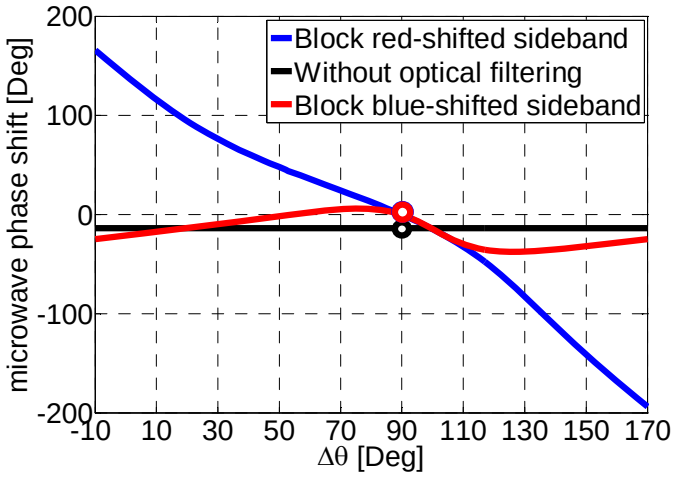

FIGURE 3.12: Numerical simulations of initial chirp dependence of an slow light based microwave phase shifter for three different optical filtering cases. The microwave phase shifts of P_{RF}(black), P_{+1}(blue) and P_{-1}(red) are induced by increasing the normalized input optical power S from 0.01 to 1.6. The microwave frequency is 19 GHz.

normalized input optical power S from 0.01 to 1.6, which corresponds to an absolute power change from -10 dBm to 12 dBm. The same parameters as in section 3.2 are used. For the conventional case without optical filtering, represented by the variable P_{RF}, it is easy to infer from Eq. (3.11) that the microwave phase of P_{RF} will not depend on $\Delta\theta$. This corresponds to the black curve in Fig. 3.12, showing a small constant phase shift of $\sim -13.8^o$. If the red-shifted sideband is blocked after propagation through the SOA, the blue curve in Fig. 3.12 shows that the final microwave phase shift greatly depends on $\Delta\theta$. When $-10^o \leq \Delta\theta < 90^o$, a microwave phase delay is induced by the slow light effect. At $\Delta\theta = 0^o$, corresponding to chirp-free modulation, a $\sim 150^o$ microwave phase shift is achieved, which is the situation discussed previously. On the other hand, a microwave phase advance is observed for $90^o < \Delta\theta \leq 170^o$. As $\Delta\theta$ approaches 90^o from either side, the

absolute value of the microwave phase shift will vanish. Notice that $\Delta\theta = 90^o$ represents a pure phase modulation, for which there is no amplitude modulation of the detected signal. When the blue-shifted sideband is blocked, the final phase shift will slightly depend on $\Delta\theta$, as shown by the red curve in Fig. 3.12. Thus, as $\Delta\theta$ increases from -10^o to 90^o, the numerical value of the microwave phase advance increases from $\sim -21.1^o$ and even flips into a phase delay of $\sim 6^o$ at $\Delta\theta = 76^o$. If $\Delta\theta$ increases continuously from 90^o to 170^o, there will be a maximum microwave phase advance of $\sim -37.6^o$, achieved at $\Delta\theta = 126^o$.

3.4.2 Experimental realization and results

To experimentally achieve a tunable chirp $\Delta\theta$, the input optical signal with two sidebands is generated by modulating a CW laser beam, at a wavelength of 1539.5 nm, using a Dual-Arm Mach-Zehnder Modulator (DA-MZM), where only one arm is biased and modulated at 19 GHz. Figure 3.13(a) gives the experimental set-up. The modulation chirp of the DA-MZM can be changed by the bias voltage [69] and the output electrical fields from the DA-MZM can be derived:

$$\begin{cases} E_0(0) = \dfrac{A_0}{2}[1 + J_0(\dfrac{V_{RF}}{V_\pi}) \cdot e^{-i\frac{V_{DC}}{V_\pi}\pi}] \equiv |E_0(0)| \cdot e^{i\theta_0} \\ E_{+1}(0) = i\dfrac{A_0}{2} \cdot J_{+1}(\dfrac{V_{RF}}{V_\pi}) \cdot e^{-i\frac{V_{DC}}{V_\pi}\pi}] \equiv |E_{+1}(0)| \cdot e^{i\theta_1} \\ E_{-1}(0) = -i\dfrac{A_0}{2} \cdot J_{-1}(\dfrac{V_{RF}}{V_\pi}) \cdot e^{-i\frac{V_{DC}}{V_\pi}\pi}] \equiv |E_{+1}(0)| \cdot e^{i\theta_1} \end{cases} \tag{3.12}$$

Here, $V_{RF} = 0.3V$, V_{DC}, and $V_\pi = 3.9V$ are the peak voltage of the microwave modulation signal, the DC bias voltage and the half-wave voltage of the modulator, respectively. According to Eq. (3.12) $\Delta\theta$ $(= \theta_1 - \theta_0)$ can be altered between 0^o and 180^o by changing the bias

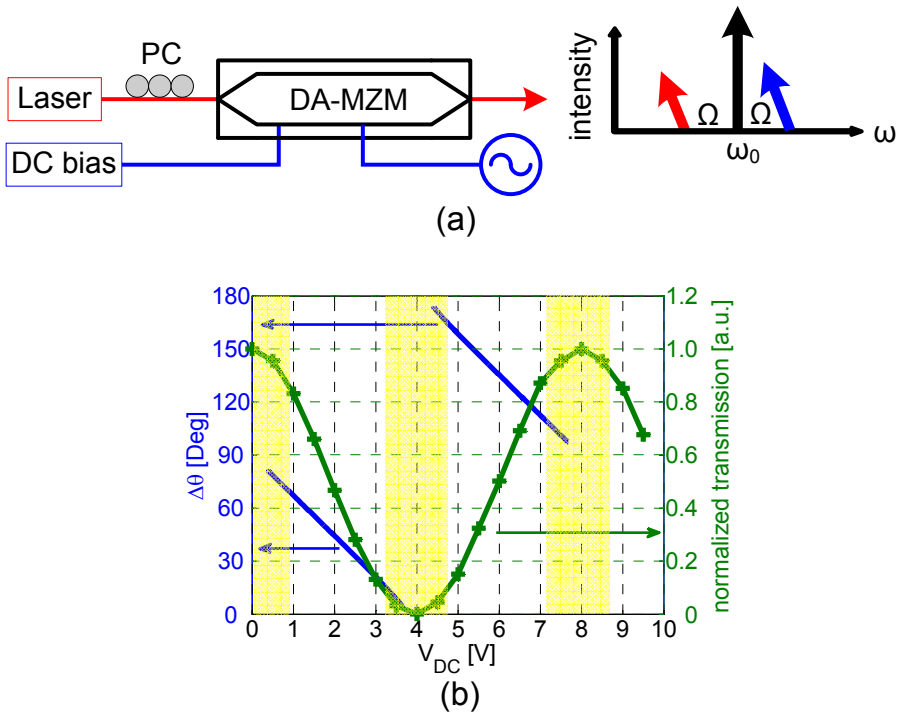

FIGURE 3.13: (a) Experimental set-up to realize a tunable initial chirp. (b) The green line shows the measured transmission curve of the DA-MZM. The blue lines represents the initial chirp $\Delta\theta$ as a function of the bias voltage of the modulator, which is calculated using Eq. (3.12).

voltage V_{DC}, as shown by the blue lines in Fig. 3.13(b). To avoid double-frequency modulation, the DA-MZM should not be biased in the yellow shaded areas, which restricts the available range of $\Delta\theta$, to the range $20^o < \Delta\theta < 80^o$ and $110^o < \Delta\theta < 160^o$. The rest of the experimental set-up is same as Fig. 3.4.

Figure 3.14 shows the measured microwave phase shifts (markers) versus input optical power for different values of the chirp parameter $\Delta\theta$ (which is changed through the DC bias voltage of the DA-MZM) for the case

where the red-shifted sideband is blocked before the detection. During the measurements, the SOA is operated at a constant injection current of 160 mA. From Fig. 3.14(a), a positive microwave phase shift (slow light) is obtained for $21^o \leq \Delta\theta \leq 67^o$. The maximum phase shift decreases as $\Delta\theta$ increases from 21^o to 67^o. If the DA-MZM is biased at a higher voltage than V_π, a negative microwave phase shift, corresponding to fast light, is achieved. The maximum obtained phase advance decreases as $\Delta\theta$ decreases from 158^o to 112^o. The measured initial chirp dependence of the microwave phase shift thus shows a good qualitative agreement with the numerical simulations in Fig. 3.12. However, at low input optical power levels, e.g. -4 dBm, the microwave phase shift does not monotonously decrease for increasing $\Delta\theta$ and the maximum values of the absolute microwave phase shift are achieved at $\Delta\theta = 44^o$ and $\Delta\theta = 135^o$, respectively. These microwave phase variations at low input optical power will be discussed by a perturbation theory presented later.

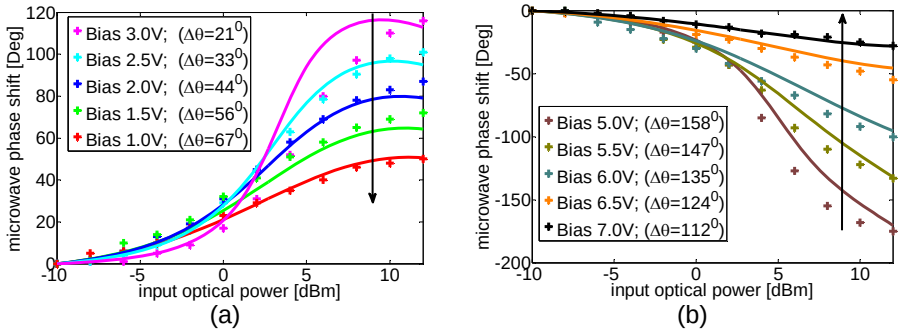

FIGURE 3.14: Measured (markers) and simulated (solid lines) microwave phase shifts as a function of the input optical power for different values of the initial chirp, which is realized by changing the DC bias voltage of the DA-MZM. In all cases the red-shifted sideband is blocked before detection. (a) $21^o \leq \Delta\theta \leq 67^o$ and (b) $112^o \leq \Delta\theta \leq 158^o$. For each of the bias voltages, the reference microwave phase is chosen at the input optical power of -10 dBm.

Figure 3.15 gives the microwave power changes corresponding to Fig. 3.14. Figure 3.15(a) and (b) are measured results. In both cases, (a) $21^o \leq \Delta\theta \leq 67^o$ and (b) $112^o \leq \Delta\theta \leq 158^o$, the magnitude of the microwave power dip decreases as the absolute microwave phase shift decreases. The microwave power dip contributes to the sharp phase change [60]. Figure 3.15(c) and (d) are calculated curves in good agreement with the experimental results. Again, these 5∼10 dB microwave power variations could be a limitation for a real microwave photonic application [63]. For instance, if these microwave phase shifts are utilized in a microwave photonic filter to enable the tunability, the accompanied microwave power variations will reduce the suppression ratio of the filter.

If the blue-shifted sideband is filtered away before detection, the maximum phase advance decreases from 15^o to 4^o when $\Delta\theta$ increases from 21^o to 67^o, and a small phase delay is observed at $\Delta\theta = 67^o$ when the input optical power is around 0 dBm, as shown in Fig. 3.16(a). If $\Delta\theta$ increases further, a larger phase delay is expected. However, this parameter range cannot be accessed in the present experiment due to the strong double-frequency modulation at the required bias voltages, cf. yellow areas in Fig. 3.13(b). On the other hand, when $\Delta\theta$ decreases from 158^o to 124^o, the microwave phase advance increases from 25^o to 35^o, shown in Fig. 3.16(b). These measured phase changes also agree well with the red line in Fig. 3.12.

As for the conventional case shown in Fig. 3.16(c), without optical filtering, a $\sim 17^o$ microwave phase advance is obtained independently of the values of the initial chirp.

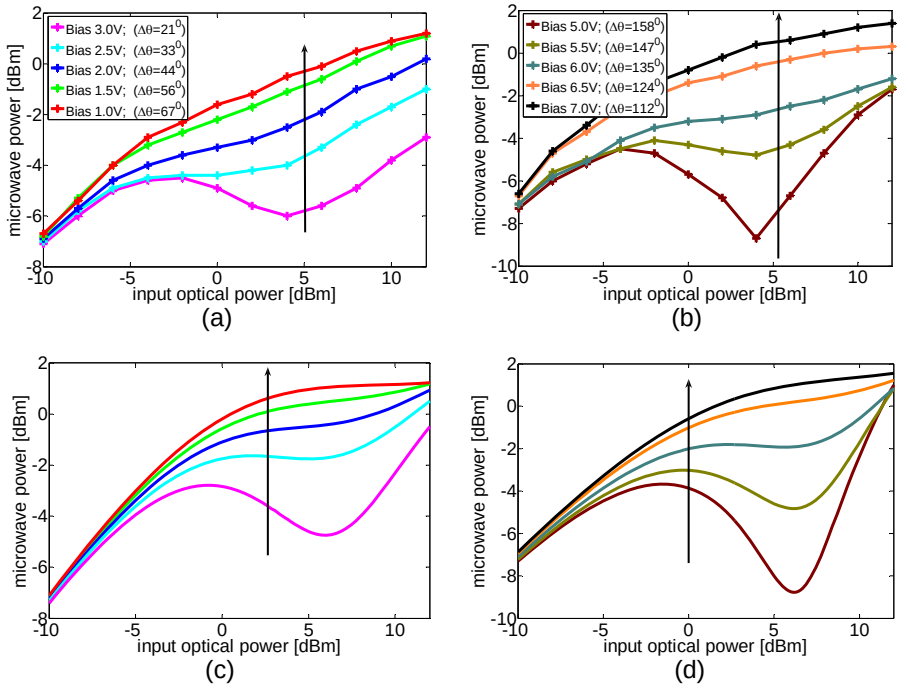

FIGURE 3.15: Measured and simulated microwave power changes as a function of the input optical power for different values of the initial chirp. In all cases the red-shifted sideband is blocked before detection. (a) $21^o \leq \Delta\theta \leq 67^o$ and (b) $112^o \leq \Delta\theta \leq 158^o$. (c) and (d) show the corresponding simulated results for the same values of the chirp parameter.

3.4.3 Perturbation theory and discussion

The results presented above can be qualitatively understood by the use of an approximate analytical perturbation theory in order to elucidate the role of the initial modulation chirp that influences the archived microwave phase shifts. Therefore, we firstly focus on the case with a very short propagation distance in the SOA. After that, we will remove this limitation and discuss the effects of the length of the SOA. Because of the significant enhancements of the microwave phase shift seen when

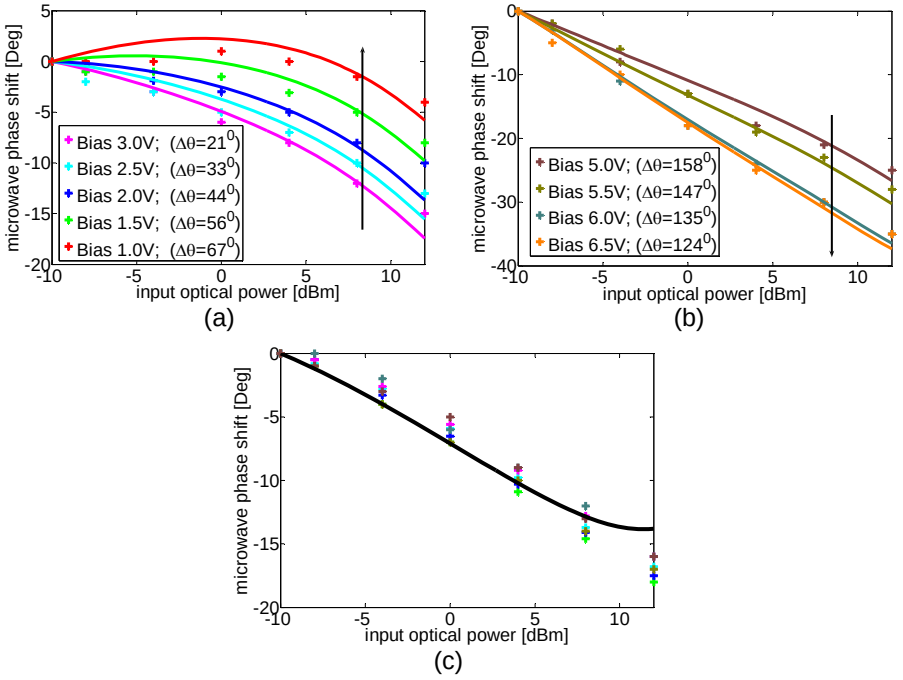

FIGURE 3.16: Measured (markers) and simulated (solid lines) microwave phase shifts as a function of the input optical power for different values of the initial chirp. (a) $21^o \leq \Delta\theta \leq 67^o$ and (b) $112^o \leq \Delta\theta \leq 158^o$ are for the case of blocking the blue-shifted sideband. (c) is the case without optical filtering.

blocking the red-shifted sideband, which is potentially interesting for applications, we will here mainly focus on this case. By taking into account the initial chirp Eq. (3.11) and following the same procedure in section 3.1.2, Eq. (3.3) can be re-written and the output microwave signals from an SOA with a short length δL, P_{RF}, P_{+1} and P_{-1}, can be

approximately derived.

$$\begin{aligned} P_{RF}(\delta L) &= P_{RF}(0) + \Delta P_{RF} \qquad (3.13) \\ &= 2|E_0 E_{+1}|cos(\Delta\theta) \cdot [1 + (g_{sat} - a + \gamma_1)\delta L + i\beta_1 \delta L] \\ P_{+1}(\delta L) &= P_{+1}(0) + \Delta P_{+1} \qquad (3.14) \\ &= |E_0 E_{+1}|cos(\Delta\theta) \cdot \{1 + (g_{sat} - a + \gamma_1 + \alpha\beta_1)\delta L \\ &\quad + i \cdot tan(\Delta\theta) + i[\beta_1 - \alpha\gamma_1 + (g_{sat} - a)tan(\Delta\theta)]\delta L\} \\ P_{-1}(\delta L) &= P_{-1}(0) + \Delta P_{-1} \qquad (3.15) \\ &= |E_0 E_{+1}|cos(\Delta\theta) \cdot \{1 + (g_{sat} - a + \gamma_1 - \alpha\beta_1)\delta L \\ &\quad - i \cdot tan(\Delta\theta) + i[\beta_1 + \alpha\gamma_1 - (g_{sat} - a)tan(\Delta\theta)]\delta L\} \end{aligned}$$

For the conventional case, without optical filtering, from Eq. (3.13), it is easy to see that the final microwave phase shift of P_{RF} does not depend on $\Delta\theta$. For the case when the red-shifted sideband is blocked, we illustrate $P_{+1}(\delta L)$ in the complex plane in Fig. 3.17(a). If the input signal is chirped, we have $\Delta\theta$ different from 0^o. The initial position of $P_{+1}(\delta L)$, illustrated by thick black arrows in Fig. 3.17(a), will then have an angle of $\Delta\theta$ with respect to the real (Re) axis. From Eq. (3.14), the approximate analytical microwave phase shift $\delta\varphi_{+1}(\delta L)$, induced by increasing the input optical power, then becomes,

$$\begin{aligned} \delta\varphi_{+1}(\delta L) &= arg[P_{+1}(\delta L)]_S - arg[P_{+1}(\delta L)]_{S_{ref}} \qquad (3.16) \\ &\simeq arctan\{cos^2(\Delta\theta) \cdot [\beta_1 - \alpha\gamma_1 - (\gamma_1 + \alpha\beta_1) \cdot tan(\Delta\theta)]\delta L\} \end{aligned}$$

For a very short propagation distance in the SOA, Eq. (3.16) demonstrates that the phase shift $\delta\varphi_{+1}(\delta L)$, strongly depends on $\Delta\theta$. Furthermore, from Eq. (3.16), the microwave phase shift will vanish, $\delta\varphi_{+1}(\delta L) =$

0, when $\Delta\theta$ satisfies either of the following conditions.

$$cos(\Delta\theta) = 0 \Rightarrow \Delta\theta = \pm 90^0 \tag{3.17}$$

$$tan(\Delta\theta) = \frac{\beta_1 - \alpha\gamma_1}{\gamma_1 + \alpha\beta_1} \tag{3.18}$$

Eq. (3.17) corresponds to the condition for a purely phase modulated signal, i.e., there is no intensity modulation of the input optical signal. On the other hand, according to Eq. (3.18), the value of the chirp parameter depends on the normalized input optical power, α factor, carrier recovery time, and microwave modulation frequency. Using the parameters in Chapter 2, $\Delta\theta$ will equal to -10^o or 170^o. Both phase delay $\delta\varphi_{+1}(\delta L) > 0$ and phase advance $\delta\varphi_{+1}(\delta L) < 0$ can be obtained for $90^o > \Delta\theta \geq -10^o$ and $170^o \geq \Delta\theta > -90^o$, respectively, as shown in Fig. 3.17(b). Therefore, $P_{+1}(\delta L)$ will always rotate towards the imaginary (Im) axis, as illustrated by the blue dotted arrows in Fig. 3.17(a).

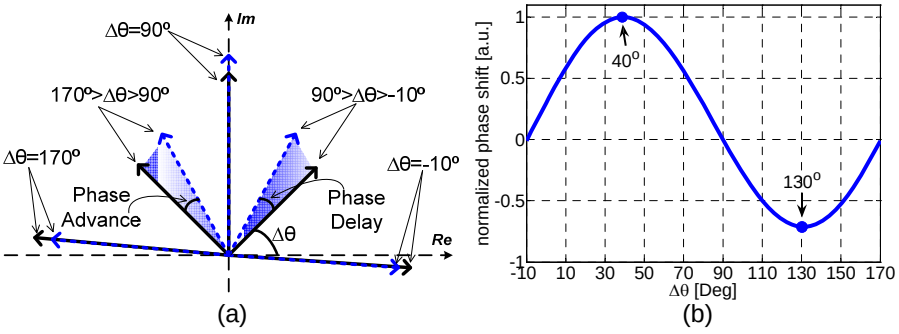

FIGURE 3.17: (a) Representation of $P_{+1}(\delta L)$ in the complex plane for different values of the initial phase difference $\Delta\theta$. The thick black arrows indicate the reference points corresponding to the minimum input optical power. Upon increasing the optical power the arrows rotate towards the dotted blue arrows, which correspond to the maximum input optical power. (b) The normalized phase shift $\delta\varphi_{+1}(\delta L)$ as a function of $\Delta\theta$ (the length of the SOA is $10\mu m$).

Compared with Eq. (3.15), derived for the case where the blue-shifted sideband is blocked, the absolute value of the real part of Eq. (3.14) decreases, rather than increases, as the input optical power increases. This means that a larger phase shift is expected when blocking the red-shifted sideband rather than the blue-shifted sideband before detection. These results are in good agreement with a more extensive model but without taking into account the effects of the generation of the conjugate waves. For this limiting case of a very short length of the SOA, the generation of the conjugate wave can be neglected. The refractive index experienced by the sideband (probe) is modified asymmetrically by the carrier (pump) due to the nonzero linewidth enhancement factor α. Therefore, the blue-shifted sideband will experience a larger group refractive index than the red-shifted sideband.

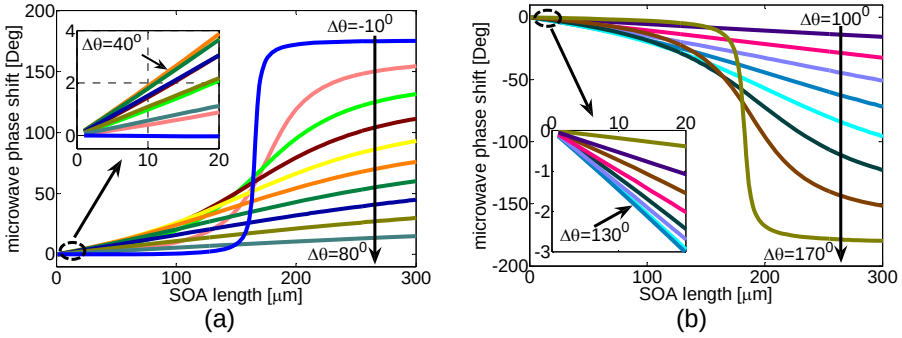

FIGURE 3.18: Calculated microwave phase shifts of P_{+1} induced by increasing S from 0.01 to 1.6 as a function of the SOA length for (a) $-10^o < \Delta\theta < 90^o$ and (b) $90^o < \Delta\theta < 170^o$. (The increment between curves is 10^o)

As the SOA length increases, saturation and propagation effects have to be properly included. We find that the generation of the conjugate wave by the FWM effect will strongly influence the propagation of the probe itself, making a simple analysis unfeasible. Full numerical calculations of

the microwave phase shift of P_{+1} as a function of SOA length are shown in Fig. 3.18. When the SOA is short, as $\Delta\theta$ increases the absolute microwave phase shift firstly increases until reaching a maximum at $\Delta\theta \approx 40^o/130^o$, and then decreases in both the slow-down regime, as shown by the inset in Fig. 3.18(a), and speed-up regime, as shown by the inset in Fig. 3.18(b). These numerical simulations show a good agreement with above perturbation theory in Fig. 3.17(b). If the SOA is long enough, the microwave phase shift of P_{+1} will monotonously decrease from 175^o to -180^o as $\Delta\theta$ increases from -10^o to 170^o.

3.5 Realization of fully tunable microwave photonic notch filters

Up to now, we have experimentally demonstrated that the microwave phase shift induced by slow and fast light effects in SOAs strongly depends on the initial modulation chirp in schemes where optical filtering is used before detection. By using different values of the input modulation chirp, $\sim 120^o$ phase delay as well as $\sim 170^o$ phase advance at 19 GHz has been realized by changing the input optical power. Numerical simulations based on a FWM model show good agreement with the experimental results. Furthermore, a simple perturbative analysis provides good insight into the physical effects at play. This characteristic of the initial chirp dependence provides a possible way to combine 120^o phase delay and 170^o phase advance for achieving a fully tunable 360^o phase shifter at different microwave frequency bands. This is highly desired for applications in microwave photonic filters [10].

One important example of interest is the microwave photonic notch filter, which has potential for broadband wireless access networks and radar

systems. In a typical radar system, the filtering of unwanted signals (noise and clutter) is highly desired and currently performed using a digital notch filter placed after frequency down-conversion to baseband and using analog to digital conversions (ADCs). In order to distinguish the desired small signal from the clutter, high-performance ADCs with 14- to 18-bit resolution are required, which becomes a major bottleneck in system performance. However, such stringent requirements for ADC performance can be alleviated if the clutter can be removed before down-conversion by using tunable analog notch filters such as tunable photonic microwave filters. To satisfy the expected bandwidth demand in the coming years, several millimeter-wave frequency bands, such as 28 GHz and 40 GHz, which can provide transfer rates higher than 2 MHz, have already been allocated for these systems [70].

During the past several decades, many approaches to realize tunable notch filters have been proposed, e.g. liquid crystal spatial light modulator [71], fiber bragg gratings [72] and arrayed waveguide gratings [73]. However, all the above techniques result in a simultaneous undesirable variation of the free spectral range (FSR) while the filters are continuously tuned. For some of radar applications, it is preferable that only the null frequency is tuned while keeping the shape of the spectral response unaltered (a constant FSR). In [74, 75], it has been shown that this desired function can be accomplished by using microwave photonic phase shifters capable of providing a tunable phase shift over the full 360^o range. Recently, several such configurations have been reported. In [76] a tuning range of 50% FSR was realized by three optical attenuators. In [75] stimulated Brillouin scattering was utilized to achieve an entire FSR tuning, but it required a 20 km long fiber. Furthermore, from an application point of view, all aforementioned schemes were performed by bulky devices, which could be also a limitation.

3.5.1 Principle of operation

Based on the discussions in last section, by choosing different values for the initial optical phase difference between the carrier and sidebands, optical filtering enhanced slow light effects in an SOA can provides a possible way to achieve a 360^o microwave phase shifter. Figure 3.19 shows the basic architecture of a tunable 360^o microwave phase shifter. The detailed method of measuring the microwave phase shift is similar to that described before. The microwave intensity modulation is imposed on a CW laser beam using a MZ-modulator. By operating the modulator at the different transmission slopes, V_{DC1} and V_{DC2}, 0^o or 180^o initial optical phase difference between the carrier and sidebands can be obtained.

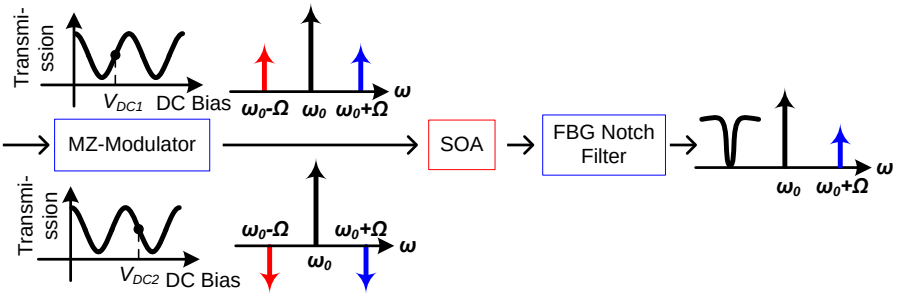

FIGURE 3.19: Schematic of a $\sim 360^o$ microwave photonic phase shifter by utilizing the initial chirp dependence. (ω_0: laser frequency; Ω: microwave modulation frequency; V_{DC1} and V_{DC2}: DC bias voltages of the modulator)

Figure 3.20 illustrates the microwave phase shifts induced by slow and fast light effects achieved by changing the injection current of the SOA for two different operating bias voltages of the modulator. For these two cases, the reference phase is chosen at the injection current of 90 mA, and the input optical power into the SOA is fixed at 9 dBm. The

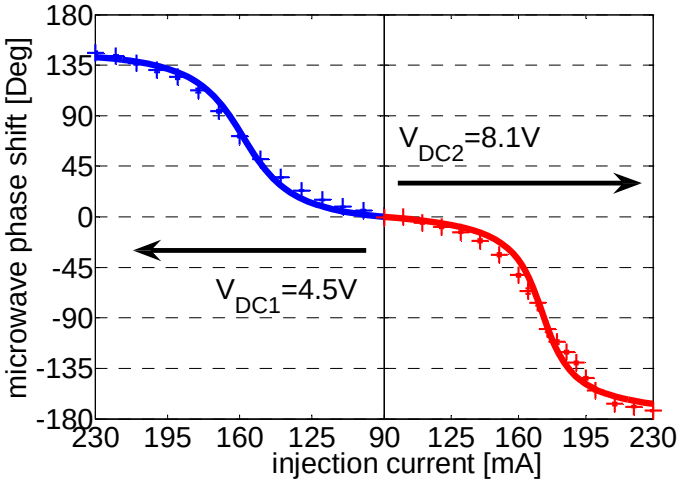

FIGURE 3.20: Microwave phase shifts as a function of injection current of the SOA when the modulator is biased at $V_{DC1} = 4.5V$ (blue curves in the left part) and $V_{DC2} = 8.1V$ (red curves in the right part). The "+" markers show experimental results and the solid lines are numerical simulations. (The modulation frequency is sweeping between 29.75 GHz and 30.25 GHz)

laser wavelength is 1552.7 nm. When the modulator is operated at the positive slope ($V_{DC1} = 4.5V$), about 150^o microwave phase delay at $\sim$30 GHz is achieved, as shown in the left part of Fig. 3.20. On the other hand, about 170^o phase advance, right part of Fig. 3.20, is obtained for the negative slope ($V_{DC2} = 8.1V$). Figure 3.20 also shows that the microwave phase sensitivity is different over the whole tuning range, $\sim 12^o$ phase shift due to a 5 mA current change at the injection current of around 170 mA and $\sim 2^o$ phase shift due to the same current change at around 90 mA or 230 mA. However, later in Chapter 4 we will discuss the possibility of achieving linear microwave phase shift. The solid lines are numerical results and show good agreement with the experimental results.

In Chapter 2, we have already shown that the optical filtering technique can increase the bandwidth of the microwave phase shifter to 100 GHz, which means that this proposed microwave phase shifter can provide $\sim 360^o$ phase shifts at other microwave frequency bands. The lower microwave frequency is limited to several GHz by the bandwidth of the optical FBG notch filter, which is employed to block the red-shifted sideband after the SOA.

3.5.2 Experimental demonstration of a fully tunable microwave notch filter with a FSR of 9.4 MHz

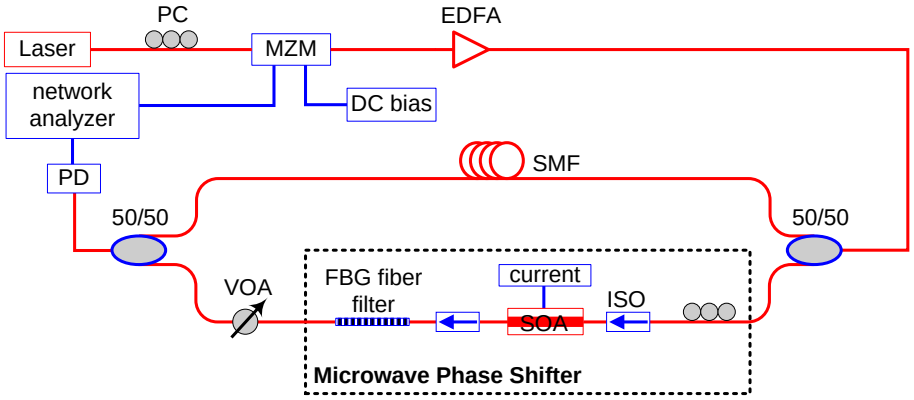

FIGURE 3.21: Experimental set-up of a tunable two-tap microwave photonic notch filter.

Figure 3.21 describes the experimental set-up. The microwave notch filter itself is a simple Mach-Zehnder interferometer composed of two arms, one of which incorporates the slow light based microwave phase shifter, shown in the dotted-line box, which is made up of an SOA followed by an FBG fiber filter. The EDFA is used to adjust the SOA input optical power to 9 dBm, in order to ensure that the SOA operates in the saturation regime. After the microwave phase shifter, a tunable

attenuator provides microwave power balance between the two arms to compensate $\sim$10 dB power change after the SOA. Tuning of the null frequency can be achieved by changing the injection current of the SOA. Through switching between the two operating stages, $V_{DC1} = 4.5V$ and $V_{DC2} = 8.1V$, of the modulator, a $\sim 330^o$ microwave phase shift, which is the sum of an $\sim 150^o$ phase delay and $\sim 170^o$ phase advance, is expected. Note that the switching between the two different operating points of the modulator will not change the spectral shape of the filter.

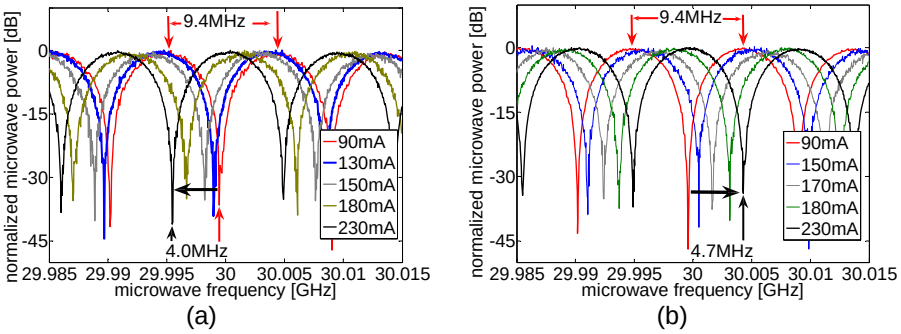

FIGURE 3.22: Tunable power response of the microwave notch filter obtained by changing the injection current of the SOA. (a) $V_{DC1} = 4.5V$ and (b) $V_{DC2} = 8.1V$.

Figure. 3.22 shows the measured filter responses for different injection currents. The FSR is 9.4 MHz, corresponding to 22 m optical fiber length difference between the two arms. The notch rejection is always larger than 30 dB over the entire tuning range. The spectral response at the SOA injection current of 90 mA is chosen as the reference for both operating stages of the MZM. For $V_{DC1} = 4.5V$, as shown in Fig. 3.22 (a), the null frequency experiences a shift of 4.0 MHz towards lower frequencies as the current increases from 90 mA to 230 mA, which corresponds to almost +50% fractional tuning range. Similarly Fig. 3.22(b) shows that if the modulator is operated at the negative slope

$V_{DC2} = 8.1V$, a 4.7 MHz shift in the other direction, corresponding to -50% fractional tuning range, is obtained also by changing the current from 90 mA to 230 mA. Note that the two initial frequency responses at 90 mA in Fig. 3.22(a) and (b) have the same position as well as the same shape.

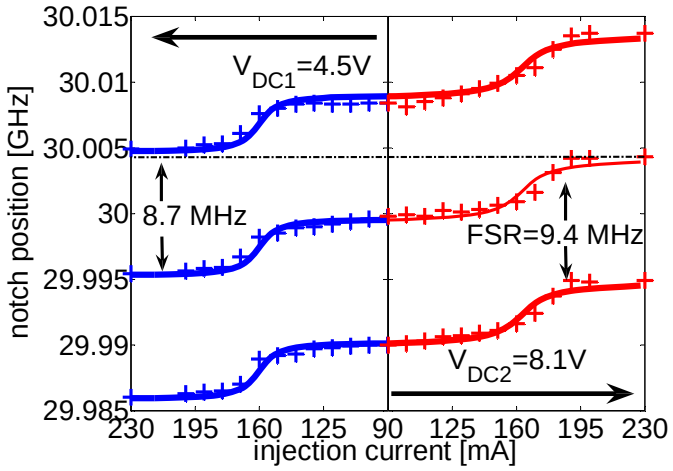

FIGURE 3.23: Measured notch frequency versus the injection current of the SOA, when the modulator is biased at $V_{DC1} = 4.5V$, (the blue curves in the left part) and $V_{DC2} = 8.1V$ (the red curves in the right part). The "+" markers and the solid lines are experimental and numerical results, respectively.

Figure 3.23 demonstrates that through switching between the two operation points of the modulator, the notch positions of the microwave photonic notch filter can be continuously tuned over 8.7 MHz, without changing the spectral shape of the response, by changing the injection current of the SOA. The solid lines are simulation results. Because the microwave phase shifts shown in Fig. 3.20 are measured over a bandwidth of 500 MHz, this almost 100% fractional tuning range will maintain for even larger filter FSRs, which can be achieved by decreasing the time difference between two arms. Notice, however, that for the time

difference on the order of or smaller than the coherence time of the laser, optical interference effects have to be taken into account.

3.6 Summary

In this chapter the refractive index dynamics related to an non-zero linewidth enhancement factor α was investigated. Two different optical filtering schemes were discussed. A theoretical analysis demonstrated that the refractive index dynamics can be exploited using the introduction of an optical notch filter after the SOA and supply an additional enhancement on slow and fast light effects. Especially when the red-shifted sideband is blocked before the detection, the absolute value of the achieved microwave phase shift can be greatly improved from $\sim 15^o$ to $\sim 150^o$, and the operating microwave bandwidth is increased from a few GHz to several tens of GHz as well.

Furthermore, an analytical solution was derived to explain the dependence of optical filtering enhanced slow light on the linewidth enhancement factor α. It showed that the microwave operating frequency of slow light based microwave phase shifters can be greatly increased even larger than 100 GHz by choosing an SOA with α factor on the order of 30. This analytical solution servers as a guide to further engineer SOAs for different application requirements on the frequency bands.

We also demonstrated that when the red-shifted sideband is blocked before the detection, the microwave phase shift induced by slow and fast light effects in SOAs strongly depends on the initial modulation chirp. By choosing different values of the input chirp, both large microwave phase delays and phase advances can be achieved.

Finally, we reported a real application in microwave photonic systems. A fully tunable microwave photonic notch filter was demonstrated. It exploits CPO based slow and fast light effects in SOAs and can realize $\sim$ 100% fractional tuning range at $\sim$30 GHz. The advantages of the proposed scheme are large tuning range, wide choice of frequency bands, low control voltage, and fast reconfiguration in the order of several hundreds of picoseconds. The demonstration shows the potential of slow light effects for the applications in the new generation of Mobile Broadband Systems operating at millimeter-wave frequency ranges.

Chapter 4

Experimental realizations of 360^o microwave phase shifters by cascaded structures

4.1 Introduction

By now, optical filtering enhanced slow and fast light effects in SOAs have been extensively discussed, and the discussion has highlighted the distinct advantages in terms of large microwave operating bandwidth, small size, prospect for integration, operation at room temperature, and low power consumption. One of the exciting motivations is their potential applications in the field of microwave photonics. In particular, 360^o microwave phase shifters can provide flexible tunability, and are thus

needed as key components in many communication circuits and applications based on phased antenna arrays (narrow band applications) and in future reconfigurable radio frequency front-ends [4]. However the large size, high cost and limited dynamic range of ferrite-based phase shifters, that are dominant in antenna arrays, prevent the widespread use of phased-arrays in public communications. Furthermore, the high losses incurred by these technologies directly impact the dynamic range of the RF signals. For a microwave phase shifter, the following parameters are very important: size, absolute magnitude of phase shift, working frequency range, operation voltage, and response time. Since most of the so far favored concepts such as active semiconductor devices and circuits based on $GaAs$ varactors do not fully meet these requirements, especially in the millimeter-wave region. There has been, in recent years, strong research effort focused on microwave phase shifters relying on new technologies.

Nonlinear dielectrics both at room temperatures and under superconductor operation (at $77K$) have been considered [77, 78]. In the first case [77], the preferred candidate are ferroelectric materials such as Barium-Strontium-Titanate which can be employed both in epitaxial thin films or in low-cost ceramic thick films to implement coplanar waveguide phase shifters capable of providing moderate/high tunability (20-38 GHz with only 360^o complete phase shift at 38 GHz), with a very fast response time ($< 1ns$). However, its operation voltages ranges from 20 V for thin film devices and 10 to 100 V for thick film configurations. Superconductor devices [78] produce limited phase shifts (up to 20^o) over a bandwidth of 7-11 GHz and require considerable operation voltage $\sim$200 V. Another interesting alternative is the use of nematic liquid crystals to implement a phase shifter based on a planar inverted-micro strip line [77]. In this case, the anisotropy induced by a control electric

field can provide much higher phase excursions 270^o at 20 GHz with the operation voltage on the order of 30 V. However the response time is on the order of several microseconds. In addition, microwave phase shifters based on Micro-Electro-Mechanical Systems (MEMS) circuits have also been reported and have the potential of being inexpensive, low loss and compatible with integrated circuit technology [79–81]. Two options have been so far suggested. The first one uses MEMS switches to route the signal along one of several possible paths [79] while the second [80, 81] employs MEMS to implement switchable varactors to periodically load a high impedance transmission. The first alternative leads to inherently digital phase shifters with only a finite number of discrete states, and quickly becomes cumbersome with increasing the number of the switched paths. Systems such as phased antenna arrays often require high resolution phase control circuits, which would become large and lossy with these types of phase shifters. The second approach however has yielded particularly impressive results in terms of a 170^o phase shift with a 1.27 dB loss at 40 GHz through a 5.3 mm long device, but its tunability range is limited as well as its response speed ($> 5\mu s$). Also, operating voltages can be considerable (several tens of volts). Implementations based on electronic phase-locked loops can achieve 640^o phase shifts at 40 GHz, but require complex designs and have a limited bandwidth ($\sim$40 MHz) [82].

Since current electrical technologies thus do not meet the desired application requirements, especially in the millimeter-wave bands, it is natural to consider the development of compact, continuously tunable microwave phase shifters by using optical methods as an alternative with additional advantages such as electromagnetic immunity and light weight [63, 83]. Much of work has been reported using different physical schemes, for example, titanium diffused $LiNbO_3$ optical waveguides [84],

wavelength conversion [85], electro-optic modulators [86], and the SOA based slow and fast light effects presented in Chapter 3. In Chapter 3, it was already presented that optical filtering enhanced slow light in SOAs can achieve a $\sim 150^o$ continually tunable microwave phase shift over a bandwidth of $\sim$100 GHz by either optically changing input optical power or electrically changing the injection current. Furthermore, through exploiting the initial chirp dependence, close to 360^o phase shifts were also demonstrated. It however requires switching between two operation stages of the modulator, which is difficult to implement in a real application system.

In this chapter, we will discuss a new scheme that enables the cascadability of the proposed microwave phase shifter, and finally leads to $> 360^o$ phase shifts.

4.2 Cascade two microwave phase shift stages

4.2.1 Basic cascaded configuration

Due to saturation effects, it is not possible to increase the absolute phase shift by increasing the length of the SOA. Furthermore, simply cascading several optical filtering assisted slow light stages can not give more microwave phase shifts either. That is because after the first slow light stage, due to the optical filtering only the optical carrier and blue-shifted sideband survive. Therefore, as already discussed in section 3.1, the optical signal with single sideband at input can not experience significant microwave phase shifts even after passing through the second slow light stage. To enable the cascading of several optical filtering enhanced slow light elements, in order to achieve an accumulated microwave phase shift

of 360^o, we introduce a regenerator between two slow light stages, with the aim of restoring the double sideband characteristic of the optical signal. Therefore, after the regeneration, the optical signal will regain the same optical spectrum as the initial input, cf. the insets (1) and (4) in Fig. 4.1. Hence, by adding the second slow light stage, the modulated optical signal will experience a similar effect as in the first stage.

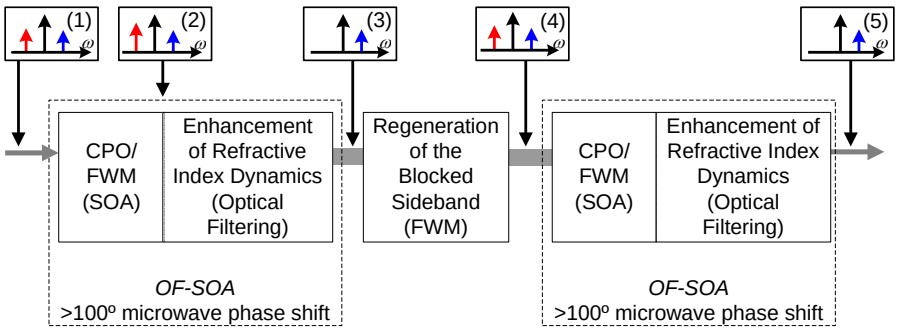

FIGURE 4.1: Configuration to cascade two optical filtering assisted slow light stages.

These optical filtering enhanced slow light effects and cascadability can be illustrated by considering the evolution of the slowly varying complex sideband amplitudes in a polar representation, as shown in Fig. 4.2. The optical phase of the strong carrier is chosen as the reference, as shown by the green arrows. At the input, the electrical fields of both the strong carrier and sidebands can be taken as real (Fig. 4.2(1)). Before optical filtering, the resulting microwave phase shift of the modulated signal has contributions from both sidebands (black shaded area in Fig. 4.2(2)), corresponding to a phase advance of a few tens of degrees at a few GHz. Now, when blocking the red-shifted sideband after the SOA, the cancelation between two sidebands is avoided and the refractive index dynamics, quantified by the linewidth enhancement factor α, contribute a large positive phase shift to the blue-shifted sideband. This phase

shift dominates the total phase shift of the microwave modulation (blue shaded area in Fig. 4.2(3)), thus corresponding to an enhanced slow light. After the red-shifted sideband is regenerated and then blocked again by the second stage, a totally doubled microwave phase shift will be expected at the final output, as Fig. 4.2(5) shows.

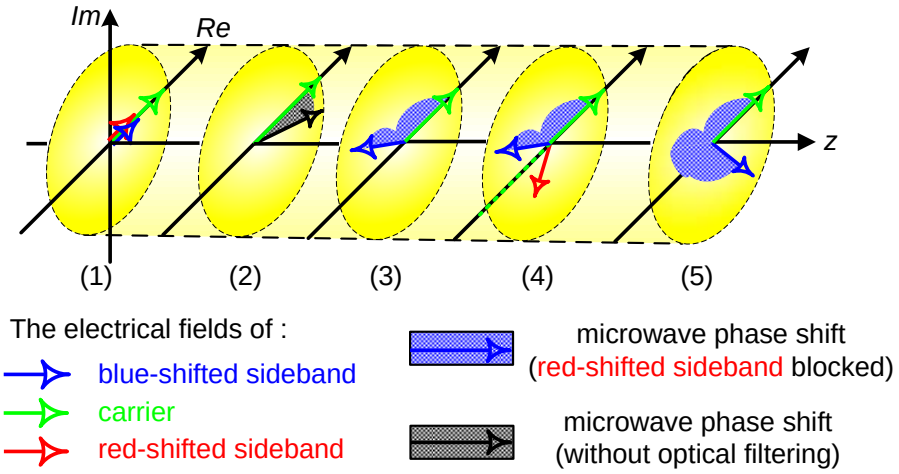

FIGURE 4.2: Illustrations of the evolution of the complex amplitudes of the sidebands in a polar representation.

The regeneration of the red-shifted sideband can be achieved using four-wave mixing effects, where the fast build-up of the conjugate signal at the mirror frequency is a well-known effect that can be achieved with high-efficiency in active semiconductor waveguides. Therefore, both the phase shift and the regeneration can be accomplished using the same technology of active semiconductor waveguides. The performance of the red-shifted sideband regeneration stage by using a SOA can be experimentally verified. After the optical filtering assisted SOA (OF-SOA), another SOA is employed as the regenerator and biased at a fixed current to provide the maximum regeneration efficiency. The experimental results, respectively, before the optical filtering ("+"), after the OF-SOA

("o"), and after the regenerator ("$*$") are presented in Fig. 4.3. Figure 4.3 brings two important points. One is that $\sim 150^o$ microwave phase shift survives even after the regenerator, which makes it possible to cascade several such microwave phase shifters. The slight decrease of the phase shift, $\sim 10^o$, after the regenerator can be explained by fast light effects contributed by the SOA as the regenerator. The other point is the distinct increase of microwave power after the regenerator, as shows in Fig. 4.3(b). We attribute it to the fast build-up of the red-shifted sideband. This $\geq$10 dB microwave power improvement reinforces the regeneration characteristic of the regenerator.

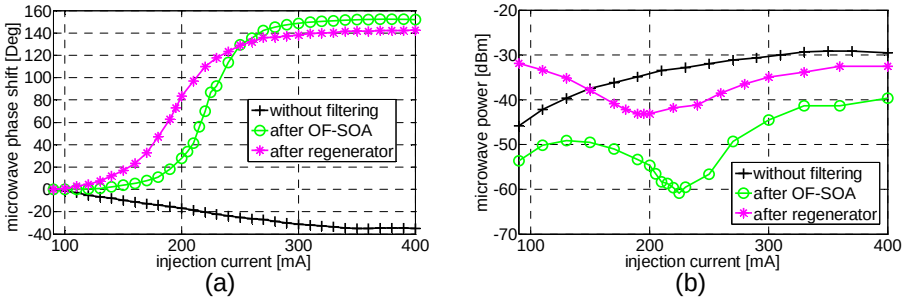

FIGURE 4.3: Experimental demonstrations of the performance of the red-shifted sideband regeneration stage. Measured (a) microwave phase shifts and (b) power changes as a function of the injection current into the OF-SOA before optical filtering, after optical filtering (OF-SOA) and after the regeneration, respectively. The microwave frequency is 40 GHz. The SOA as the regenerator is biased at a constant current to achieve the maximum regeneration efficiency.

4.2.2 Experimental results of cascaded microwave phase shifts

The actual experimental set-up is depicted in Fig. 4.4. The initial modulated signal is nearly chirp free. The power level is boosted, by

an EDFA, up to 10 dBm. The injection current I_1 of SOA-1 can be changed between 10 mA and 230 mA. After the regeneration of the red-shifted sideband by another SOA, which is operated at 180 mA during all the measurements reported here, the second slow light stage, SOA-2 followed by optical filtering is employed to double the microwave phase shift, and also allows the possibility of controlling the microwave power. The injection current I_2 can be tuned from 30 mA to 180 mA. The microwave frequency is 19 GHz.

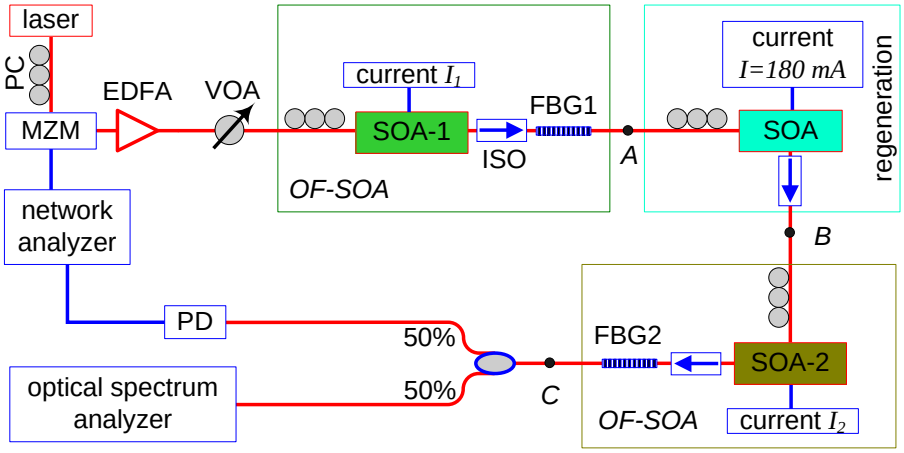

FIGURE 4.4: Experimental set-up to cascade two optical filtering enhanced slow light stages. (OF: Optical spectral Filtering)

Figure 4.5 shows the measured microwave phase shifts and power changes and demonstrates the ability to double the microwave phase shift by cascading two optical filtering assisted SOAs. The reference phase is chosen for $I_1 = 20mA$ and $I_2 = 30mA$. During the measurement, FBG1 is fixed to block the red-shifted sideband, while FBG2 is tuned to block either the red-shifted or the blue-shifted sideband. Firstly, I_1 is fixed at 20 mA. The input optical signal into SOA-2 has a similar optical spectrum because the red-shifted sideband blocked by FBG1 is restored after the

regeneration. For three different FBG2 filtering cases, microwave phase shifts and power changes by changing the injection current of SOA-2, I_2, from 30 mA to 180 mA are shown in the left part of Fig. 4.5. The influence of the optical filter FBG2 agrees well with the results Fig. 3.5 reported in the previous chapter, except that the current dependence of the phase shift, when the red-shifted sideband is blocked, is not as sharp as seen in Fig. 3.5 and the maximum phase delay of $\sim 100^o$ is smaller. We attribute these differences to the chirp of the optical signal acquired by propagation in SOA1 and regenerator prior to injection into SOA-2.

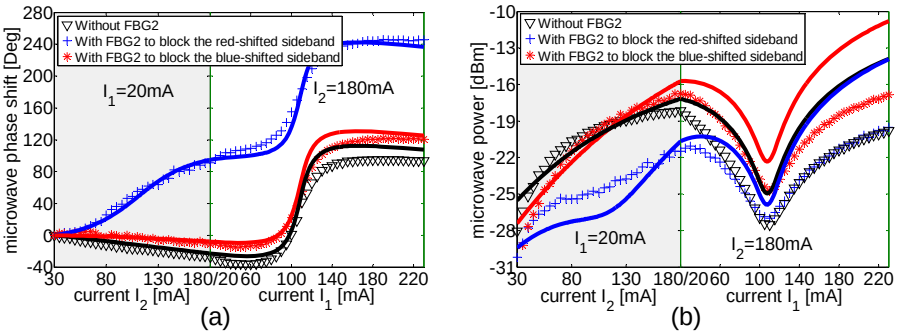

FIGURE 4.5: (a) Microwave phase shifts and (b) microwave powers as a function of the injection currents of SOA-1 and SOA-2. The markers and solid lines are experimental and simulation results, respectively.

Next, I_2 is kept fixed at 180 mA. By increasing I_1 from 20 mA to 230 mA, the input optical signal into SOA-2 experiences a $\sim 150^o$ phase delay induced by SOA-1, which will be added to the phase shift imposed by SOA-2, independently of the filtering action of FBG2, as shown in the right part of Fig. 4.5(a). Figure 4.5(a) shows that when FBG2 is employed to block the red-shifted sideband, the final microwave phase delay is successfully doubled to $\sim 250^o$ by cascading two optical filtering assisted SOAs. The corresponding microwave power changes are presented in Fig. 4.5(b). The $\sim 250^o$ microwave phase shift is accompanied

by a $\sim$12 dB power variation. The power-dip seen in the right part of Fig. 4.5(b) is correlated to the sharp phase change and caused by SOA-1 when blocking the red-shifted sideband using FBG1. The initial chirp induced by SOA-1 and the regenerator will reduce the power dip caused by SOA-2, when the red-shifted sideband is blocked by FBG2, as shown by the blue curves in the left part of Fig. 4.5(b). The solid lines are simulation results. The good agreement with the experimental results confirms our interpretation of the physical mechanisms responsible for the microwave phase shift.

4.2.3 Flexible controls on both microwave phase and power

As an ideal microwave phase shifter, the microwave power is desired to be constant over the whole tuning range of the microwave phase. However, both perviously reported results [84–86] and those presented earlier in this Thesis inevitably induce more than 10 dB microwave power variation, which could hamper their applications. To overcome this drawback, the proposed cascaded structure provides a feasible method to greatly suppress the induced microwave power variation by simultaneously controlling two currents injected into two cascaded slow light stages. Figure 4.6 presents the contours of measured microwave phase shift and power change as a function of the injection currents of SOA-1 and SOA-2. It is important to notice that the contour lines for the microwave phase shift and power change are nearly orthogonal, or at least not parallel, for a large fraction of the parameter space. This implies that by adjusting both currents, I_1 and I_2, the microwave phase and power can, for a large range of parameters, be changed independently. As an example, Fig. 4.7 demonstrates the possibility of achieving a large microwave phase shift and simultaneously maintaining a small power variation by

adjusting both I_1 and I_2 to follow, e.g., the 6 dB power contour line in Fig.4.6. In this case, $(I_1, I_2) = (20mA, 50mA)$ is chosen as the reference point. Figure 4.7 shows a continuously tunable $\sim 240^o$ microwave phase shift at 19 GHz with an power variation of less than 1.6 dB. The power variation could be decreased further by more careful control of I_1 and I_2.

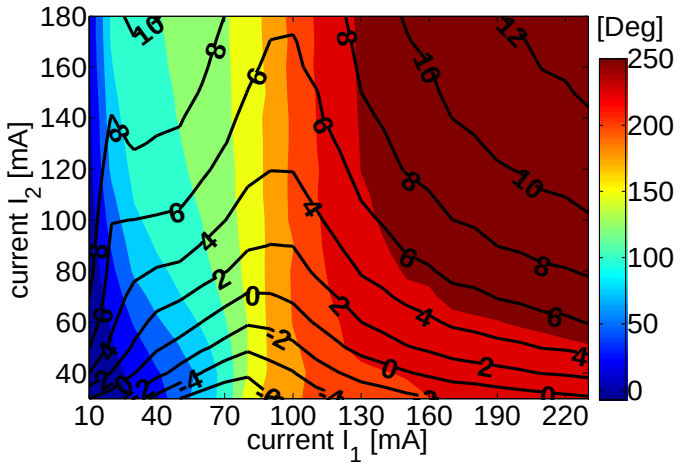

FIGURE 4.6: Contour plots of measured microwave phase shift (in degrees, colour contour) and microwave power change (in dB, black line contour) as a function of the injection currents of SOA-1 and SOA-2. The reference point of zero phase and zero power change is set at $I_1 = 10mA$ and $I_2 = 30mA$.

Therefore, the need to control several currents is similar to the control problem encountered in the case of continuously tunable multi-section laser diodes. By properly choosing the combination of the currents, the flexible controls on both microwave phase and power can be achieved.

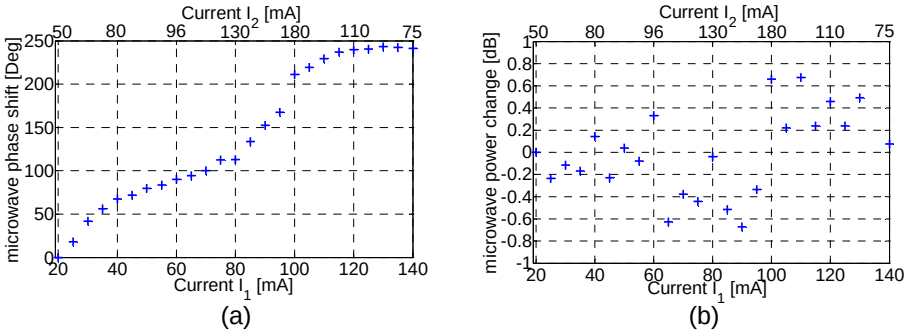

FIGURE 4.7: Measured (a) microwave phase shift and (b) power change when varying the injection currents of SOA-1 (bottom axis) and SOA-2 (top axis) to follow the 6 dB power contour line in Fig. 4.6.

4.3 Cascade three stages for 360^o microwave phase shifters

In this section, the situation will be extended further. In order to achieve an accumulated microwave phase shift of 360^o, a third slow light stage is incorporated, as shown in Fig. 4.8. The six insets depict how the optical spectrum of the signal evolves in the whole structure.

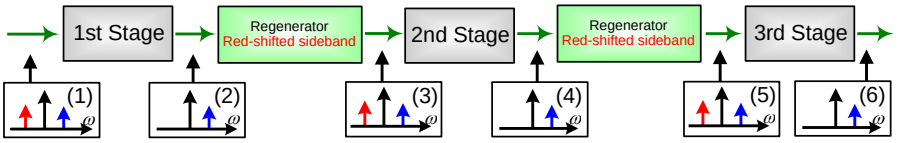

FIGURE 4.8: Configuration of a 360^o microwave phase shifter by cascading three slow light stages.

The contour plots in Fig. 4.9 show the calculated microwave phase shifts when the injection currents (I_1, I_2, I_3) of the three SOAs in three phase shift stages are increased, one by one, from the transparent current 20 mA to the maximum value 300 mA. The two regeneration SOAs are

biased at a fixed current to get the maximum regeneration efficiency. The main simulation parameters are same as what we used in Chapter 3. For the conventional case without optical filtering, as shown in Fig. 4.9(a), the CPO effects in an SOA induce the fast light and thus give a total $\sim -180^o$ microwave phase shift at 5 GHz. When the red-shifted sidebands are blocked by optical filtering within three slow light stages, Figure 4.9(b) demonstrates $> 360^o$ microwave phase shifts at microwave operating frequencies between 6 GHz and 40 GHz. The simulation results are capable of theoretically demonstrating the scalability of the optical filtering enhanced light slow-down and the possibility of achieving a continuously tunable 360^o microwave phase shift over a bandwidth of several tens of GHz, a feature which is difficult to achieve either in conventional microwave phase shifters or in those based on the alternative approaches previously discussed.

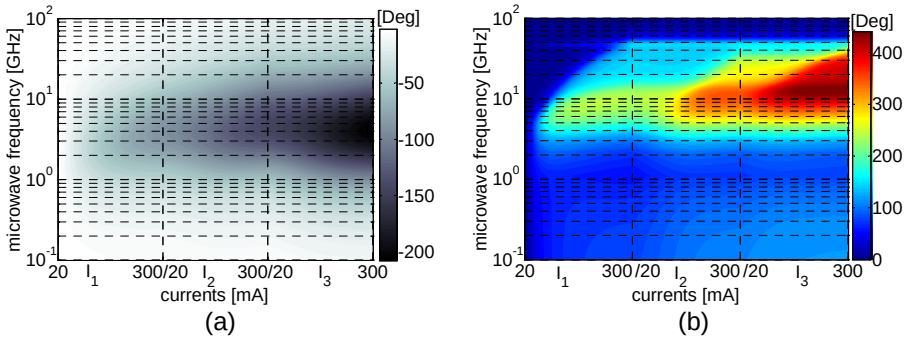

FIGURE 4.9: Calculated microwave phase shift as a function of both microwave frequency and the injection currents of three SOAs. (a) Conventional case without optical filtering, which corresponds to simply cascading five SOAs. (b) Blocking the red-shifted sidebands within each slow light stage.

4.3.1 Experimental realizations at microwave operating frequencies up to 19 GHz

To experimentally verify the achievement of 360^o microwave phase shift by cascading three slow light stages, the experimental set-up in Fig. 4.10 is employed, which is similar to that for two cascaded structures except that one more pair of regenerator and slow light stage is inserted before the detection. The three injection currents of the slow light stages I_1, I_2, and I_3 can be tuned between 20 mA and 210 mA, 40 mA and 190 mA, 40 mA and 190 mA, respectively. The two regenerators of the blocked red-shifted sideband are biased at fixed currents, 180 mA and 470 mA, during the experiment. The microwave phase is measured relative to a reference point of $(I_1, I_2, I_3) = (20mA, 40mA, 40mA)$. The maximum microwave frequency is limited to 19 GHz by the bandwidth of the modulator.

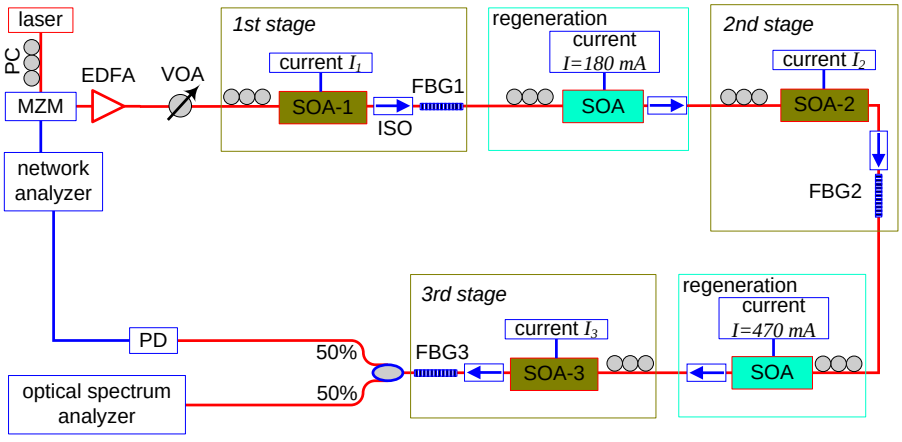

FIGURE 4.10: Experimental set-up to achieve 360^o microwave phase shift by cascading three optical filtering-SOAs.

The microwave modulation frequency is firstly fixed at 19 GHz. Figure 4.11(a) shows measured and calculated microwave phase shifts as

a function of the injection currents of SOA-1, SOA-2, and SOA-3. For comparison with the conventional unfiltered case, the black "Δ" markers give the results when the three FBGs are removed from the set-up. In this case five cascaded SOAs induce a $\sim 90^o$ microwave phase advance by increasing I_1, I_2, and I_3 in sequence, which corresponds to a $\sim 20^o$ microwave phase shift for each SOA and agrees well with previously published results. When the three FBGs are tuned to block the red-shifted sidebands, $\sim 165^o$, $\sim 105^o$, and $\sim 100^o$ phase delays are obtained by increasing I_1, I_2, and I_3, respectively. The total 370^o microwave phase shift at 19 GHz and the good agreement with theoretical results verify the scalability of the proposed scheme. The corresponding microwave power changes are also shown in Fig. 4.11(b).

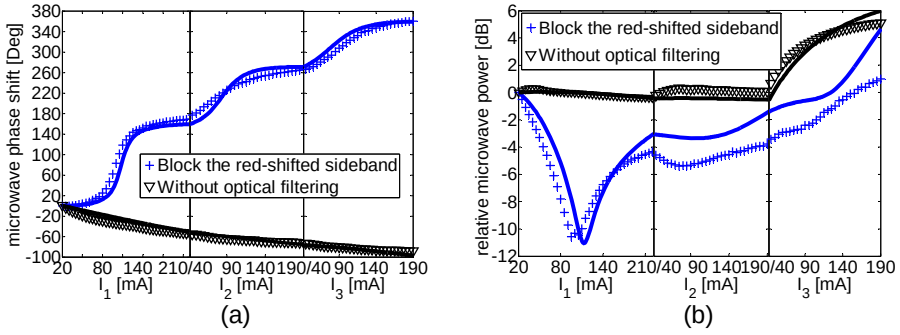

FIGURE 4.11: (a) Microwave phase shifts and (b) relative power changes at a microwave frequency of 19 GHz by cascading three slow light stages. The blue "+" markers correspond to blocking the red-shifted sidebands by three FBGs. The black "Δ" markers correspond to both sidebands being detected (without optical filtering). The experimental results are shown as symbols, and the calculations as solid lines.

Now we have three currents to control. When the current combination (I_1, I_2, I_3) increases from the reference $(20mA, 40mA, 40mA)$ to the maximum $(210mA, 190mA, 190mA)$, the microwave phase of the optical

signal will shift from 0^o to $\sim 360^o$. This situation can be considered as two points in the 3-dimension space. In principle, there are infinite ways to connect these two points. As already discussed in section 4.2.3, this infinity also enables the flexible controls on the microwave phase and power. One of the most interesting examples is a linear microwave phase shift. Figure 4.12(a) demonstrates a possibility of achieving a linear microwave phase shift, up to $\sim 360^o$, as a function of I_1 by properly choosing (I_2, I_3). Therefore, from Fig. 4.7 and 4.12, it is concluded that both nearly linear phase shifts and suppressing microwave power variation can probably be achieved by optimizing the current combination (I_1, I_2, I_3).

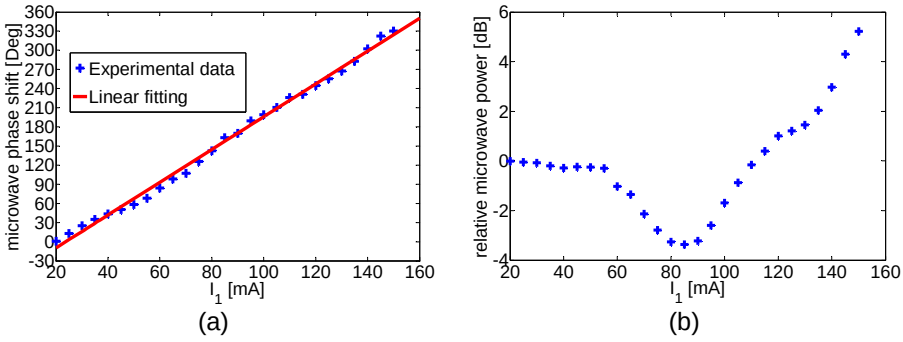

FIGURE 4.12: (a) A linear microwave phase shift by combining injection currents of three cascaded slow light stages. (b) The corresponding microwave power change. The microwave frequency is 19 GHz.

We have also investigated the modulation frequency dependence, and the results are plotted in Fig. 4.13. For the conventional case, without optical filtering, the maximum microwave phase shift decreases as the modulation frequency increases, as shown by the lines below the reference. However, when the red-shifted sidebands are blocked by the FBGs, through increasing the injection currents I_1, I_2, and I_3 one by one,

$> 360^o$ phase delay, above the reference line in Fig. 4.13, is obtained in the entire frequency range from 9 GHz to 19 GHz. Furthermore, based on the theoretical simulations in Fig. 4.9, these 360^o microwave phase shifts can be expected for even higher microwave frequencies.

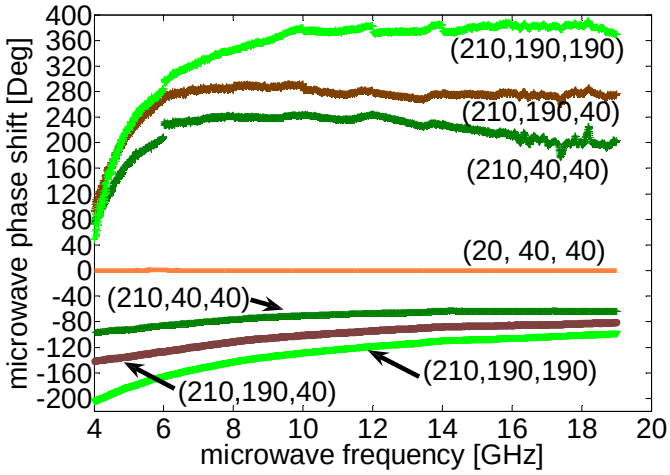

FIGURE 4.13: Measured microwave phase shift as a function of the microwave modulation frequency when (I_1, I_2, I_3) increases from $(20mA, 40mA, 40mA)$ to $(210mA, 190mA, 190mA)$ in sequence. The individual curves are labeled by the combination of currents (I_1, I_2, I_3) used for the measurements. The reference phase is set at $(20mA, 40mA, 40mA)$. The curves above the reference correspond to the red-shifted sidebands being blocked by the FBGs. The curves below the reference are both sidebands detected (without optical filtering).

4.3.2 Experimental realizations at microwave operation frequencies up to 40 GHz

There are additional issues involved in experimentally shifting the microwave operation frequency to higher frequency band. Firstly, the modulator must be able to operate at the higher microwave frequencies, such

as 40 GHz. Secondly, the linewidth enhancement factor of the SOA has to be large enough to expand the operation frequency up to 40 GHz. Thirdly, the removed red-shifted sideband should be effectively regenerated by the regenerators. The first two issues are easily resolved by, respectively, using a different modulator with a bandwidth of 50 GHz (from Valencia) and three similar SOAs for nonlinear applications (from CIP). For the regenerator stage, as the microwave frequency increases, the regeneration efficiency will decrease. Furthermore, the Amplified Spontaneous Emission (ASE) could significantly reduce the carrier population, which in turn weakens the regeneration efficiency. To avoid this situation, three bandpass optical filters are included after each SOAs within the three phase shift stages in the experimental set-up shown in Fig. 4.10.

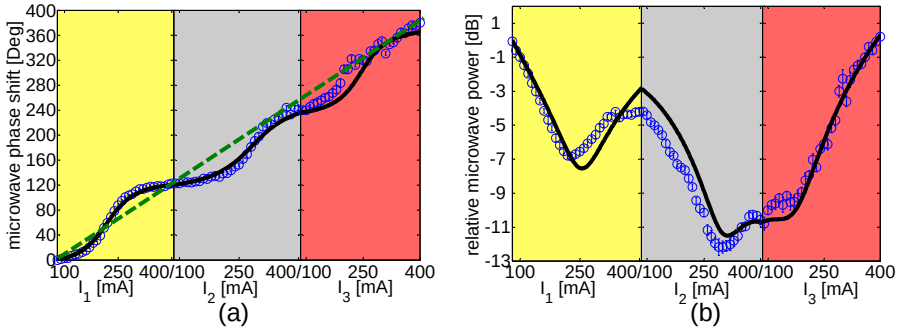

FIGURE 4.14: (a) Microwave phase shift and (b) power changes at the microwave frequency of 40 GHz. The injection currents (I_1, I_2, I_3) are increased from 80 mA to 400 mA consecutively. The markers are experimental data and the black solid lines are numerical simulations. The green dashed line shows a linear fit.

Figure 4.14 gives measured microwave phase shifts and power changes at a microwave frequency of 40 GHz. Similar simulations as those in Fig. 4.11 are also plotted. All these results confirm the achievement of

360^o microwave phase shifts at 40 GHz by cascading three optical filtering enhanced slow light stages. Figure 4.15 shows measured microwave frequency dependence from 20 GHz to 40 GHz. Combined with that from 9 GHz to 19 GHz in Fig. 4.13, it verifies the theoretical prediction shown in Fig. 4.9.

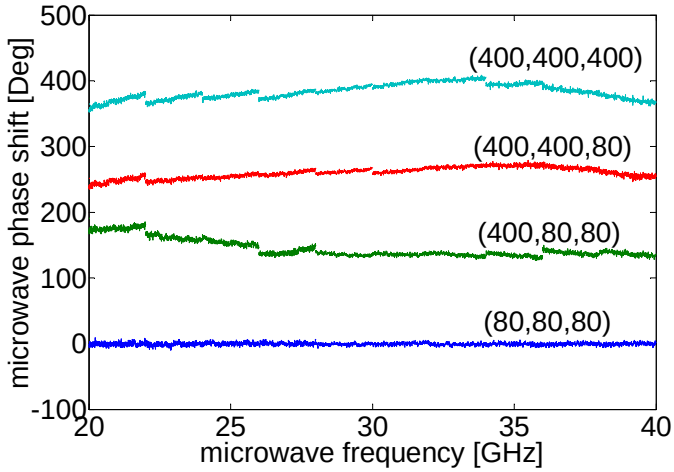

FIGURE 4.15: Measured microwave frequency dependence of phase shifter from 20 GHz to 40 GHz. The injection currents (I_1, I_2, I_3) are consecutively increased from 80 mA to 400 mA.

4.3.3 Fully tunable microwave notch filter with a FSR of ~300 MHz

Based on an cascaded structure, we already reported that a 360^o microwave phase shifter over a bandwidth of ~40 GHz can be achieved by solely slow light effects in SOAs. Compared with 360^o phase shifts achieved by exploiting the initial chirp dependence in Chapter 3, this is simpler and more practical for applications. In section 3.5, a preliminary microwave notch filer is reported. However as already mentioned,

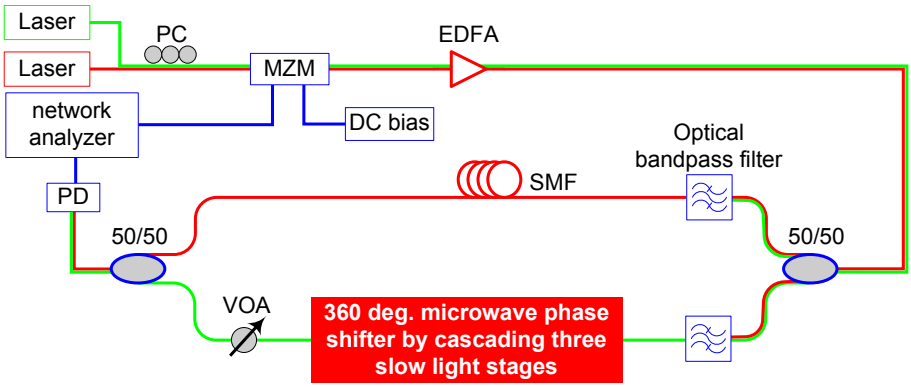

FIGURE 4.16: Experimental set-up of a tunable two-tap microwave photonic notch filter with a FSR of 300 MHz.

its main limitation is the requirement of changing the operation voltage of the modulator. Here, we utilize the reported 360^o microwave phase shift by cascading three slow light stages to re-perform the implementation of a tunable microwave photonic notch filter. Another improvement is, in order to demonstrate 100% fractional tuning range for even larger filter FSRs, for instance 300 MHz, the propagation time difference between two arms is provided by two different laser wavelengthes, as shown in Fig. 4.16.

The measured microwave power response is presented in Fig. 4.17. A tuning range coving a whole FSR of 300 MHz is realized by changing three injection currents (I_1, I_2, I_3) increases from $(80mA, 80mA, 80mA)$ to $(400mA, 400mA, 400mA)$. It should be noted that at some current combinations, the response is a little bit noisy and the notch suppression is just 10 dB. We however believe that these performances could be improved by optimizing the current combination and carefully balancing the microwave powers of two arms.

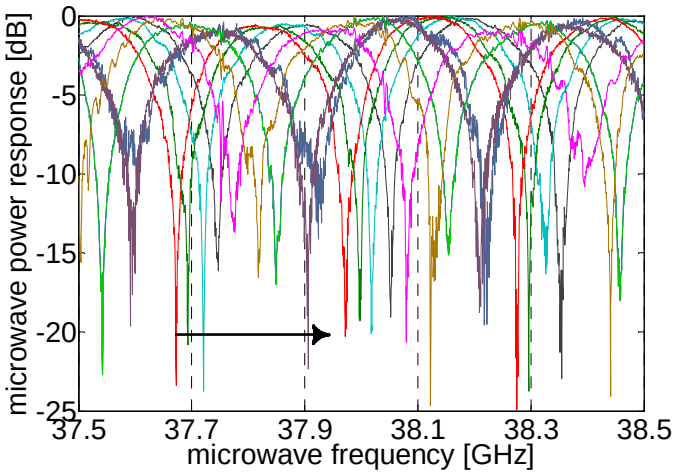

FIGURE 4.17: Tunable power response of the microwave notch filter obtained by changing injection currents of three cascaded slow light stages.

4.4 Summary

In this chapter, we have proposed a new configuration and, to the best of our knowledge, experimentally demonstrated, for the first time, the realization of a tunable 360^o microwave photonic phase shifter based on slow light effects in semiconductor waveguides. A $> 360^o$ phase shift has been achieved over a broad frequency range up to 40 GHz, and further improvement of the bandwidth is feasible. The demonstration is based on the cascading of several semiconductor optical amplifiers, with in-between stages of optical filtering and regeneration. The microwave phase shift and regeneration are realized using coherent population oscillations and four-wave mixing in SOAs. The proposed phase shifter can be reconfigured on a sub-nanosecond time-scale and the operation voltage is on the order of 1 volt. Finally, the suggested approach allows

large flexibility in tailoring the linearity and frequency response of the system.

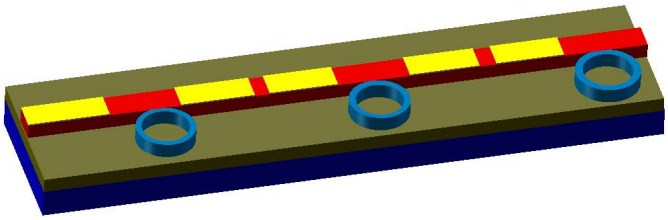

FIGURE 4.18: Sketch of a possible monolithic implementation of a microwave photonic phase shifter with micro-rings to realize optical filtering.

Furthermore, if the optical filtering is realized monolithically, e.g. by micro-ring structures, surface gratings or Bragg filters, this scheme allows a fully integrated device. An important issue in such a design is to avoid feedback effects from the integrated filters, which could lead to undesirable lasing effects. Figure 4.18 shows a schematic of a possible implementation of such a monolithically integrated microwave photonic phase shifter.

Chapter 5

Noise investigation

5.1 Motivation and introduction

In the last chapter, we discussed the realization of a 360^o microwave phase shifter by cascading several optical filtering enhanced slow light devices. Furthermore, their capability to be operated even at 100 GHz was investigated theoretically. All these properties make them promising for microwave photonic applications. However, for most applications, slow light based devices have to meet stringent requirements in order not to degrade the system performance [87], especially regarding the spectral purity of the microwave signal [51–53, 88]. In particular, active devices, such as SOA based slow light devices discussed in this thesis, inevitably add noise and may distort the signal. In [89–91], the signal to noise ratio (SNR), the spurious free dynamic range and harmonic distortion were investigated for SOA based phase shifters and it was reported that slow light effects inevitably degrade the SNR [89]. However, in the microwave community, the single sideband (SSB) phase noise is one of

the most important parameters for describing the spectral purity of the microwave signal. In this chapter, we will mainly discuss the SSB phase noise property of the proposed slow light based microwave phase shifter.

An ideal microwave signal at a frequency of Ω is a single line in the frequency spectrum, as illustrated by the green curve in Fig. 5.1, and can be described as $V(t) = V_0 \cdot e^{i\Omega t}$. Here V_0 is the electrical amplitude of the microwave signal. But such perfect spectral purity is not achievable in a practical situation, as shown by the red curve in Fig. 5.1. The spreading of the spectra line caused by any effect in the system must be investigated carefully. A realistic microwave signal can be expressed,

$$V(t) = [V_0 + \Delta V(t)] \cdot e^{i\Omega t + i\Delta\phi_e(t)} \tag{5.1}$$

where $\Delta V(t)$ and $\Delta\phi_e(t)$ are the amplitude and phase noise, respectively. Compared with the phase noise, the amplitude noise is negligible, $\Delta V(t) \approx 0$, because in most commercial synthesizers the amplitude noise can be strongly reduced, if needed, using automatic level control systems or simple amplitude limiting amplifiers [92]. The phase term, $\Delta\phi_e(t)$, represents random phase fluctuations and is commonly denoted as phase noise.

One of the most common descriptions of phase noise is the one sided spectral density of phase fluctuations per unit bandwidth, called SSB phase noise and referred to as the spectral density, and describes the energy distribution as a continuous function, expressed in units of energy per Hz bandwidth [92]. SSB phase noise $P_{ssb}(f)$ is typically specified in dBm/Hz at a given frequency offset f from the carrier Ω, as the black shaded area illustrated in Fig. 5.1. It can also be expressed in dBc/Hz relative to the carrier power $P_{carrier}(\Omega)$, $L(f) = \frac{P_{ssb}(f)}{P_{carrier}(\Omega)}$.

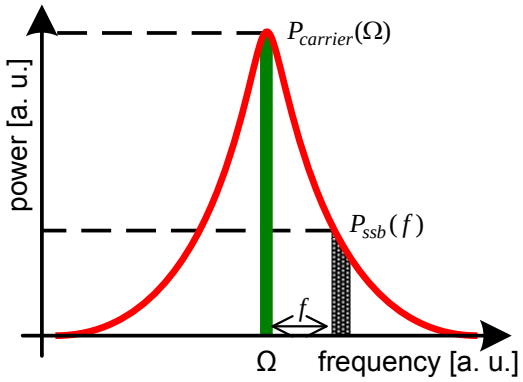

FIGURE 5.1: Example of the single sideband phase noise of a signal at a microwave frequency of Ω. The green line shows a perfect microwave signal without any noise. The red curve illustrates a practical microwave signal.

Furthermore, in the field of microwave photonic systems, one of the major noise sources that degrade the performance of a photonic link is the intensity noise of the optical source [93, 94]. The intensity noise is normally measured by detecting the intensity (or power) with a fast PD and evaluating the noise spectrum with an electronic spectrum analyzer. Therefore, the intensity noise is measured in the same units, dBm/Hz, as that of the SSB phase noise. Normally, intensity noise is quantified as Relative Intensity Noise (RIN) in dB/Hz, i.e. as noise power divided by the average optical power. We will start by discussing the relation between the intensity noise of an optical source and the SSB phase noise of an microwave source for an optically generated microwave signal.

5.2 Intensity noise and SSB phase noise of an optically generated microwave signal

The input optical microwave signal is generated by an external modulator, as depicted in Fig. 5.2.

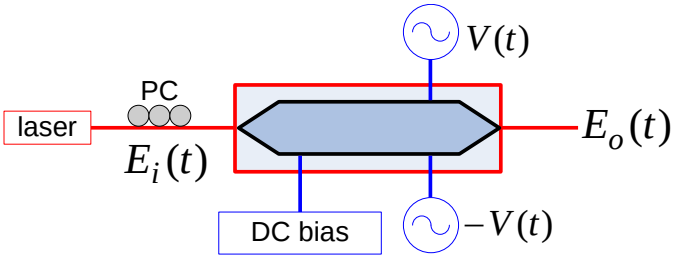

FIGURE 5.2: Set-up to optically generate the input microwave signal. Example of a MZ-modulator is shown, which is biased by a DC voltage and operated in the push-pull configuration to provide chirp free modulation.

By including the intensity noise RIN, the laser output, $E_i(t)$, can be expressed,

$$E_i(t) = [A_0 + \Delta A(t)] \cdot e^{i\omega t + i\Delta\phi_o(t)} \tag{5.2}$$

Here A_0 is the average electrical field amplitude, $\Delta A(t)$ is the amplitude noise related to the RIN of the laser source, ω is the optical frequency, and $\Delta\phi_o(t)$ is the phase noise of the laser. The MZ-intensity modulator is operated in the push-pull configuration in order to provide chirp-free modulation. The electrical microwave modulation signal is described by Eq. (5.1). Assuming small-signal modulation and neglecting higher-order optical sidebands, the electrical field, $E_o(t)$, after the MZ-intensity

modulator can be expressed,

$$\begin{aligned} E_o(t) \approx & \frac{\sqrt{2}}{2}[A_o + \Delta A(t)] \cdot J_0(\gamma) \cdot e^{i\omega t + i\Delta\phi_o(t)} \\ & -\frac{\sqrt{2}}{2}[A_o + \Delta A(t)] \cdot J_1(\gamma) \cdot e^{i(\omega+\Omega)t + i\Delta\phi_e(t) + i\Delta\phi_o(t)} \\ & -\frac{\sqrt{2}}{2}[A_o + \Delta A(t)] \cdot J_1(\gamma) \cdot e^{i(\omega-\Omega)t - i\Delta\phi_e(t) + i\Delta\phi_o(t)} \end{aligned} \quad (5.3)$$

Here, $\gamma = \frac{\pi}{2} \cdot \frac{V_0}{V_\pi}$ is the modulation index, V_π is the half-wave voltage of the modulator, and J_0 and J_1 are Bessel functions of the first kind. From Eq. (5.3), the optical intensity is,

$$\begin{aligned} P_o(t) = & \frac{1}{2}[A_o + \Delta A(t)]^2 \cdot [J_0^2(\gamma) + 2J_1^2(\gamma)] \\ & +2[A_o + \Delta A(t)]^2 \cdot J_o(\gamma)J_1(\gamma) \cdot cos(\Omega t + \Delta\phi_e) \end{aligned} \quad (5.4)$$

Then, the average optical intensity is,

$$\overline{P_o(t)} = \frac{1}{2}A_0^2 \cdot [J_0^2(\gamma) + 2J_1^2(\gamma)] \quad (5.5)$$

and the intensity fluctuation term is,

$$\begin{aligned} \Delta P(t) = & \frac{1}{2}[2A_0\Delta A + \Delta A^2] \cdot [J_0^2(\gamma) + 2J_1^2(\gamma)] \\ & +2[A_o + \Delta A(t)]^2 \cdot J_o(\gamma)J_1(\gamma) \cdot cos(\Omega t + \Delta\phi_e) \end{aligned}$$

The first term in $\Delta P(t)$ originates from the intensity noise of the laser. The second term describes the contribution from the electrical microwave signal and is negligible compared with the first one. From Eq. (5.4), the generated microwave signal after the PD can be expressed as,

$$V_{RF} = 2\Re \cdot [A_0 + \Delta A(t)]^2 \cdot J_0(\gamma)J_1(\gamma) \cdot cos(\Omega t + \Delta\phi_e) \quad (5.6)$$

where $\Re$ is the responsivity of the PD. Eq. (5.6) demonstrates that:

1. The optical phase noise $\Delta\phi_o(t)$ of the laser completely drops out because of the correlation between the carrier and the sidebands, as explained in [52].

2. The phase noise of the detected microwave signal is completely determined by the electrical source.

3. The intensity noise (RIN) of the optical source is converted into amplitude noise of the optically generated microwave signal. Therefore, when the noise spectrum of the optically generated microwave signal is discussed, both intensity noise from the optical domain and phase noise from the microwave domain contribute to the total noise spectrum. Furthermore, it is important to clarify which noise source is dominant when investigating the noise property of an optically generated microwave signal or specific device in a microwave photonic system.

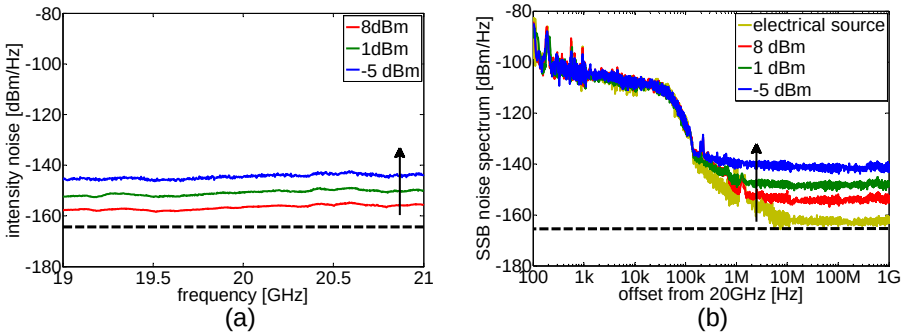

FIGURE 5.3: (a) Intensity noise without microwave modulation and (b) SSB phase noise spectra for microwave frequency of 20 GHz. The signals are measured at the output of the EDFA for several different input power into the EDFA from -5 dBm to 8 dBm. The original microwave synthesizer is also shown in (b) as a reference.

To experimentally investigate whether the main of the noise originates from the intensity noise of the optical source or phase noise of the microwave source, an EDFA is employed after the modulator. When the input optical signal into the EDFA is relatively weak, the EDFA will introduce substantial intensity noise [95], which provides a way to achieve an optical signal source with variable intensity noise. Figure 5.3(a) shows that the intensity noise after the EDFA can be changed around 15 dB by varying the input optical power into the EDFA. To avoid any effect of the PD (which is especially important for noise measurements), during the measurements, a fixed optical power level of 3 dBm at the PD is maintained through a tunable attenuator. Figure 5.3(b) shows the measured SSB noise spectra of the detected microwave signal after the EDFA when the laser is modulated at a microwave frequency of 20 GHz. The electrical spectrum analyzer has a noise floor of -164 dBm/Hz. Based on Eq. (5.6), both the intensity noise, $\Delta A(t)$, of the optical source and the phase noise, $\Delta\phi_e$, of the electrical source contribute to the SSB noise spectrum. In Fig. 5.3(b), the SSB noise spectrum of the original microwave source is also shown as a reference. By comparing it with the intensity noise shown in Fig. 5.3(a), the phase noise, $\Delta\phi_e(t)$, from the electrical source completely dominates for frequency offsets $<$500 kHz. Hence, the SSB noise spectrum of the optically generated microwave signal is exactly same as the electrical reference. However, for frequency offsets $>$500 kHz, the intensity noise is larger than the phase noise of the electrical source. Therefore, the SSB spectrum of the generated optical signal will be determined by and follow the level of the intensity noise. For this regime, the main noise of the optically generated microwave signal can be attributed to the intensity noise from the optical domain. Consequently, if one calculates the total noise power of the generated optical signal by taking an integral of the SSB noise spectrum over a

bandwidth of interests, for instance 1 GHz here, the total noise power will mainly originate from the optical intensity noise.

5.3 Noise properties of slow light based microwave phase shifters

In order to investigate the noise properties of slow light based microwave phase shifters, the experimental set-up shown in Fig. 5.4 is used. The previously discussed optical signal is injected into the slow light devices as the initial optical input. The modulator is operating in the chirp-free configuration. Similar measurements are performed at three different positions, ❶ after SOA-1, ❷ after the optical filter and ❸ after the regenerator, of the microwave phase shifter to investigate how the quality of the microwave signal evolves. By comparing the noise measurements at these different positions with that at the initial input, we are able to quantify how the slow light device and regenerator influence the signal quality.

5.3.1 Electrical spectra of slow light based microwave phase shifters

Firstly, the microwave frequency from the network analyzer is set at the maximum 40 GHz. The measured phase shifting performance and the electrical microwave power of the microwave phase shifter are re-plotted from Fig. 4.2. To investigate the noise properties, Figure 5.5(b) further shows the noise power (the power level at 1 GHz offset from the microwave carrier frequency) for each case. The following four conclusions can be drawn:

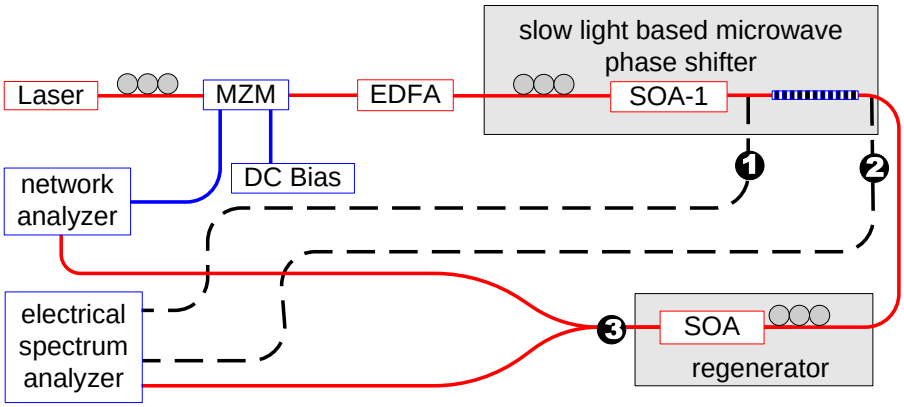

FIGURE 5.4: Experimental set-up to measure electrical frequency spectra after a slow light based microwave phase shifter.

1. The SOAs, either inside the slow light stage or the regenerator, always decrease the microwave signal power comparing with the initial input. This is partly because the SOAs are operated in the deep saturation regime [96] and partly because of the insertion loss related to all employed devices.

2. a $\sim$20 dB microwave power drop accompanies the phase shift enhancement by optical filtering.

3. The regenerator not only restores the red-shifted sideband, but also boosts the microwave signal power.

4. During the propagation in the proposed slow light based microwave phase shifter, there is no visible or measurable increase of the noise compared with the input noise level.

The main conclusion in this section is that although the slow light based microwave phase shifter does decrease the signal power, they do not cause any noise increase, at least under our experimental conditions.

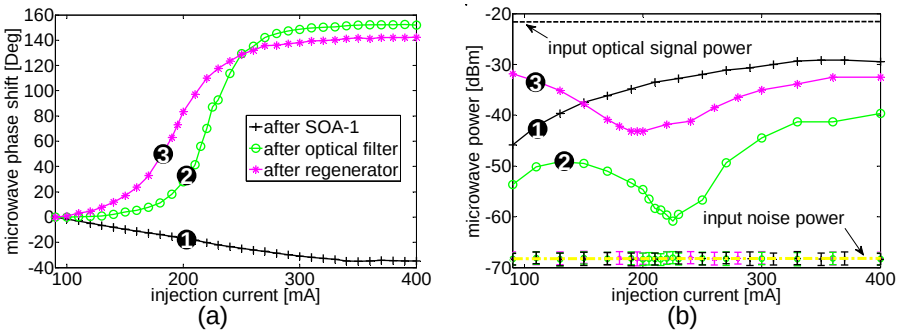

FIGURE 5.5: Measured evolution of (a) microwave phase shift and (b) electrical microwave power at three positions of the set-up as the injection current of SOA-1 is increased: ❶ at the output of SOA-1, ❷ at the output of the optical filter and ❸ at the output of the regenerator. The symbols with error bars show the noise powers for each case. The black and yellow dashed lines refer to the microwave signal and noise power at the input of SOA-1, respectively.

5.3.2 Intensity noise spectra of slow light based microwave phase shifters

To better understand the measurements and conclusion presented in the previous section, a more detailed noise measurement can be performed to clarify which noise source dominates. Here a lightwave component analyzer is used instead of the electrical spectrum analyzer shown in Fig. 5.4 to measure the intensity noise and SSB noise spectrum. Due to the bandwidth limitation of the lightwave component analyzer, the electrical microwave frequency is changed to 20 GHz. As already discussed in section 5.2, intensity noise at input is a main noise contribution at a frequency offset larger that 500 kHz. Therefore, it is natural to start with discussion the effect of the SOAs on the intensity noise. In [53, 97], it has already been demonstrated that an SOA can be used to suppress the intensity noise of the laser. This property can be easily understood

through the optical modulation response of an SOA [97–99]. For the concerned case in this thesis, where SOAs are working in the deep saturation regime, Figure 5.6 shows an example of a measured optical modulation response at different injection currents. For a small signal modulation and by using the expression of optical modulation power P_{RF} in Eq. (2.7), the optical modulation response of an SOA can be defined as the ratio of the output optical modulation power $P_{RF}(output)$ to the input optical modulation power $P_{RF}(input)$. This definition enables the theoretical calculation by using the model presented in Chapter 2. The simulation results are also plotted by solid lines. Note that all the results are normalized to a reference response measurement without the SOA.

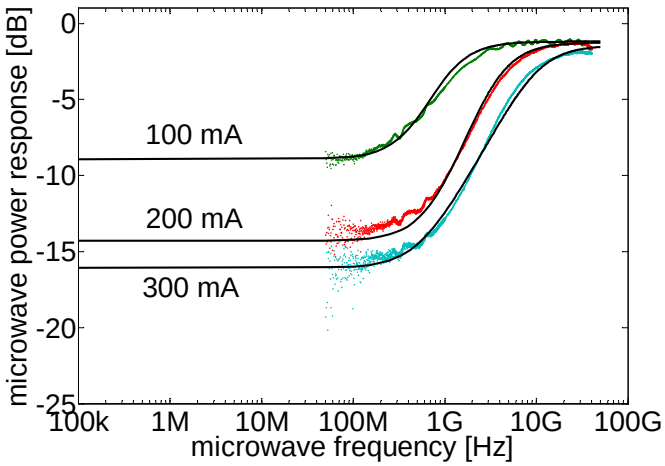

FIGURE 5.6: A typical optical modulation response of an SOA under deep saturation operation. The dotted colored lines are experimental measurements. The solid black lines are theoretical calculations.

As Fig. 5.6 shows, at high microwave frequencies, such as 20 GHz, because the SOA can not follow the optical power variation at the input, the response is flat and is proportional to the CW power gain. The response at 20 GHz is ∼-2 dB, which means that the output microwave power is 2 dB less than the input microwave power and can be attributed

to the deep saturation operation and insertion loss [96]. Along with the decrease of the modulation frequency, SOAs can response the optical power variation, and hence the response sharply decreases, which can be explained by the dependence of gain on the input optical power [100]. Furthermore, this reaction is enhanced as the injection current increases. The measured results are consistent with theoretical simulations, which are calculated by using the model presented in Chapter 2. Therefore, the SOAs will have a reduced sensitivity to any optical power fluctuations at the input, for our case about 2 dB suppression at high microwave frequencies and >10 dB at low frequencies. These suppressions naturally imply that the intensity noise at the input will be damped. In view of Eq. (5.6), this intensity noise suppression by the SOA can reduce the noise power of the final detected microwave signal.

Figure 5.7(a) shows how the intensity noise evolves in the microwave phase shifter. During the measurements, the received optical power at the lightwave component analyzer is kept at 3 dBm to avoid any noise floor changes induced by the shot noise. It clearly shows that the intensity noise is reduced by ∼4 dB after the SOA-1 within the phase shift stage, which matches ∼-2 dB response suppression shown in Fig. 5.6 (taking into account a factor of two difference in decibels dB difference between electrical and optical units.). Although optical filtering slightly increases the intensity noise as the injection current increases, the absolute value is still 2 dB lower than the signal at the input.

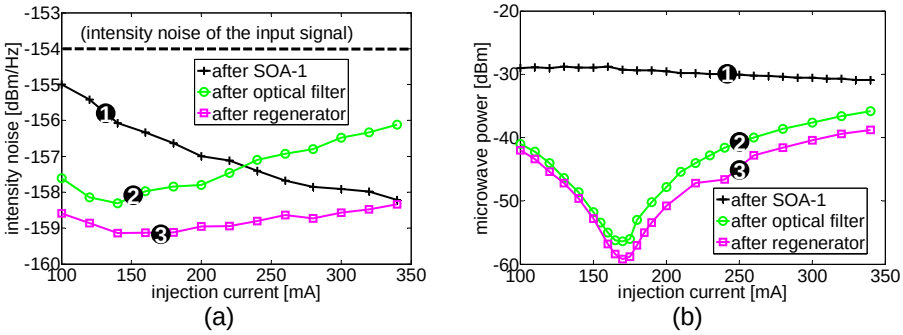

FIGURE 5.7: Measured (a) intensity noise and (b) microwave signal power at three different locations of the set-up shown in Fig. 5.4. The microwave modulation frequency is 20 GHz.

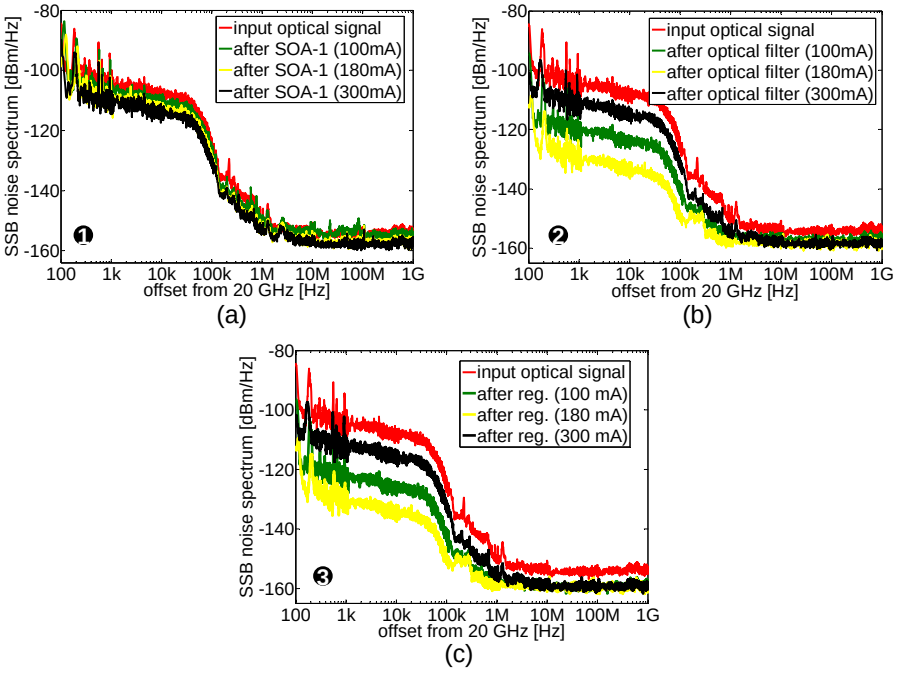

FIGURE 5.8: SSB noise measurements for three representative injection currents at three different locations in fig. 5.4. (a) ❶ at the output of SOA-1. (b) ❷ at the output of the optical filter. (c) ❸ at the output of the regenerator.

5.3.3 SSB noise spectra of slow light based microwave phase shifters

Based on the discussion in section 5.3.2, the SOA-induced intensity noise reduction will thus decrease the SSB noise power at frequency offsets larger than 500 kHz. Figure 5.8 gives the measured SSB noise spectra for three representative injection currents after the SOA ❶, after the optical filter ❷, and after the regeneration ❸, respectively. In order to understand these results, let's back to Fig. 5.7(b) which shows the microwave signal power change while the microwave phase is shifted. It is expected that the SSB noise spectrum should follow the microwave power changes plotted in Fig. 5.7(b). However, from the measured SSB noise spectra shown in Fig. 5.8, this is only true when the frequency offset is smaller than 500 kHz. When the frequency offset is larger than 500 kHz, the variation of the SSB noise spectrum is limited and determined by the changes of the intensity noise illustrated in Fig. 5.7(a) instead of the microwave power changes.

If the SNR ($= P_{signal,dB} - P_{noise,dB}$) is calculated, the noise power is the integral of the measured SSB noise spectrum over a bandwidth of interest, for instance 1 GHz. Therefore, the intensity noise of the input optical signal at frequency offsets > 500 kHz will dominate the total noise power. To clearly comprehend how the optical intensity noise impact the SNR of the detected microwave signal, Figure 5.9 shows a schematic representation by focusing on the effects of the optical intensity noise. For an extreme situation where, compared with the noise from the synthesizer, all optical noise can be neglected, the SNR is only determined by the synthesizer. Now, as the microwave modulation part of the optical signal is attenuated, the SSB noise spectrum will be reduced accordingly, as Fig. 5.9(a) shows. Therefore, the calculated SNR

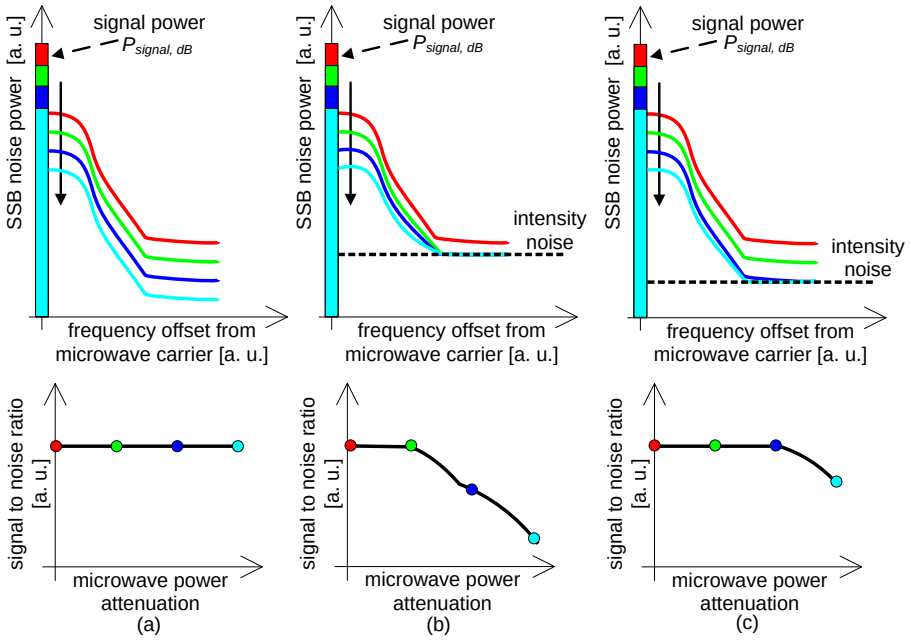

FIGURE 5.9: Top row: Microwave signal power (color bars at the carrier frequency) and SSB noise spectrum for the cases (a) without any optical noise, (b) with optical intensity noise, and (c) with suppressed optical intensity noise, respectively. Bottom row: The corresponding signal to noise ratio. The different colors stand for different values of the microwave power attenuation. This attenuation is achieved by optically decreasing the microwave modulation part without altering the average optical power.

is constant because $P_{signal,dB}$ and $P_{noise,dB}$ experience the same drop. If we take the optical intensity noise into account, it will set a limitation on the SSB noise measurements. This limitation can be considered as "white" over the microwave bandwidth of interest, which is represented by the black dashed lines in Fig. 5.9(b) and (c). Because the microwave power attenuation does not change the optical intensity noise, it can be

inferred from Fig. 5.9(b) that, as the microwave signal decreases, the intensity noise dominates the SSB noise spectrum, especially at larger frequency offsets. Therefore, compared with the decreases of $P_{signal,dB}$, the noise power $P_{noise,dB}$ will drop smaller and smaller, even be unchanged. This is why the calculated SNR decrease, as the bottom plot illustrates in Fig. 5.9(b). However, the SNR deterioration could be avoided by suppressing the optical intensity noise, as shown by Fig. 5.9(c). This possibility was theoretically confirmed in [101]. But one should keep in mind that when the intensity noise is decreased to the same order of, or even smaller than, the noise induced by the SOA itself, the SNR will decrease again due to the domination by the SOA induced noise.

The intensity noise of the laser used in our experiments is -154 dBm/Hz. Firstly, we can calculate the SNR of the input optical signal, ~35 dB, by integrating the red curve, in Fig. 5.8, over a bandwidth of 1 GHz. By propagating through the microwave phase shifter, the detected microwave signal experiences a 20 dB drop at the injection current of 180 mA. Based on the previous discussions, this 20 dB drop can deteriorate the SNR due to that the noise power could be dominated by the intensity noise of the input optical signal. The measured SNR as a function of the injection current of the SOA-1 is plotted as the dotted line in Fig. 5.10 and confirms the predicted SNR deterioration at ~180 mA, also in good agreement with published results in [89]. However, if we take a simplified situation where the SOA induced noise and measurement floor can be totally neglected, a 15 dB SNR improvement could be expected, as indicated by the solid line in Fig. 5.10, by using a laser with a shot noise limited RIN of -172 dBm/Hz [102]. But even when the SOA induced noise is considered, based on the theoretical analysis in [101], a certain degree of the SNR improvement is still expected. These issues

could be quantitatively investigated using well-known theory of noise in SOAs [101, 103].

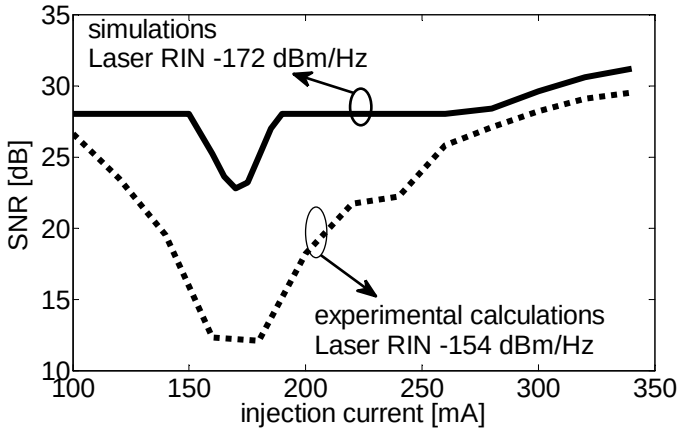

FIGURE 5.10: SNR as a function of injection current for two lasers with different RIN. The RIN of the laser used here is -154 dBm/Hz. The simulation curve (the solid line) neglect the effects of amplified spontaneous emission noise in the SOA.

5.4 Discussions

In this Chapter, the noise properties of the slow light based microwave phase shifters were discussed. In the microwave community, SSB phase noise is a commonly used parameter to evaluate the spectral purity of the microwave signal. In the optical community, intensity noise is considered as one of the major noise contributions to the microwave photonic system. An analytical model was introduced for describing how the intensity noise and SSB phase noise combine and impact the spectral quality of the microwave signal. The experimental measurements confirm the model and demonstrate that it is important to clarify which noise source is dominant. Under the experimental situation analyzed in

this chapter, the intensity noise of the input optical signal dominates the SSB noise spectrum at a frequency offset larger than 500 kHz.

The model was used to investigate, in more detail, the noise properties of the proposed microwave phase shifter and the regenerator stage. The measurements verified that the SOA based microwave phase shifter and regenerator did not result in measurable increase of the microwave noise. Furthermore, because the SOAs were operated in the regime of deep saturation, the intensity noise can be suppressed up to 4 dB, which led to a 4 dB decrease of the SSB phase noise at >500 kHz frequency offsets.

Based on this improved understanding, it could be expected that by using an input optical signal with lower RIN, the SNR of slow light based microwave phase shifters can be significantly improved, rendering these devices promising for microwave photonics applications. However, one should notice that when the intensity noise of the input signal is lower than the noise from the saturated SOAs, the situation will be different, because in this case, the SOAs induced noise will dominate instead of the intensity noise of the input optical signal.

Chapter 6

Microwave photonic true time delay based on cross gain modulation in SOAs

Up to now, we have investigated CPO effects induced slow and fast light phenomenon in SOAs. By exploiting the refractive index dynamics, 360^o microwave phase shifts over a bandwidth of several tens of GHz were realized. As an application, fully tunable microwave notch filters over the whole FSR were demonstrated. However, as already mentioned in Chapter 1, the other interesting application, phase array antennas, has not been discussed. To satisfy the broadband requirement of current antennas and avoid the beam squinting effects, slow light based devices have to provide a microwave true time delay, which refers to invariance of time delay with microwave frequency. Based on the relation between microwave phase shift and time delay, $\Delta\varphi = 2\pi f_{RF}\Delta t$, a microwave true time delay corresponds to a linear phase change as a function of

the microwave frequency. It can be concluded from Fig. 4.13 and Fig. 4.15 that CPO effects based slow light can not achieve a microwave true time delay. In this chapter, we will introduce a new slow light scheme, which is achieved by cross gain modulation (XGM) effects in an SOA. Although this scheme requires two independent lasers, one as control signal and the other as probe, it is able to provide a microwave true time delay over a microwave bandwidth of $\sim$40 GHz.

6.1 Introduction

Since the first demonstration of optically steered phased array antenna [12], the study of photonic microwave true time delay has become a hot topic in microwave photonics. Photonic realizations of true time delay possess promising advantages over the traditional microwave delay lines, such as light weight, huge bandwidth, and immunity to electromagnetic interference. Up to now, a common scheme is based on dispersion induced time delay by tuning the laser wavelength and propagating through high dispersion fibers or chirped fiber gratings [12, 104, 105]. This scheme is, however, relatively bulky and complex. As an alternative, slow light effects have been exploited to achieve true time delays [50, 65]. Especially slow light in semiconductor waveguides can provide very fast tuning speed, compact size and low power consumption. However, as mentioned in this thesis, it is still difficult to achieve true time delay over a broadband microwave frequency, e.g. several tens of GHz.

Here, we investigate the possibility to achieve microwave true time delays in an SOA by exploiting the XGM effects. It is well-known that XGM in a SOA can be used to perform wavelength conversion and optical switching [38, 39]. As reported in [61, 62], the XGM response has a

low-pass filter profile, which is because the SOA can not follow the optical power variation when the intensity modulation frequency is larger than the inverse of the carrier lifetime. For the counter-propagation configuration, where the signal beam and CW probe beam propagate in opposite directions in the SOA, the XGM response drops off significantly faster with the microwave modulation frequency compared to the co-propagation case [62]. Based on the Kramers-Krönig relation, altering the slope of the fall-off edge of the XGM response will lead to group velocity changes of the converted probe beam after the SOA. In this chapter, we experimentally examine both configurations, co-propagation and counter-propagation, and confirm that due to the fast drop of the XGM response, the counter-propagation scheme can provide tunable true time delays in the range up to 10.5 ps over a microwave frequency band from a few GHz to 35 GHz.

6.2 Experimental results

6.2.1 Co-propagation configuration

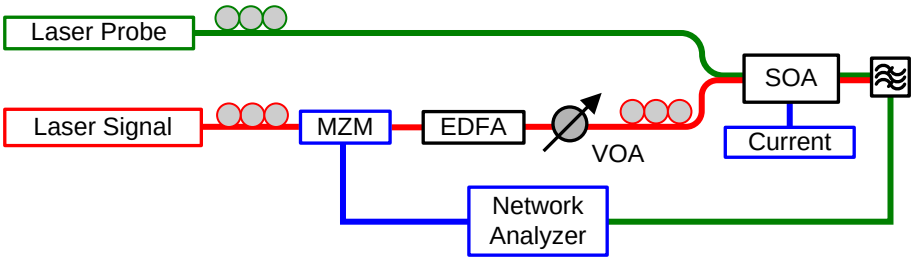

FIGURE 6.1: Co-propagation experimental set-up to measure the time delay induced by XGM effects in an SOA.

Figure 6.1 shows the experimental setup with the signal and probe co-propagating through the SOA. The wavelength of the CW probe is 1550

nm with -5 *dBm* optical power injected into the SOA. The signal laser is intensity modulated by a microwave signal from the network analyzer. The wavelength of the signal laser is 1540 *nm* and the optical power can be tuned by a variable optical attenuator. The SOA is electrically biased at 340 *mA* to achieve maximum XGM efficiency. After the SOA, an optical band-pass filter is employed to select the probe wavelength before the detection by the network analyzer.

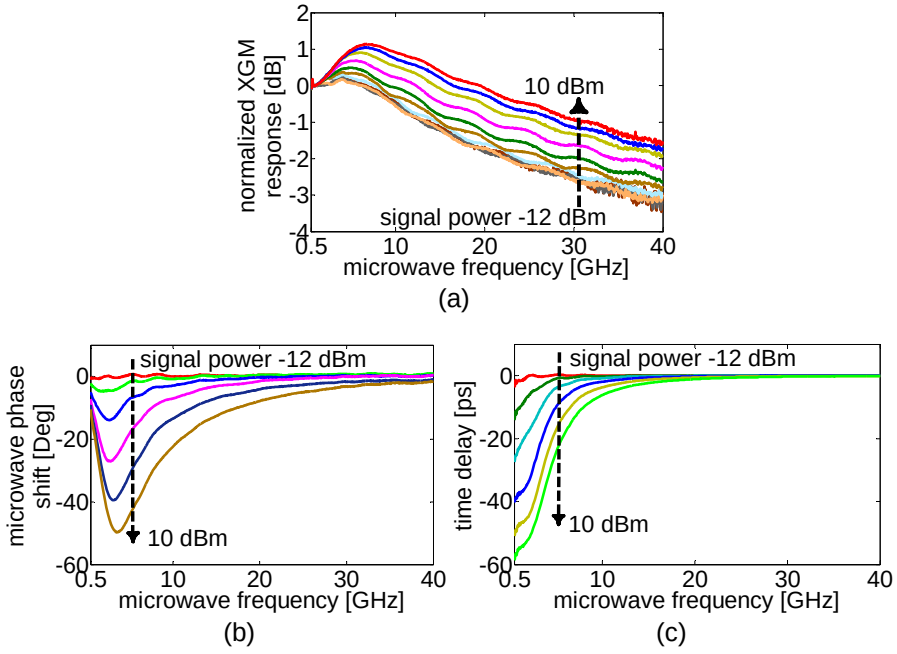

FIGURE 6.2: Measured (a) XGM responses, (b) microwave phase shifts and (c) time delays for different optical signal power levels in the co-propagation configuration.

Figure 6.2 (a) presents the measured XGM response of the probe beam as a function of the microwave modulation frequency for different signal laser levels. To clearly compare the slopes, each curve is normalized to the value at the lowest modulation frequency. The resonance peak

appearing at a few GHz is related to the carrier lifetime. At microwave frequencies below 15 GHz, the slope is seen to change with the input signal power. Consequently the microwave phase will experience a shift, as shown in Fig. 6.2(b), and its value can be controlled optically via the signal power level. The obtained microwave phase shifts are similar to those achieved by the conventional CPO based slow light effects (without optical filtering). Therefore, it can also be explained by the gain dynamics. Figure 6.2(c) gives the corresponding time delays, which are apparently not true time delays.

6.2.2 Counter-propagation configuration

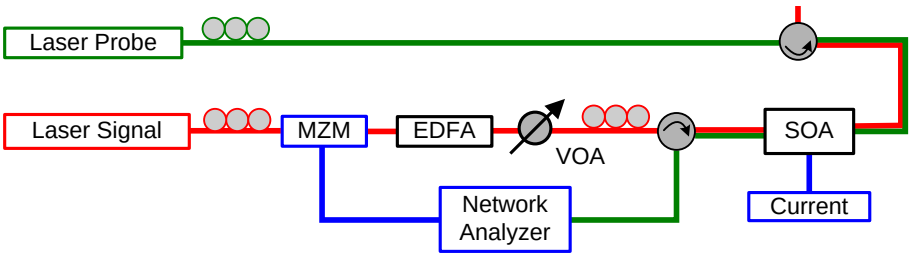

FIGURE 6.3: Counter-propagation experimental set-up to measure the time delay induced by an SOA.

Using the set-up depicted in Fig. 6.3, we also investigate the time delay obtained in the counter-propagation configuration. Two optical circulators are employed, instead of the optical band-pass filter, to separate the probe and signal beams. All other devices are operated under conditions identical to the co-propagation configuration.

Compared to the co-propagation case, the slope of the XGM response experiences a larger change over the entire investigated microwave frequency, as Fig. 6.4(a) shows. The microwave phase versus frequency

relationship, in Fig. 6.4(b), is seen to be nearly linear, with a slope that increases as the input signal power increases from -5 dBm to 9 dBm. Therefore this significant slope increase results in a tunable true time delay. A $\sim$10.5 ps continuous true time delay over a frequency range from 5 GHz to 35 GHz is successfully obtained in Fig. 6.4(c).

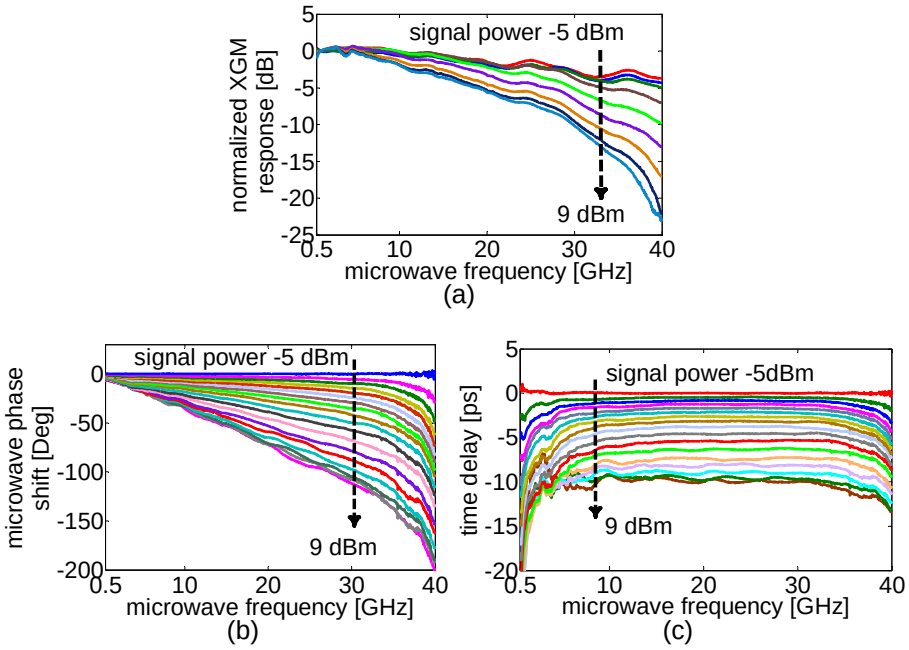

FIGURE 6.4: Measured (a) XGM responses, (b) microwave phase shifts and (c) time delays for different optical signal power levels in the counter-propagation configuration.

6.3 Summary

In conclusion, we experimentally demonstrated a photonic microwave time delay line realized by a semiconductor optical amplifier. The operation principle is cross gain modulation. Both co-propagation and

counter-propagation configurations were investigated. In the co-propagation configuration, a time delay of several tens of picoseconds at a few GHz is realized, which is limited by the carrier lifetime. However, in the counter-propagation case, due to the fast fall-off of the XGM response with the microwave frequency, a 10.5 ps continuously tunable true time delay over a microwave bandwidth of several tens of GHz is achieved. The maximum time delay and microwave operation frequency could be further improved by engineering the structure of the SOA.

Chapter 7

Conclusion and outlook

7.1 Conclusion

Control of the group velocity of light, well known as slow and fast light, brings a new opportunity to manipulate light, and hence has stimulated a lot of research on the fascinating physics and potential applications in optical signal processing. For a modulated optical beam at a microwave frequency, controlling the speed of light naturally provides microwave phase shifts or delay lines, which are highly desired for microwave photonic systems and still difficult to realize by traditional technologies, especially at millimeter-wave bands. Recently a lot of work has focused on microwave phase shifts realized by slow and fast light effects in semiconductor materials, especially SOAs or EAs. In this case, the process of coherent population oscillations (CPO) leads to the control of the group velocity. However, due to their relatively long carrier recovery times, slow and fast light effects can provide only 150^o microwave phase shifts

operating at a microwave frequency of 1 GHz with a few-GHz bandwidth, and inevitably cause 20 dB microwave power variation [43–46]. These limitations, small bandwidth, limited phase shift, and large microwave power variation, seriously hamper their applications.

This thesis has investigated SOA based slow and fast light devices for applications in microwave photonics, theoretically as well as experimentally. The main objective is to resolve the aforementioned problems or limitations of current slow light devices, and further prove the potential of slow and fast light effects for real applications within microwave photonic systems.

At first, we theoretically investigated the limitations of the achievable microwave phase shifts by CPO effects enabled slow and fast light effect in SOAs. It turns out that the refractive index dynamics in the SOA cancels out due to the double-sideband detection. Therefore, the obtained microwave phase shift is solely determined by the gain dynamics. To exploit the refractive index dynamics we experimentally proposed a novel and simple scheme, which utilized an optical filtering, after the SOA, to block the red-shifted sideband. A ten-fold increase of the absolute phase shift as well as the microwave operation bandwidth was achieved. Additionally, perturbation theory provided a physical understanding on the optical filtering enhanced slow light effects. We then investigated in more detail the proposed new structure. The initial modulation chirp dependence and the microwave operation frequency limitations were analyzed both theoretically and experimentally. Because the detected microwave signal is generated by the beating between the optical carrier and sidebands, both microwave phase delay and phase advance were demonstrated by utilizing the initial optical phase difference between the carrier and sidebands. This led to the implementation of a

100 percent tunable microwave photonic notch filter over its whole FSR. The microwave operation bandwidth of the proposed slow light devices was analyzed by an approximate analytical solution, which highlights that the microwave operation frequency is greatly expanded through the linewidth enhancement factor and gives directions for further engineering the SOA to make it operate at a specific microwave frequency band of interest.

In order to cascade slow light based phase shifters, we introduced a red-shifted sideband regenerator between two phase shift stages. The principle of regeneration is four wave mixing by an SOA. This new configuration not only enabled the cascadability of several microwave phase shifters, but also provided the possibility to control the microwave power independently. A doubling of the microwave phase shift with less than 1.6 dB power change at 19 GHz was successfully demonstrated. This cascadability finally enabled the achievement of 360^o microwave phase shifts by slow light effects in SOAs. To confirm the phase shifting capability at even higher microwave operation frequency, a MZ-modulator with a bandwidth of 40 GHz was used. $> 360^o$ microwave phase shifts over a microwave frequency from $\sim$9 GHz to 40 GHz were demonstrated by cascading three optical filtering enhanced slow light stages. This is, to the best of our knowledge, the first-ever demonstration of 360^o microwave phase shift by slow light effects in terms of both the magnitude of achieved phase shifts and the microwave operation frequency. Furthermore, the control of three injection currents offers more flexible manipulations of microwave phase and power. As an example, a $\sim 330^o$ linear microwave phase shift was demonstrated. Therefore, all these achievement by slow light effects show a promising potential with advantages and unprecedented characteristics in terms of losses,

tuning speed, phase shift, bandwidth and flexible controls of both the microwave phase and the power.

The noise properties of the proposed structure were also examined experimentally. Two commonly discussed noise sources in microwave photonic systems, intensity noise of the laser and SSB phase noise of the microwave source, were investigated by a theoretical model. The model shows that both the intensity noise of the optical signal and phase noise of the electrical synthesizer contribute to the SSB noise spectrum of the optically generated microwave signal, which was also confirmed by the experimental measurements. Furthermore, at frequency offsets $<$ 500 kHz the SSB noise spectrum is dominated by the phase noise of the synthesizer. Otherwise, when the frequency offset is larger than 500 kHz it is dominated by the intensity noise of the optical signal. Therefore, when the SNR is calculated, the intensity noise at the large frequency offsets could be a main contribution to the total noise power. By including the slow light based microwave phase shifter, we experimentally concluded that the proposed phase shift stages do not introduce any measurable noise increases, which is because the intensity noise at the input optical signal is dominant. This results in a possibility to improve the SNR, to a certain extent, by suppressing the intensity noise of the input signal.

Finally, to apply the SOAs based slow light effects in optically steered phased array antennas, a microwave true time delay is highly desired instead of a microwave phase shifter. Especially for a broadband antenna, a true time delay is able to remove the beam squinting effects. To implement a microwave true time delay, we experimentally proposed and investigated an XGM based slow light scheme. By operating the scheme in a counter-propagation configuration, the slope of the fall-off

edge of the XGM response led to a linear microwave phase change with the microwave frequency. Consequently, a 10.5 ps continuously tunable true time delay over a microwave bandwidth of several tens of GHz was achieved. The demonstration expands the possible applications of SOAs based slow light effects in broadband antennas.

7.2 Outlook

Though we have shown the potential of slow light effects in SOAs by achieving 360^o microwave phase shifts over a microwave bandwidth of several tens of GHz, there are still some points which are not properly covered in this thesis. Firstly, all presented results in this thesis were achieved by using a sinusoidal microwave carrier, which means that no actual RF signal propagated through the slow light based microwave devices. Therefore, from an application point of view, launching a microwave signal with a finite bandwidth into the proposed device is of course more interesting. Another very interesting topic missing from this work is the implementation of phased array antennas. From the results shown in this thesis, CPO based slow light effects can not provide a true time delay over a large microwave bandwidth, which is a limitation for broadband antennas. But there is still potential for narrow band phased array antennas [106]. Also, the SOAs we used here are commercially available with bulk or quantum well structures. It would be worthwhile investigating other nano-engineered SOAs, such as quantum dots, which could have very different properties, for instance fast carrier recovery time, low saturation power and giant linewidth enhancement factor. All these parameters could enhance the performance of the proposed devices. In this work, we did not discuss the noise contribution

from SOAs because in our case it was inferior to the intensity noise at the input. If the intensity noise can be suppressed to a sufficiently low level, the noise from the SOAs will dominating. Finally, recently several photonic microwave phase shifters based on different principles were proposed too, such as silicon microring resonator based schemes [107]. Up to 360^o phase shifts at a microwave frequency of 40 GHz was demonstrated by using a dual-microring resonator [108]. Therefore, it is considered important, from an application point of view, to compare these different schemes and establish their respective pros and cons.

Appendix A

Ph.D. Publications

A.1 Journal

1. Weiqi Xue, Salvador Sales, José Capmany, and Jesper Mørk, "Wideband 360 microwave photonic phase shifter based on slow light in semiconductor optical amplifiers," *Optics Express* 18, 6156-6163 (2010)

2. Weiqi Xue, Salvador Sales, José Capmany, and Jesper Mørk, "Microwave phase shifter with controllable power response based on slow- and fast-light effects in semiconductor optical amplifiers," *Optics Letters* 34, 929-931 (2009)

3. Weiqi Xue, Salvador Sales, Jesper Mørk, and José Capmany, "Widely tunable microwave photonic notch filter based on slow and fast light effects," *IEEE Photonics Technology Letters* 21, 167-169 (2009)

4. Weiqi Xue, Yaohui Chen, Filip Öhman, and Jesper Mørk, "The role of input chirp on phase shifters based on slow and fast light

effects in semiconductor optical amplifiers," *Optics Express* 17, 1404-1413 (2009)

5. Weiqi Xue, Yaohui Chen, Filip Öhman, Salvador Sales, and Jesper Mørk, "Enhancing light slow-down in semiconductor optical amplifiers by optical filtering," *Optics Letters* 33, 1084-1086 (2008)

6. Weiqi Xue, Filip Öhman, Søren Blaaberg, Yaohui Chen, Salvador Sales, and Jesper Mørk, "Broadband microwave photonic phase shifter based on polarisation rotation," *Electronics Letters*, 44, 684-685 (2008)

7. Minhao Pu, Liu Liu, Weiqi Xue, Yunhong Ding, Haiyan Ou, Kresten Yvind, and Jørn M. Hvam, "Widely tunable microwave phase shifter based on silicon-on-insulator dual-microring resonator," *Optics Express* 18, 6172-6182 (2010)

8. Minhao Pu, Liu Liu, Weiqi Xue, Yunhong Ding, L. H. Frandsen, Haiyan Ou, Kresten Yvind, and Jørn M. Hvam, "Tunable microwave phase shifter based on silicon-on-insulator microring resonator," *IEEE Photonics Technology Letters* 22, 869-871 (2010)

9. Jesper Mørk, Per Lunnemann Hansen, Weiqi Xue, Yaohui Chen, Per Kær Nielsen and Torben Roland Nielsen, "Slow and fast light in semiconductor waveguides," *Semiconductor Science and Technology*, 25, 083002 (2010)

10. Lei Wei, Weiqi Xue, Yaohui Chen, Thomas Tanggaard Alkeskjold, and Anders Bjarklev, "Optically fed microwave true-time delay based on a compact liquid-crystal photonic-bandgap-fiber device," *Optics Letters* 34, 2757-2759 (2009)

11. Enbo Zhou, Xianbin Yu, Xinliang Zhang, Weiqi Xue, Yu Yu, Jesper Mørk, and Idelfonso Tafur Monroy, "Photonic generation of ultrawideband monocycle and doublet pulses by using a semiconductor-optical-amplifier-based wavelength converter," *Optics Letters* 34, 1336-1338 (2009)

12. Yaohui Chen, Weiqi Xue, Filip Öhman, and Jesper Mørk, "Theory of optical-filtering enchanced slow and fast light effects in semiconductor optical waveguides," *IEEE/OSA Journal of Lightwave Technology* 26, 3734-3743 (2008)

13. Salvador Sales, Weiqi Xue, Jesper Mørk, and Ivana Gasulla, "Slow and fast light effects and their applications to microwave photonics using semiconductor optical amplifiers," Joint Special Issue of the *IEEE Transactions on Microwave Theory and Techniques* and the *IEEE/OSA Journal of Lightwave Technology* on Microwave Photonics, Invited paper, to be published.

A.2 Conference

1. Weiqi Xue, and Jesper Mørk, "Microwave photonic true time delay based on cross gain modulation in semiconductor optical amplifiers," in the 15th Opto-Electronics and Communications Conference (OECC), Sapporo, Japan (2010)

2. Weiqi Xue, Salvador Sales, José Capmany, and Jesper Mørk, "Experimental demonstration of 360 tunable RF phase shift using slow and fast light effects," in Slow and Fast Light, OSA Technical Digest (CD), paper SMB6, Honolulu, USA (2009)

3. Weiqi Xue, Yaohui Chen, Salvador Sales, S. Blaaberg, Jesper Mørk, José Capmany, "Microwave photonics processing controlling the speed of light in semiconductor waveguides," in the Conference of the 11th International Conference on Transparent Optical Networks (ICTON),Invited talk, Azores, Portugal (2009)

4. Weiqi Xue, Salvador Sales, Jesper Mørk, and José Capmany, "Demonstration of tunable microwave photonic notch filters using slow and fast light effects in semiconductor optical amplifiers," in Optical Fiber Communication Conference, OSA Technical Digest (CD), paper OTuE2, San Diego, USA (2009)

5. Weiqi Xue, Yaohui Chen, Filip Öhman, Salvador Sales, José Capmany, and Jesper Mørk, "Slow and fast light in semiconductor waveguides for applications in microwave photonics," SPIE Photonics West, Invited talk, 7226-7232, San Jose, USA (2009)

6. Weiqi Xue, Yaohui Chen, Filip Öhman, Salvador Sales, and Jesper Mørk, "Chirp dependence of filter assisted slow and fast light effects in semiconductor optical amplifiers," in Slow and Fast Light, OSA Technical Digest (CD), paper JMB12, Boston, USA (2008)

7. Weiqi Xue, Filip Öhman, Yaohui Chen, Salvador Sales, and Jesper Mørk, "Experimental demonstration of strongly enhanced light slow-down in semiconductor optical amplifiers by optical filtering," in Slow and Fast Light, OSA Technical Digest (CD), paper STuA5, Boston, USA (2008)

8. Weiqi Xue, Filip Öhman, S. Blaaberg, Y. Chen, Jesper Mørk, and Salvador Sales, "Microwave phase shifter based on Mach-Zehnder intensity modulator and polarization rotation in an SOA," in Conference on Lasers and Electro-Optics/Quantum Electronics

and Laser Science Conference and Photonic Applications Systems Technologies, OSA Technical Digest (CD), paper CMP2, San Jose, USA (2008)

9. Jing Xu, Yunhong Ding, Weiqi Xue, Christophe Peucheret, Jorge Seoane, Beta Zsigri, Palle Jeppesen, and Jesper Mørk, "Experimental validation of efficient methods for the prediction of patterning effects in SOA-based optical switches," accepted in the 36th European Conference and Exhibition on Optical Communication (ECOC), Turin, Italy (2010)

10. Minhao Pu, Weiqi Xue, Liu Liu, Haiyan Ou, Kresten Yvind, and Jrn Hvam, "360 degree tunable microwave phase shifter based on silicon-on-insulator dual-microring resonator" in the 15th European Conference on Integrated Optics (ECIO), paper WeD3, Cambridge, UK (2010)

11. Minhao Pu, Liu Liu, Weiqi Xue, Lars Frandsen, Haiyan Ou, Kresten Yvind, and Jrn Hvam, "Microwave photonic phase shifter based on tunable silicon-on-insulator microring resonator" in Conference on Lasers and Electro-Optics/Quantum Electronics and Laser Science Conference and Photonic Applications Systems Technologies (CLEO/QELS), paper CThJ2, San Jose, CA, USA, (2010)

12. Jesper Mørk, Weiqi Xue, Yaohui Chen, Filip Öhman, Per Kær Nielsen, Henri Thyrrestrup Nielsen, and Torben Roland Nielsen, "Exploring carrier dynamics in semiconductors for slow light," IEEE/LEOS Winter Topicals Meeting Series, Invited talk, 150-151, Innsbruck, Austria (2009)

13. Jesper Mørk, Weiqi Xue, Yaohui Chen, S. Blaaberg, Salvador. Sales, and Jose Capmany, "Controlling the speed of light in semiconductor waveguides: physics and applications," in Conference on Lasers and Electro-Optics/International Quantum Electronics Conference, OSA Technical Digest (CD), Invited talk, paper JTuF4, Baltimore, USA (2009)

14. Lei Wei, Weiqi Xue, Yaohui Chen, T. T. Alkeskjold, and B. Anders, "Compact optically-fed microwave true-time delay using liquid crystal photonic bandgap fiber device," in Slow and Fast Light, OSA Technical Digest (CD), paper JTuB27, Honolulu, USA (2009)

15. José Capmany, Salvador Sales, Weiqi Xue, Yaohui Chen, S. Blaaberg and Jesper Mørk, "Optical signal processing using slow and fast light technologies" in Conference on 14th European Conference on Networks and Optical Communications (NOC), Invited talk, 351-359, Valladolid, Spain (2009)

16. Enbo Zhou, Xinliang Zhang, X. Yu, J. Dong, Weiqi Xue, and I. T. Monroy, "Photonic Generation of UWB monocycle pulses using a cascaded semiconductor optical amplifier and electroabsorption modulator," in Optical Fiber Communication Conference, OSA Technical Digest (CD), paper JWA49, San Diego, USA (2009)

17. Jesper Mørk, Filip Öhman, Weiqi Xue, Yaohui Chen, Søren Blaaberg, Salvador Sales, "Slow and fast light effects in semiconductor waveguides for applications in microwave photonics" IEEE International Topical Meeting on Microwave Photonics, Invited talk, 310-313, Queens land, Australia (2008)

18. Yaohui Chen, Weiqi Xue, Filip Öhman, and Jesper Mørk, "Semi-analytical model of filtering effects in microwave phase shifters

based on semiconductor optical amplifiers," in Slow and Fast Light, OSA Technical Digest (CD), paper JMB14, Boston, USA (2008)

19. Jesper Mørk, Filip Öhman, Mike van der Poel, Yaohui Chen, Weiqi Xue, Per L. Hansen, and Kresten Yvind, "Carrier dynamics and slow light in semiconductor nanostructures," in Conference on Lasers and Electro-Optics/Quantum Electronics and Laser Science Conference and Photonic Applications Systems Technologies, OSA Technical Digest (CD), Invited talk, paper CTuJ1, San Jose, USA (2008)

List of Figures

Bibliography

[1] A. Sommerfeld. Ein einwand gegen die relativtheorie der elektrodynamik und seine beseitigung. *Physikalische Zeitschrift*, 8: 841–842, 1907.

[2] L. Brillouin. *Wave propagation and group velocity.* June 1960.

[3] Federal Communications Commission. Millimeter wave 70-80-90 gigahertz service. March 2005.

[4] R. Jakoby, P. Scheele, S. Mller, and C. Weil. Nonlinear dielectrics for tunable microwave components. *15th International Conference on Microwaves, Radar and Wireless Communications*, 2:10, 2004.

[5] A. J. Seeds and K. J. Williams. Microwave photonics. *IEEE/OSA Journal of Lightwave Technology*, 24(12):4628–4641, December 2006.

[6] J. Capmany and D. Novak. Microwave photonics combines two worlds. *Nature Photonics*, 1:319–330, June 2007.

[7] A. Vilcot, B. Cabon, and J. Chazelas. *Microwave photonics: from components to applications and systems.* 2003.

[8] R. Levy and S. B. Cohn. A history of microwave filter research, design and development. *IEEE Transactions on Microwave Theory and Technique*, 32(9):1055–1067, September 1984.

[9] R. W. Simon, R. B. Hammond, S. J. Berkowitz, and B. A. Willemsen. Superconducting microwave filter systems for cellular telephone base stations. *Proceedings of the IEEE*, 92(10):1585–1596, October 2004.

[10] J. Capmany, B. Ortega, and D. Pastor. A tutorial on microwave photonic filters. *IEEE/OSA Journal Lightwave Technology*, 24(1): 201–229, January 2006.

[11] R. J. Mailloux. Phased array theory and technology. *Proceedings of the IEEE*, 70(3):246–291, March 1982.

[12] W. Ng, A. A. Walston, G. L. Tangonan, J. J. Lee, I. L. Newberg, and N. Bernstein. The first demonstration of an optically steered microwave phased array antenna using true-time-delay. *IEEE/OSA Journal of Lightwave Technology*, 9(9):1124–1131, September 1991.

[13] I. Frigyes and A. J. Seeds. Optically generated true-time delay in phased-array antennas. *IEEE Transactions on Microwave Theory and Techniques*, 43(9):2378–2386, September 1995.

[14] J. A. Carruthers and T. Bieber. Pulse velocity in a self-locked He-Ne laser. *Journal of Applied Physics*, 40(1):426–428, January 1969.

[15] F. R. Faxvog, C. N. Y. Chow, T. Bieber, and J. A. Carruthers. Measured pulse velocity greater than c in a Neon absorption cell. *Applied Physics Letters*, 17(5):192–193, September 1970.

[16] L. Casperson and A. Yariv. Pulse propagation in a high-gain medium. *Physical Review Letters*, 26(6):293–295, February 1971.

[17] S. Chu and S. Wong. Linear pulse propagation in an absorbing medium. *Physical Review Letters*, 48(11):738–741, March 1982.

[18] L. V. Hau, S. E. Harris, Z. Dutton, and C. H. Behroozi. Light speed reduction to 17 meters per second in an ultracold atomic gas. *Nature*, 397(6720):594–598, February 1999.

[19] R. W. Boyd. *Nonlinear optics*. Academic Press, 2003.

[20] A. Yariv. *Quantum electronics*. Wiley, 1989.

[21] M. M. Kash, V. A. Sautenkov, A. S. Zibrov, L. Hollberg, G. R. Welch, M. D. Lukin, Y. Rostovtsev, E. S. Fry, and M. O. Scully. Ultraslow group velocity and enhanced nonlinear optical effects in a coherently driven hot atomic gas. *Physical Review Letters*, 82 (26):5229–5232, June 1999.

[22] M. D. Lukin and A. Imamoğlu. Controlling photons using electromagnetically induced transparency. *Nature*, 413:273–276, September 2001.

[23] M. S. Bigelow, N. N. Lepeshkin, and R. W. Boyd. Superluminal and slow light propagation in a room-temperature solid. *Science*, 301:200–202, July 2003.

[24] M. S. Bigelow, N. N. Lepeshkin, and R. W. Boyd. Observation of ultraslow light propagation in a Ruby crystal at room temperature. *Physical Review Letters*, 90:113903, March 2003.

[25] P.-C. Ku, F. Sedgwick, C. J. Chang-Hasnain, P. Palinginis, T. Li, H. Wang, S. Chang, and S.-L. Chuang. Slow light in semiconductor quantum wells. *Optics Letters*, 29:2291–2293, October 2004.

[26] Y. Okawachi, M. S. Bigelow, J. E. Sharping, Z. Zhu, A. Schweinsberg, D. J. Gauthier, R. W. Boyd, and A. L. Gaeta. Tunable all-optical delays via brillouin slow light in an optical fiber. *Physical Review Letters*, 94:153902, April 2005.

[27] D. Dahan and G. Eisenstein. Tunable all optical delay via slow and fast light propagation in a Raman assisted fiber optical parametric amplifier: a route to all optical buffering. *Optics Express*, 13:6234–6249, August 2005.

[28] J. Sharping, Y. Okawachi, and A. L. Gaeta. Wide bandwidth slow light using a Raman fiber amplifier. *Optics Express*, 13:6092–6098, August 2005.

[29] L. Thévenaz. Slow and fast light in optical fibers. *Nature Photonics*, 2:474–481, August 2008.

[30] A. Wiatrek, K. Jamshidi, R. Henker, S. Preuler, and T. Schneider. Nonlinear Brillouin based slow-light system for almost distortion-free pulse delay. *Journal of the Optical Society of America B-Optical Physics*, 27:544–549, March 2010.

[31] K. J. Vahala. Optical microcavities. *Nature*, 424:839–846, August 2003.

[32] Y. A. Vlasov, M. OBoyle, H. F. Hamann, and S. J. McNab. Active control of slow light on a chip with photonic crystal waveguides. *Nature*, 438:65–69, November 2005.

[33] K. Totsuka, N. Kobayashi, and M. Tomita. Slow light in coupled-resonator-induced transparency. *Physical Review Letters*, 98: 213904, May 2007.

[34] V. Yannopapas, E. Paspalakis, and N. V. Vitanov. Electromagnetically induced transparency and slow light in an array of metallic nanoparticles. *Physical Review B*, 80:035104, May 2009.

[35] C. J. Chang-Hasnain and S. L. Chuang. Slow and fast light in semiconductor quantum-well and quantum-dot devices. *IEEE/OSA Journal of Lightwave Technology*, 24(12):4642–4654, December 2006.

[36] J. Mørk, F. öhman, M. van der Poel, Y. Chen, P. Lunnemann, and K. Yvind. Slow and fast light: Controlling the speed of light using semiconductor waveguides. *Laser & Photonics Reviews*, 3 (1-2):30–44, August 2009.

[37] S. Chang, P. K. Kondratko, H. Su, and S. L. Chuang. Slow light based on coherent population oscillation in quantum dots at room temperature. *IEEE Journal of Quantum Electronics*, 43(2):196–205, February 2007.

[38] T. Durhuus, B. Mikkelsen, C. Joergensen, S. L. Danielsen, and K. Stubkjr. All-optical wavelength conversion by semiconductor optical amplifiers. *IEEE/OSA Journal of Lightwave Technology*, 14:942–954, June 1996.

[39] K. E. Stubkjær. Semiconductor optical amplifier-based all-optical gates for high-speed optical processing. *IEEE Journal of Selected Topics in Quantum Electronics*, 6:1428–1435, November/December 2000.

[40] O. Leclerc, B. Lavigne abd E. Balmefrezol, P. Brindel, L. Pierre, D. Rouvillain, and F. Seguineau. Optical regeneration at 40 Gb/s and beyond. *IEEE/OSA Journal of Lightwave Technology*, 21: 2779–2790, November 2003.

[41]

[42] P.C. Ku, C.J. Chang-Hasnain, and S.L. Chuang. Variable semiconductor all-optical buffer. *Electronics Letters*, 38:1581–1583, November 2002.

[43] J. Mørk, R. Kjær, M. van der Poel, and Kresten Yvind. Slow light in a semiconductor waveguide at gigahertz frequencies. *Optics Express*, 13:8136–8145, October 2005.

[44] H. Su, P. K. Kondratko, and S. L. Chuang. Variable optical delay using population oscillation and four-wave-mixing in semiconductor optical amplifiers. *Optics Express*, 14:4800–4807, May 2006.

[45] F. öhman, K. Yvind, and J. Mørk. Voltage-controlled slow light in an integrated semiconductor structure with net gain. *Optics Express*, 14:9955–9962, October 2006.

[46] P. K. Kondratko and S. L. Chuang. Slow-to-fast light using absorption to gain switching in quantum-well semiconductor optical amplifier. *Optics Express*, 15:9963–9969, August 2007.

[47] F. G. Sedgwick, B. Pesala, J. Lin, W. S. Ko, X. Zhao, and C. J. Chang-Hasnain. THz-bandwidth tunable slow light in semiconductor optical amplifiers. *Optics Express*, 15:747–753, January 2007.

[48] B. Pesala, F. G. Sedgwick, A. V. Uskov, and C. Chang-Hasnain. Ultrahigh-bandwidth electrically tunable fast and slow light in semiconductor optical amplifiers. *Journal of the Optical Society of America B*, 25:C46–C54, December 2008.

[49] B. Pesala, F. G. Sedgwick, A. V. Uskov, and C. Chang-Hasnain. Greatly enhanced slow and fast light in chirped pulse semiconductor optical amplifiers: Theory and experiments. *Optics Express*, 17:2188–2197, February 2009.

[50] F. öhman, K. Yvind, and J. Mørk. Slow light in a semiconductor waveguide for true-time delay applications in microwave photonics. *IEEE Photonics Technology Letters*, 19:1145–1147, August 2007.

[51] J. J. O'Reilly, P.M. Lane, R. Heidemann, and R. Hofstetter. Optical generation of very narrow linewidth millimetre wave signals. *Electronics Letters*, 28:2309–2311, December 1992.

[52] G. Qi, J. Yao, J. Seregelyi, S. Paquet, C. Belisle, X. Zhang, K. Wu, and R. Kashyap. Phase-noise analysis of optically generated millimetre-wave signals with external optical modulation techniques. *IEEE/OSA Journal of Lightwave Technology*, 24: 4861–4875, December 2006.

[53] D. Eliyahu, D. Seidel, and L. Maleki. RF amplitude and phase-noise reduction of an optical link and opto-electronic oscillator. *IEEE Transactions on Microwave Theory and Techniques*, 56:449–456, February 2008.

[54] G. P. Agrawal. Population pulsations and nondegenerate 4-wave mixing in semiconductor-lasers and amplifiers. *Journal of the Optical Society of America B*, 5:147–159, January 1988.

[55] A. Uskov, J. Mørk, and J. Mark. Wave mixing in semiconductor laser amplifiers due to carrier heating and spectral-hole burning. *IEEE Journal of Quantum Electronics*, 30:1769–1781, August 1994.

[56] W. Xue, Y. Chen, F. öhman, and J. Mørk. The role of input chirp on phase shifters based on slow and fast light effects in semiconductor optical amplifiers. *Optics Express*, 17:1404–1413, February 2009.

[57] A. Uskov and C. Chang-Hasnain. Slow and superluminal light in semiconductor optical amplifiers. *Electronics Letters*, 41(16): 55–56, August 2005.

[58] M. van der Poel, J. Mørk, and J. Hvam. Controllable delay of ultrashort pulses in a quantum dot optical amplifier. *Optics Express*, 13(20):8032–8037, October 2005.

[59] A. Uskov, F. Sedgwick, and C. Chang-Hasnain. Delay limit of slow light in semiconductor optical amplifiers. *IEEE Photonics Technology Letters*, 18(6):731–733, March 2006.

[60] W. Xue, Y. Chen, F. öhman, S. Sales, and J. Mørk. Enhancing light slow-down in semiconductor optical amplifiers by optical filtering. *Optics Letters*, 33:1084–1086, May 2008.

[61] D. A. O. Davies. Small-signal analysis of wavelength conversion in semiconductor laser amplifers via gain saturation. *IEEE Photonics Technology Letters*, 7(6):617–619, June 1995.

[62] D. D. Marcenac, A. E. Kelly, and D. Nesset. Nonlinear optical amplifiers for ultra-high speed all-optical wavelength conversion and switching. *OSA topical meeting: Optical Amplifiers and Their Applications*, 5:SD8, July 1996.

[63] J. Capmany, B. Ortega, D. Pastor, and S. Sales. Discrete-time optical processing of microwave signals. *IEEE/OSA Journal of Lightwave Technology*, 23(2):702–723, February 2005.

[64] R. A. Minasian. Photonic signal processing of microwave signals. *IEEE Transactions on Microwave Theory and Techniques*, 54(2): 832–846, February 2006.

[65] M. Bashkansky, Z. Dutton, A. Gulian, D. Walker, F. Fatemi, and M. Steiner. True-time delay steering of phased array radars using slow light. *Proceedings of SPIE*, 7226(13):72260A, 2009.

[66] M. Nielsen and J. Mrk. Increasing the modulation bandwidth of semiconductor-optical-amplifier-based switches by using optical filtering. *Journal of the Optical Society of America B*, 21(9):1606–1619, September 2004.

[67] B. Dagens, A. Markus, J. X. Chen, J.-G. Provost, D. Make, O. Le Gouezigou, J. Landreau, A. Fiore, and B. Thedrez. Giant linewidth enhancement factor and purely frequency modulated emission from quantum dot laser. *Electronics Letters*, 41(6):323–324, March 2005.

[68] F. Koyama and K. Iga. Frequency chirping in external modulators. *IEEE/OSA Journal of Lightwave Technology*, 6(1):87–93, January 1988.

[69] G. H. Smith, D. Novak, and Z. Ahmed. Overcoming chromatic-dispersion effects in fiber-wireless systems incorporating external modulators. *IEEE Transactions on Microwave Theory and Techniques*, 45(8):1410–1415, August 1997.

[70] IEEE Standard for Local and Metropolitan Area Networks. *Air interface for fixed and mobile broadband wireless access systems.* Part 16, 2006.

[71] D. Dolfi, J. Tabourel, O. Durand, V. Laude, and J. Huignard. Optical architectures for programmable filtering and correlation of microwave signals. *IEEE Transactions on Microwave Theory and Techniques*, 56(8):1467–1472, August 1997.

[72] D. Pastor, J. Capmany, and B. Ortega. Broadband tunable microwave transversal notch filter based on tunable uniform fiber bragg gratings as slicing filters. *IEEE Photonics Technology Letters*, 13(7):726–728, July 2001.

[73] F. Coppinger, S. Yegnanarayanan, P. D. Trinh, B. Jalali, and I. L. Newberg. Nonrecursive tunable photonic filter using wavelength-selective true time delay. *IEEE Photonics Technology Letters*, 8 (9):1214–1216, September 1996.

[74] F. Coppinger, S. Yegnanarayanan, P. D. Trinh, and B. Jalali. Continuously tunable photonic radio-frequency notch filter. *IEEE Photonics Technology Letters*, 9(3):339–341, March 1997.

[75] A. Loayssa, J. Capmany, M. Sagues, and J. Mora. Demonstration of incoherent microwave photonic filters with complex coefficients. *IEEE Photonics Technology Letters*, 18(16):1744–1746, August 2006.

[76] N. You and R. A. Minasian. A novel tunable microwave optical notch filter. *IEEE Transactions on Microwave Theory and Techniques*, 49(10):2002–2005, October 2001.

[77] C. Weil, S. Müller, P. Scheele, Y. Kryvoshapka, G. Lüssem, P. Best, and R. Jakoby. Ferroelectric- and liquid crystal tunable microwave phase-shifters. *the 33rd European Microwave Conference, Munich, Germany*, 3:1431–1434, October 2003.

[78] P. Wang, C. Y. Tan, Y. G. Ma, W.N. Cheng, and C. K. Ong. Planar tunable high-temperature superconductor microwave broadband phase shifter with patterned ferroelectric thin film. *Superconductor Science and Technology*, 20(1):77–80, January 2007.

[79] B. Lakshminarayanan and T. Weller. MEMS phase shifters using cascaded slow-wave structures for improved impedance matching and/or phase shift. *IEEE MTT-S International Microwave Symposium Digest*, 2:725– 728, June 2004.

[80] N. S. Barker and G. M. Reveis. Distributed MEMS true-time delay phase shifters and wide-band switches. *IEEE Transactions on Microwave Theory and Techniques*, 46:1881–1890, November 1998.

[81] G. McFeetors and M. Okoniewski. Distributed MEMS analog phase shifter with enhanced tuning. *IEEE Microwave and Wireless Components Letters*, 16(1):34–36, January 2006.

[82] T. Kim, D. Woo, C. Lee, and K. W. Kim. A new 40 Ghz analog phase shifter using phase-locked loops. *the 35th European Microwave Conference, Paris, France*, 2, October 2005.

[83] P. F. Mcmanamon, T. A. Dorschner, D. L. Corkum, L. J. Friedman, D. S. Hobbs, M. Holz, S. Liberman, H. Q. Nguyen, D. P. Resler, R. C. Sharp, , and E. A. Watson. Optical phased array technology. *Proceeding of the IEEE*, 84(2):268–298, February 1996.

[84] K. Matsumoto, M. Izutsu, and T. Sueta. Microwave phase shifter using optical waveguide structure. *IEEE/OSA Journal of Lightwave Technology*, 9(11):1523–1527, November 1991.

[85] M. R. Fisher and S. L. Chuang. A microwave phase-shifter based on wavelength conversion in a DFB laser. *IEEE Photonics Technology Letters*, 18(16):1714–1716, August 2006.

[86] Y. Yu and J. P. Yao. A tunable microwave photonic filter with a complex coefficient using an optical RF phase shifter. *IEEE Photonics Technology Letters*, 19(19):1472–1474, October 2007.

[87] C. H. Cox, E. I. Ackerman, G. E. Betts, and J. L. Prince. Limits on the performance of RF-over-fiber links and their impact on device design. *IEEE Transactions on Microwave Theory and Techniques*, 54(2):906–920, February 2006.

[88] M. Bibey, F. Deborgies, M. Krakowski, and D. Mongardien. Very low phase-noise optical links - experiments and theory. *IEEE Transactions on Microwave Theory and Techniques*, 47(12):2257–2262, December 1999.

[89] E. Shumakher, S. O. Duill, and G. Eisenstein. Signal-to-noise ratio of a semiconductor optical amplifier based optical phase shifter. *Optics Letters*, 34(13):1940–1942, July 2009.

[90] P. Berber, J. Bourderionnet, M. Alouini, F. Bretenaker, and D. Dolfi. Theoretical study of the spurious-free dynamic range of a tunable delay line based on slow light in SOA. *Optics Express*, 17(22):20584–20597, October 2009.

[91] J. Gasulla, J. Sancho, J. Lloret, S. Sales, and J. Capmany. Harmonic distortion in microwave photonic phase shifters based on coherent population oscillations in SOAs. *IEEE Photonics Technology Letters*, 22(12):899 – 901, June 2010.

[92] E. Rubiola. *Phase noise and frequency stability in oscillators*. 2008.

[93] X. S. Yao and L. Maleki. Optoelectronic oscillator for photonic systems. *IEEE Journal of Quantum Electronics*, 32(7):11411149, July 1996.

[94] C. W. Nelson, A. Hati, and D. A. Howe. Relative intensity noise suppression for RF photonic links. *IEEE Photonics Technology Letters*, 20(18):1542–1544, September 2008.

[95] N. A. Olsson. Lightwave systems with optical amplifiers. *IEEE/OSA Journal of Lightwave Technology*, 7(7):1071–1082, July 1989.

[96] R. Boula-Picard, M. Alouini, J. Lopez, N. Vodjdani, and J.-C. Simon. Impact of the gain saturation dynamics in semiconductor optical amplifiers on the characteristics of an analog optical link. *IEEE/OSA Journal of Lightwave Technology*, 23(8):2420–2426, August 2005.

[97] K. Sato and H. Toba. Reduction of mode partition noise by using semiconductor optical amplifiers. *IEEE Journal of Selected Topics in Quantum Electronics*, 7(2):328–333, March/April 2001.

[98] J. Mørk, A. Mecozzi, and G. Eisenstein. The modulation response of a semiconductor laser amplifier. *IEEE Journal of Selected Topics in Quantum Electronics*, 5(3):851–860, May/June 1999.

[99] M. L. Nielsen, D. J. Blumenthal, and J. Mørk. A transfer function approach to the small-signal response of saturated semiconductor optical amplifiers. *IEEE/OSA Journal of Lightwave Technology*, 18(12):2151–2157, December 2000.

[100] G. P. Agrawal and N. A. Olsson. Self-phase modulation and spectral broadening of optical pulses in semiconductor laser amplifiers. *IEEE Journal of Quantum Electronics*, 25(11):2297–2306, November 1989.

[101] F. öhman, S. Bischoff, B. Tromborg, and J. Mørk. Noise and regeneration in semiconductor waveguides with saturable gain and absorption. *IEEE Journal of Quantum Electronics*, 40(3):245–255, March 2004.

[102] G. Baili, M. Alouini, D. Dolfi, F. Bretenaker, I. Sagnes, and A. Garnache. Shot-noise-limited operation of a monomode high-cavity-finesse semiconductor laser for microwave photonics applications. *Optics Letters*, 32(6):650–652, March 2007.

[103] M. Shtaif, B. Tromborg, and G. Eisenstein. Noise spectra of semiconductor optical amplifiers: relation between semiclassical and quantum descriptions. *IEEE Journal of Quantum Electronics*, 34 (5):869–878, May 1998.

[104] J. L. Corral, J. Marti, J. M. Fuster, and R. I. Laming. True time-delay scheme for feeding optical controlled phased-array antennas using chirped-fiber gratings. *IEEE Photonics Technology Letters*, 9(11):1529–1531, November 1997.

[105] Y. Liu, J. Yang, and J. Yao. Continuous true-time-delay beamforming for phased array antenna using a tunable chirped fiber grating delay line. *IEEE Photonics Technology Letters*, 14(8): 1172–1174, August 2002.

[106] H. Hashemi, G. Xiang, A. Komijani, and A. Hajimiri. A 24-Ghz SiGe phased-array receiver-LO phase-shifting approach. *IEEE*

Transactions on Microwave Theory and Techniques, 53(2):614–626, February 2005.

[107] Q. Chang, Q. Li, Z. Zhang, M. Qiu, T. Ye, and Y. Su. A tunable broadband photonic RF phase shifter based on a silicon microring resonator. *IEEE Photonics Technology Letters*, 21(1):60–62, January 2009.

[108] M. Pu, L. Liu, W. Xue, Y. Ding, H. Ou, K. Yvind, and J. M. Hvam. A tunable broadband photonic RF phase shifter based on a silicon microring resonator. *Optics Express*, 18(6):6172–6182, March 2010.